DIPLOMARBEIT

Titel der Diplomarbeit

Towards Cavity Cooling of a Molecular Beam

angestrebter akademischer Grad

Magister der Naturwissenschaften (Mag. rer.nat.)

Verfasserin / Verfasser:	Peter ASENBAUM
Matrikel-Nummer:	0501797
Studienrichtung (lt. Studienblatt):	Diplomstudium Physik 411
Betreuerin / Betreuer:	Prof. Dr. Markus ARNDT

Wien, am
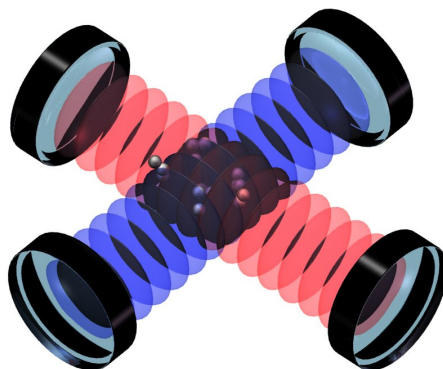
Towards Cavity Cooling of a Molecular Beam

Diplomarbeit zur Erlangung des akademischen Grades
Magister der Naturwissenschaften

eingereicht von
Peter Asenbaum

Juli 2009

durchgeführt bei
Prof. Dr. Markus Arndt

Universität Wien

Abstract

The ability to provide dense samples of cold molecules offers great opportunities in various different research fields. Unfortunately, the successful techniques available for cooling and trapping of atoms cannot be applied to molecules. Off-resonant cavity cooling is a very promising candidate to cool molecules even to ultracold temperatures. This method can be, in principle, applied to every polarizable particle, which is non-absorptive at the wavelength that is used.

Using off-resonant light results in low absorption, but also in weak molecule-field coupling. Fortunately, above a critical laser intensity threshold the low coupling can be compensated by a high particle density. Nevertheless, the requirements for cavity cooling of molecules are challenging. Until now (cavity assisted) laser cooling of molecules has not been realized for any molecular species anywhere in the world.

The aim of this experiment is to achieve the first optical cooling of molecules ever. By utilizing the features of a molecular beam, by enhancing the molecule-field coupling in a highly degenerate cavity mode structure and by amplifying the pump laser in a second high-finesse cavity this major goal has come into the reach based on the present Diploma thesis.

By now the whole experiment has been designed and constructed. The high-finesse cavities have been manufactured and characterized, the vacuum chamber including the molecule source and detection are fully functional and the optical setup is aligned. Therefore the first experiments exploring this novel molecular cooling scheme are about to begin.

4

Zusammenfassung

Die Fähigkeit, kalte Moleküle mit hoher räumlicher Dichte herzustellen, eröffnet völlig neuartige Möglichkeiten in diversen Forschungsdisziplinen. Die direkte Anwendung der sehr erfolgreichen Kühl- und Fallen-Techniken für Atome auf Moleküle ist bisher nicht möglich. Nicht-resonantes Laserkühlen mit Hilfe optischer Resonatoren (Cavity Kühlen) eröffnet eine neue Perspektive kalte Moleküle herzustellen. Im Prinzip ist diese Methode auf jedes polarisierbare Teilchen anwendbar, welches das Kühllicht bei der gewählten Wellenlänge zwar streut, aber möglichst wenig absorbiert.

Die Verwendung von nicht-resonantem Licht resultiert zum einen in einer schwachen Absorption, zum anderen in einer schwachen Kopplung zwischen Molekül und elektrischem Feld. Erreicht man jedoch eine kritische Laserleistung und molekulare Teilchendichte, so kann die schwache Molekül-Feld Kopplung ausgeglichen werden. Nichts desto weniger stellt das Cavity-Kühlen von Molkülen eine große Herausforderung dar. Bis heute konnte noch keine (Cavity-) Laser-Kühlmethode auf irgendein Molekül erfolgreich angewendet werden.

Das Ziel dieses Experiments ist es, Moleküle zum allerersten Mal mit Hilfe von Licht zu kühlen. Durch Nutzung der vorteilhaften Eigenschaften eines Molekularstrahls, der verbesserten Molekül-Feld Kopplung in einem Resonator mit hochgradig entarteter Modenstruktur und der Verstärkung des Laser-Pumpfeldes in einer zweiten high-finesse Cavity ist dieses lang ersehnte Ziel durch diese Diplomarbeit in experimenteller Reichweite.

Bisher wurde der gesamte Versuch geplant und aufgebaut. Die zwei high-finesse Resonatoren wurden hergestellt und charakterisiert, die Vakuum-Kammer, die darin enthaltene Molekül-Quelle und Detektion sind voll funtkionstüchtig und das optische Setup ist justiert. Somit können die ersten Messungen dieser neuartigen Kühlmethode für Moleküle beginnen.

Contents

1 Introduction

The basic idea of laser cooling is to manipulate the motion of massive particles with light towards lower temperatures. Since the first proposal of laser cooling by Hänsch and Schawlow for neutral atoms [1], and by Wineland and Dehmelt for ions [2] in 1975 , many different schemes have been realized [3], including cavity assisted laser cooling [4, 5].

I will first present well known laser cooling techniques of atoms to underline their physical origin. This will be important to understand the difference to cavity assisted laser cooling.

In the wide-spread *Doppler-cooling* scheme, atoms are irradiated with photons of momentum $\hbar k$. Due to the motion of the atoms the frequency of the incident light appears Doppler-shifted. If the laser frequency is chosen to be red-detuned with respect to the dominant electronic transition, atoms moving towards the light source will absorb more photons than those moving in any other direction. Once they have absorbed a photon, the atoms are in an excited state. They have the possibility either to emit spontaneously or to undergo stimulated emission in the presence of already existing laser photons. In the case of stimulated emission the photon is emitted with the same momentum as during the absorption. Hence the momentum of the atom does not change.

While all absorption processes add the same momentum to the atom, spontaneous emission is isotropic. The total effect of all emission processes is a momentum diffusion of the atom, where the average momentum remains zero while its variance grows linearly with the number of scattered photons.

This velocity dependent momentum exchange can be used to modify the trans-
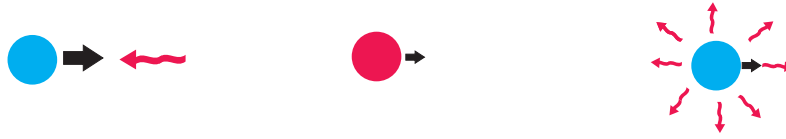
Figure 1.1: An atom absorbs a photon. The atom is excited and the momentum is reduced by $\hbar$k. Then the atom decays spontaneously and emits the photon isotropically. After N absorption processes the net momentum will change by $N \cdot \hbar k$ in the direction of the exciting light beam.

lational state of an atom [6].[1] The maximum deceleration force is given by $|\mathbf{F}| = \hbar k\gamma/2$ and the achievable Temperature T, limited by photon diffusion, is given by $k_B T = \hbar\gamma/2$ (Doppler-limit) [6]. Here, γ is the natural line width of the transition, which is the inverse of the excited state life time.

This Doppler temperature limit can be surpassed by *polarization gradient cooling* [11]. For linear $\perp$ linear polarization gradient cooling the mechanism is of a Sisyphus type. Due to the AC Stark shift the Zeeman sublevels of an atom experience different potential energies along the laser beam axis. While moving along an optical potential the atom converts kinetic into potential energy and vice versa. At positions of high potential energy the atom is optically pumped into another sublevel, which has a lower potential energy at this position. When reaching the potential energy hill of this new sublevel, the atom is optically pumped back to the original sublevel. Therefore the atom climbs the potential hills until it is cooled to the temperature limit.

In the case of $\sigma^+ - \sigma^-$ polarization gradient cooling the polarization is always linear and rotates around the beam axis. For a $J_g = 1 \rightarrow J_e = 2$ transition linearly polarized light pumps the atoms into the sublevel with $M_g = 0$. This sublevel has a more negative AC Stark shift (light shift) than the $M_g = \pm 1$ sublevels. For an atom at rest the particle will be in the $M_g = 0$ state. However, due to the changing polarization direction along the beam axis the quantization axis rotates also. This means a moving atom is constantly distorted into the $M_g = 0$ and a small fraction into $M_g = \pm 1$ [2] state. Again the linearly polarized light pumps the atom back into the $M_g = 0$, which is bound more deeply (stronger

---

[1]see also the Nobel lectures by Chu, Cohen-Tannoudji and Philips [7–9]. A more theoretical overview will be given in [10].

[2]The sign is determined by the direction of propagation along the beam axis.

light shift). Therefore motional energy of the particle is transferred to the light field. It has to be noted that this cooling scheme works for $J_g \geq 1$ [12].

The cooling mechanism is therefore provided by the continuous change to lower bounded internal states by optical pumping. The achievable temperature for these two cooling schemes is approximately given by the recoil energy. The recoil energy is defined by the kinetic energy of an atom with the momentum of a photon, $\hbar k$.

Laser cooling even below the recoil limit has been achieved either by *velocity-selective coherent population trapping* (VSCPT) [13] or by *Raman cooling* [14]. The main idea behind these cooling schemes is to protect the atom from the momentum diffusion due to spontaneous emission (recoil heating).

In the case of VSCPT atoms can evolve into dark states, that interact weakly with the applied light fields. Weak interaction implies that the atom remains in this dark state longer. The smaller the momentum of an atom the weaker it interacts. For zero momentum the atom does not interact and is therefore trapped in this state. The dark state protects the atom from recoil heating. Due to the momentum diffusion from the spontaneous emission atoms with nonzero momentum can accidentally end up with a momentum close to zero. For a finite interaction time with the light fields the atoms are arranged in states with very small momentum uncertainty.

In the case of Raman cooling a Raman transition between two hyperfine ground states can be used to excite very narrow velocity classes. The high velocity particles are pumped into the higher hyperfine state by two light pulses into the higher hyperfine state. The line width of transitions between two ground states is only limited by the line width of the laser pulses, therefore these transitions can be very velocity selective. One can excite very narrow velocity classes without exciting the low velocity particles. The particles in the higher hyperfine state are then excited by another laser to a further above lying state and decay again to the lower ground state. Again, due to the random momentum kick from the spontaneous emission particles may end up in the low velocity class, wherein the particles are trapped.

A common way to cool ions in alternating current traps is side band cooling [15]. The ion oscillates in the trap with a certain frequency ω_T. The ion is irradiated with a light field of frequency ω_l. Due to the oscillations the ion experiences a light

field with frequency ω_l (carrier) but also a small fraction of light with frequency $\omega_l \pm \omega_T$ (sidebands). By choosing $\omega_l + \omega_T$ to be resonant with an optical transition ω_o, energy from the oscillation can be transferred into an electronic excitation. After the decay to the electronic ground state the oscillation of the ion is cooled. All the discussed cooling schemes require a so called 'closed cycle'. This means that the atoms return to the desired ground state after one cycle of absorption and emission, in order to remain in the cooling cycle. For a few atomic species almost closed transitions can be found. For a cesium atom one can use the transition $6S_{1/2}, F_g = 4 \rightarrow 6P_{3/2}, F = 5_e$, see figure 1.2.
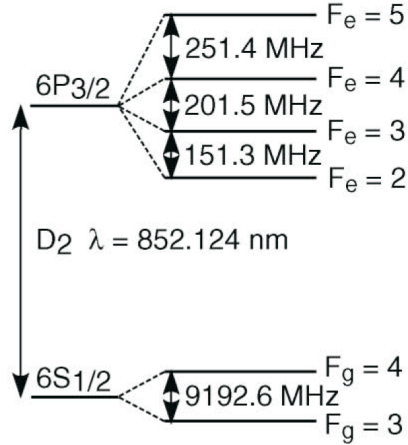
Figure 1.2: $6S_{1/2}, F_g = 4 \rightarrow 6P_{3/2}, F = 5_e$ transition of cesium. The graph is taken from *Chan et al* [16].

This transition is favorable, because the atom can only decay to the $F_g = 4$ state due to the selection rules. However, the excited state hyperfine levels $F = 4, 5_e$ are only separated by 250 MHz ($\gamma/2\pi = 5MHz$). Therefore the atom can also be excited to $F_e = 4$, where it can decay to $F_g = 3$. In the $F_g = 3$ state the atom is no longer resonant with the $F_g = 4 \rightarrow F_e = 5$ and is lost from the cycle. This problem can be solved by introducing a repump laser, which pumps the atom back in the $F_e = 4$.

Hence, by introducing a single repump laser the cycle can be closed again. With additional repump lasers, laser cooling techniques can be applied to alkali, alkaline earth and metastable noble gas atoms.

Laser Cooling of Molecules   Extending these techniques to molecules involves several problems.   On the one hand molecules offer not only electronic but also rotational and vibrational degrees of freedom.   These states are coupled to each other by radiative or non-radiative transitions. Repumping all these different states would be highly impracticable. It has been proposed that for some molecules a finite number of repump lasers would be sufficient to achieve a quasi-closed cooling cycle [17–19]. However, until now these techniques could not be implemented. On the other hand the lifetimes of rotational and vibrational levels in the electronic ground state are very long. The energy of an absorbed photon can be partly reemitted (fluorescence, phosphorescence) and partly distributed over the many of freedom. Any attempt to slow down a molecule by a laser beam would therefore lead to a continuous increase of internal energy and most likely to its thermal dissociation.

As we have seen, spontaneous emission is not an appropriate dissipation channel for cooling molecules. An alternative method was therefore proposed in 1997 by the group of Helmut Ritsch [20], namely the so called cavity assisted laser cooling (cavity cooling). The spatial dependence of the cavity field is given by the mode function. Close to the cavity axis this mode function reads $\cos(kx)$. The field intensity is then proportional to $\cos^2(kx)$.
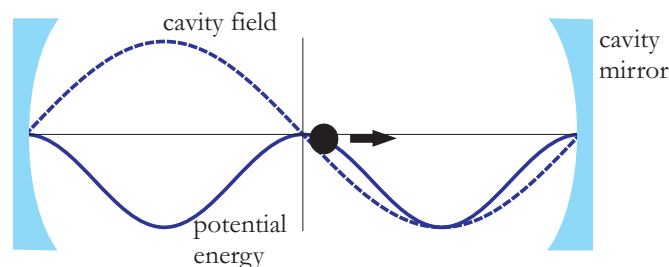

Figure 1.3: Coupling of a polarizable particle to the electric field of a cavity mode. The dashed curve denotes the cavity field along the cavity axis. The solid curve indicates the potential energy of the particle. The antinodes of the field indicate strong and the nodes weak particle-field coupling. The nodes of the cavity field coincide with zero potential energy.

For further discussions it is advisable to introduce the light shift per cavity photon $U(x) = U_0 \cos^2(kx)$ with the dimension s^{-1}. The corresponding energy shift is

given by $\hbar U(x)$ [3]. This periodic energy shift can also be interpreted as a potential energy surface along the cavity axis, see figure 1.3. Additionally, the presence of a particle inside a cavity shifts the resonance of this system by $U(x)$. On the one hand U_0 describes the impact of the cavity field on the particle (potential energy). On the other hand it characterizes the change of the cavity resonance due to the presence of the particle. Therefore U_0 denotes the particle-field coupling strength.

We assume the cavity to be pumped by light, which is red detuned to the cavity resonance and far red detuned from any molecular resonance, i.e. in the region of normal dispersion, where the polarizability is positive and U_0 negative[4]. If the particle is located near an antinode of the cavity field, the resonance of the cavity is shifted to the red. Therefore more photons from the pump beam can leak into the cavity mode, which results in a stronger cavity field. If the particle is located near a node of the cavity field only few photons can leak into the cavity. This will affect the photon number inside the cavity on a timescale of the cavity response time κ^{-1}, where κ is the line width of the cavity resonance. While the photon number is still increased the particle moves up the potential energy hill and loses kinetic energy. Arriving at a node of the field the photon number has decreased, see figure 1.4. Moving on to the next antinode at a low photon
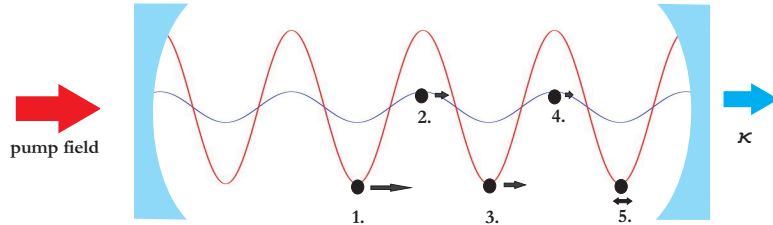
Figure 1.4: Particle moving in cavity pumped by red detuned light. The curves denote the potential energy of the particle, the color indicates the resonance frequency for a given particle position. For strong coupling the resonance of the cavity system is shifted to the red. This results in a high photon number and therefore deep potential wells. While moving along the cavity axis the particle is slowed down until it is finally trapped. The cavity decay rate κ determines how fast energy can be transferred to the dissipating environment.

number, the particle regains only a part of its initial kinetic energy. The difference

---

[3]This energy equals the AC Stark shift of the particle.

[4]By detuning the pump light to the blue with respect to the cavity resonance the particle will not be cooled but accelerated.

in the kinetic energy is transferred to the cavity field, which leaks out by the rate κ. The arising cooling effect is of a Sisyphus type, because the particle has to climb higher potential hills than it can go down. This mechanism is similar to polarization gradient cooling of atoms, which, however, emerges from a different physical origin. In the case of polarization gradient cooling the state of atoms is changed towards lower potential energy. In the case of cavity cooling, the state of the cavity is changed, which results in lower potential energy of the particle.

For large detuning from any resonance the moving particle is not excited and therefore not spontaneously emitting any photons either. In this scheme the cavity leakage rate κ provides a cooling mechanism, which is independent of the energy level structure of the particles. This new light-mediated friction force was experimentally observed for the first time in 1999 [21]. The group of Gerhard Rempe used single rubidium atoms falling from a magneto optical trap. Later experiments achieved trapping [22, 23] and cooling due to the cavity mediated light forces [4, 5, 24, 25] for rubidium and cesium atoms.

However, this cooling method has a certain disadvantage in the scaling to larger particle numbers [26–28]. In the case of strong coupling, i.e. when $U_0 \approx \kappa$, the presence and motion of several independent particles can actually disturb or eliminate the cooling process [26]. To see that, let us assume two particles moving in the same cavity, with the same velocity, direction and with a relative displacement of $\lambda/4$. While one particle is moving to an antinode, the other one is leaving it. Therefore the frequency shift stays constant and no cooling force can arise, see figure 1.5.
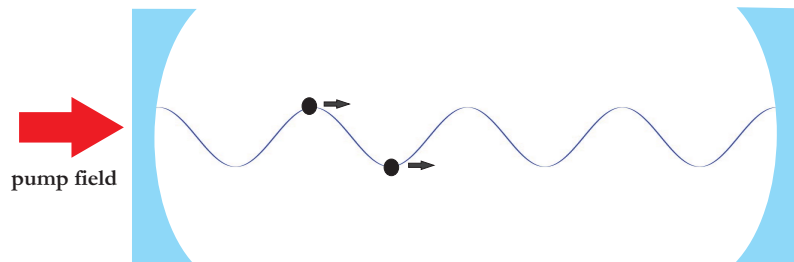

Figure 1.5: Two particles strongly coupled to the cavity mode. Due to the disturbance of the second particle the frequency shift stays constant and the photon number inside the cavity is low all the time.

This is just one case, where the net influence on the cavity field is compensated

by the motion of more than one particles [29]. For weakly coupled particles ($U_0 \ll \kappa$) the mutual influence is rather small and the cooling rate is independent of the particle number. Unfortunately, the cooling times get very long for small U_0 [28].

Far away from any resonance even highly polarizable large molecules have a very low U_0, in our experiment with fullerenes $U_0/\kappa = 10^{-9}$. The mentioned experiments with atoms were carried out in the strong coupling regime, $U_0 \approx \kappa$. This scheme seems to be unfeasible. Fortunately, by changing in setup a small U_0 can be compensated by a large particle number inside the cavity. Instead of pumping the cavity mode directly, the particles are pumped by a laser beam oriented perpendicular to the cavity axis [30].
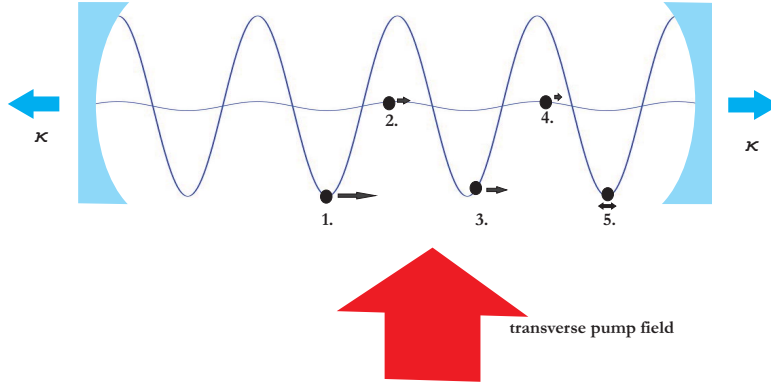
Figure 1.6: The cavity is blue detuned with respect to the transverse pump. Around an antinode of the cavity field the particle scatters light into the cavity mode. In a node of the cavity field the particle cannot scatter light inside the cavity. Therefore the photon number of the cavity field is even more dependent on the particle's position compared to the cavity pump scheme 1.4.

Now the cavity field arises from the light that is scattered by the particles, see figure 1.6. For randomly distributed particles the phase of the scattered photons is arbitrary. For low pumping intensities the scattered light from different particles interferes destructively and no cavity field can build up. But if the pumping strength is increased above a certain threshold, the particles self-organize into a regular lattice with a period of λ along the cavity axis, see figure 1.7. This means that constructive interference will further enhance the scattering rate into the cavity. This effect is known as superradiance or Bragg-scattering.

The self-organization process starts with small density perturbation with period

λ. Due to this perturbation a cavity field can arise, which attracts particles to every second antinode of the mode function. The particles at these antinodes are displaced by λ and therefore scatter in phase. The field gets larger and attracts more particles, which again leads to a stronger cavity field. After a certain time the particles are finally ordered in a molecular lattice of periodicity λ.

Once the particles are organized, the cooling force is maximal. To achieve efficient cooling this pattern has to be triggered. The cavity setup for transverse pumping will be discussed in more in chapter 2.
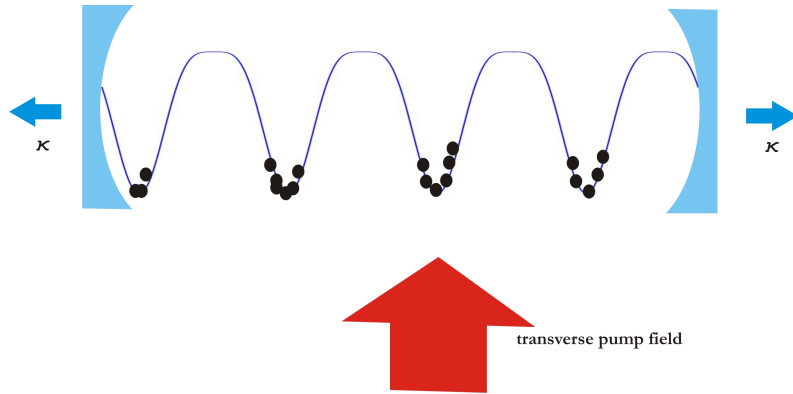

Figure 1.7: The particles have self-organized in a period of λ. In this phase the intensity of the scattered light is proportional to N^2.

The phase transition to collectively enhanced cooling has already been observed and studied in detail for atoms by the group of Vladan Vuletic [16,31]. They used up to 10^7 cesium atoms that were falling from a magneto-optical-trap at T=50 μK into a confocal cavity underneath. The pump light was detuned up to a few GHz from an atomic transition of cesium ($\gamma/2\pi = 5MHz$). Despite the far detuning, their coupling strength ($U_0 \approx 10^2$ Hz) is still very strong in comparison with molecules ($U_0 \approx 10^{-3}$ Hz). Due to the mentioned collective effects the research group was able to cool and even trap parts of the cloud.

The aim of our experiments is quite similar with completely different parameters, though. The threshold laser intensity for molecular self-organization in the cavity is proportional to $U_0^{-2}N^{-1}$. This implies that a very high pumping power and a high particle number are needed to initiate the phase transition into a molecular lattice.

A high pumping power can be achieved in a high-finesse pumping cavity, which
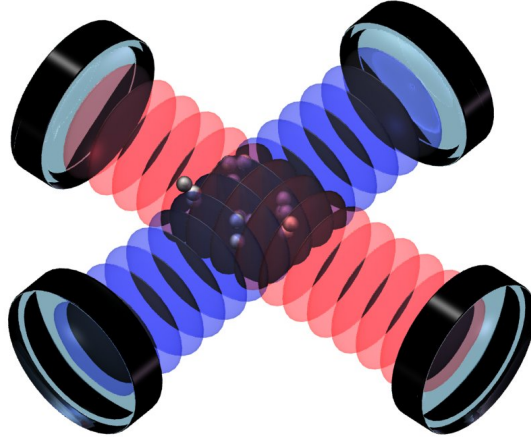
Figure 1.8: The blue detuned cooling cavity is orientated perpendicular to the pumping cavity. The molecules inside this intersection scatter the pump photons preferentially into the cooling cavity.

can enhance the power of a laser by several orders of magnitude. By positioning the molecule source close to the cavity a high particle density can be achieved inside the cavity mode. Another crucial increase of the coupling U_0 can be achieved by using a resonator with a highly degenerate mode structure (e.g. a confocal cavity). A higher mode density naturally leads quite naturally to an increased scattering rate.

Cavity assisted cooling of large molecules was already described by [32, 33]. However, there are several differences between these earlier simulations and the present experiment. First of all, the simulations were performed for particle clouds entering and leaving the cavity mode, where the optical field was built up by the entering particles. However, in our experiment we are working with a continuous molecular beam. For large particle numbers (up to 10^8 inside the cavity mode) the dynamics of the system was interpolated using the results of lower particle numbers. Additionally, the dynamic behavior of the pumping cavity and the effect of the degenerate modes is not fully understood.

Therefore, we search for a more profound understanding of the interaction of a molecular beam with a confocal cavity and of the phase transition to the

self-organized molecular structure. The insights of this novel experiment will be important for future implementations of molecular cavity cooling.

2 Theory

For low temperatures, weak pumping and non-negligible photon absorption quantum fluctuations play an important role. In this case a quantum optical treatment is required to describe the cavity-particle system appropriately [34]. However, in our experiment the laser wavelength is far from any molecular resonance, we apply strong pumping fields and we will not reach low temperatures. In this regime the semi-classical equations, derived from a quantum master equation, and classical electrodynamical equations are identical. After deriving a closed set of equations from the Maxwell equations, we will take a short look at the particle's self-organization process and on the friction force mediated by the cavity field.

2.1 Electrodynamical Approach

The following derivation stays close to that presented in [33, 35]. We consider particles with polarizability α. Far off resonance α is real and we ignore the effect of absorption. A non-vanishing but weak absorption would be an additional loss term, which is negligible compared to the cavity decay rate κ. On the contrary the internal energy of the particles would be changed significantly, which is , however, not considered here. The total applied electric field $\mathbf{E}_T$ induces a dipole moment $\mathbf{p}$.

$$\mathbf{p} = \alpha \mathbf{E}_T \tag{2.1}$$

The total electric field $\mathbf{E}_T$ inside the cavity is given by

$$\mathbf{E}_T = \mathbf{E} + \mathbf{H}, \tag{2.2}$$

where $\mathbf{H}$ is the electric field of the transversally pumping laser and $\mathbf{E}$ the cavity field. The N particle polarization $\mathbf{P}$ can be written as

$$\mathbf{P} = \sum_{j}^{N} \mathbf{p}_j(t)\delta^{(3)}(\mathbf{x} - \mathbf{x}_j(t)). \tag{2.3}$$

The electric field inside the cavity is coupled to the surrounding by the current density $\mathbf{J}$. $\mathbf{J}$ consists of the field leaking out $2\epsilon_0\kappa\mathbf{E}$ and the cavity pump field $2\epsilon_0\kappa\mathbf{E}_{ext}$.

$$\mathbf{J} = 2\epsilon_0\kappa(\mathbf{E} - \mathbf{E}_{ext}) \tag{2.4}$$

For a system without free charges and permeability $\mu = 1$ the Maxwell equations read

$$\nabla \times \mathbf{E} = -\partial_t\mathbf{B} \tag{2.5}$$

$$\nabla \times \mathbf{B} = \frac{1}{c^2\epsilon_0}\mathbf{J} + \frac{1}{c^2}\partial_t\mathbf{E} + \frac{1}{c^2\epsilon_0}\partial_t\mathbf{P} \tag{2.6}$$

$$\nabla\mathbf{E} = 0 \tag{2.7}$$

$$\nabla\mathbf{B} = 0. \tag{2.8}$$

Eliminating $\mathbf{B}$ one gets an equation for the cavity field $\mathbf{E}$

$$(-c^2\Delta + \partial_t^2)\mathbf{E}(\mathbf{x}, t) = -1/\epsilon_0\partial_t^2\mathbf{P}(\mathbf{x}, t) - 1/\epsilon_0\partial_t\mathbf{J}(\mathbf{x}, t). \tag{2.9}$$

Inserting equation 2.4 into 2.9 gives

$$(-c^2\Delta + \partial_t^2 + 2\kappa\partial_t)\mathbf{E}(\mathbf{x}, t) = -1/\epsilon_0\partial_t^2\mathbf{P} + 2\kappa\partial_t\mathbf{E}_{ext}. \tag{2.10}$$

The spatial part of the above equation is the well known Helmholtz equation. For a certain direction of field propagation one can find an approximate solution (paraxial approximation) [36]. For cylindrical boundary conditions (e.g. round mirrors) the eigenmodes are Laguerre-Gauss functions, for cartesian boundary conditions (e.g. square aperture) Hermite-Gauss functions. These eigenmodes form a complete and orthogonal set of functions. They are characterized by three mode numbers, a longitudinal and two transverse mode numbers, see equation 3.8. Generally different mode numbers result in different frequencies. For special

cavity geometries (e.g. confocal cavity) a large number of modes can be degenerate, see section 3.1. Therefore we assume M modes to be degenerate at the frequency ω_c. Furthermore ω_c is close to the transverse pump frequency ω_p. The cavity field can now be written in terms of these degenerate mode functions f_n with time dependent amplitudes $E_n(t)$.

$$E_n = 1/V \int d^3x \mathbf{E}(\mathbf{x}, t) f_n(\mathbf{x}) \tag{2.11}$$

$$E(\mathbf{x}, t) = \sum_n^M E_n(t) f_n(x) \tag{2.12}$$

$$\int f_n(\mathbf{x}) f_m(\mathbf{x}) d^3x = \delta_{n,m} V, \tag{2.13}$$

where V is the mode volume. All other modes are neglected. Also $\mathbf{P}$ and $\mathbf{E}_{ext}$ can be written in terms of the mode functions f_n

$$\mathbf{P}_n(t) = \frac{1}{V} \sum_j^N \mathbf{p}_j(t) f_n(\mathbf{x}_j) \tag{2.14}$$

$$\mathbf{E}_n^{ext} = 1/V \int d^3x \mathbf{E}_{ext}(\mathbf{x}, t) f_n(\mathbf{x}). \tag{2.15}$$

The mode functions are orthogonal, therefore each $\mathbf{E}_n(t) f_n(\mathbf{x})$ alone satisfies equation (2.10). Eliminating the mode function leads to

$$\ddot{\mathbf{E}}_n + 2\kappa \dot{\mathbf{E}}_n + \omega_c^2 \mathbf{E}_n = -1/\epsilon_0 \ddot{\mathbf{P}}_n + 2\kappa \dot{\mathbf{E}}_n^{ext}. \tag{2.16}$$

The term proportional to ω_c^2 arises from $-c^2 \Delta f_n$. Further we assume, that the fields $(\mathbf{E}_n, \mathbf{E}_n^{ext}, \mathbf{H}, \mathbf{P}_n)$ can be separated in fast times slowly varying amplitudes. The fast varying amplitudes oscillate with transverse pump frequency ω_p. The slowly varying amplitudes describe effects due to the circulation of electric fields inside the cavity mirrors. Therefore the frequency of the slowly varying amplitude is upper bounded by the free spectral ν_{FSR} (inverse round trip time). For reasonable cavity lengths (a few cm) ν_{FSR} is in the GHz range. However, for high reflectivity mirrors the frequency of the slow amplitudes is on the order of the cavity line width κ (decay rate). In our setup (reflectivity ≥ 0.9998 and cavity length = 2.5 cm) κ equals 1.2 MHz, which is nine orders of magnitude slower

than the transverse pump frequency $\omega_p = 1.2 \cdot 10^{15}$Hz. Consequently we write

$$\mathbf{E}_n = \mathbf{e}_n(t)e^{-i\omega_p t} + c.c. \tag{2.17}$$

$$\mathbf{E}_n^{ext} = \mathbf{e}_n^{ext}(t)e^{-i\omega_p t} + c.c. \tag{2.18}$$

$$\mathbf{H} = \mathbf{h}(t)e^{-i\omega_p t} + c.c. \tag{2.19}$$

$$\mathbf{P}_n = \mathbf{p}_n(t)e^{-i\omega_p t} + c.c., \tag{2.20}$$

where c.c. stands for the complex conjugated term. One can choose the frequency of the cavity pump field $\mathbf{E}_n^{ext}$ to be slightly different than the transverse pumping frequency ω_p. However, these small frequency deviations from ω_p can be put in the slowly varying amplitudes. Inserting the equations 2.17-2.20 into 2.16 and eliminating $e^{-i\omega_p t}$ yields

$$\dot{\mathbf{e}}_n = \frac{i\omega_p}{2\epsilon_0}\mathbf{p}_n - \kappa\mathbf{e}_n - \frac{i\omega_c^2}{2\omega_p}\mathbf{e}_n + \frac{i\omega_p}{2}\mathbf{e}_n + \kappa\mathbf{e}_n^{ext} - \frac{1}{\epsilon_0}\dot{\mathbf{p}}_n - \frac{i\kappa}{\omega_p}\dot{\mathbf{e}}_n + \frac{i\kappa}{\omega_p}\dot{\mathbf{e}}_n^{ext} - \frac{i}{2\epsilon_0\omega_p}\ddot{\mathbf{p}}_n - \frac{i}{2\omega_p}\ddot{\mathbf{e}}_n. \tag{2.21}$$

The next step is to take the slowly varying amplitude approximation into account. This implies $|\dot{\mathbf{e}}_n| << \omega_p |\mathbf{e}_n|$;the analog statements also hold for $\mathbf{p}_n$, $\mathbf{e}_n^{ext}$ and $\mathbf{h}$. It follows that

$$\dot{\mathbf{e}}_n = \frac{i\omega_p}{2\epsilon_0}\mathbf{p}_n - \kappa\mathbf{e}_n - \frac{i\omega_c^2}{2\omega_p}\mathbf{e}_n + \frac{i\omega_p}{2}\mathbf{e}_n + \kappa\mathbf{e}_n^{ext}. \tag{2.22}$$

Now we apply the relation $\omega_p - \omega_c^2/\omega_p = 2\Delta_C$, where the detuning between cavity and pump laser frequency is defined by $\Delta_C = \omega_p - \omega_c$.

$$\dot{\mathbf{e}}_n = (i\Delta_C - \kappa)\mathbf{e}_n + \frac{i\omega_p}{2\epsilon_0}\mathbf{p}_n + \kappa\mathbf{e}_n^{ext} \tag{2.23}$$

We insert expression 2.1 and combine several parameters to from the new parameter U_0, which is the light shift per cavity photon as already introduced in chapter 1.

$$U_0 = -\frac{\alpha\omega_p}{2\epsilon_0 V} \tag{2.24}$$

This parameter describes on the one hand the potential energy per cavity photon $\hbar U_0 f_n(\mathbf{x})^2$(without transverse pumping), see 2.30, and the shift of the cavity

resonance $U_0 f_n(\mathbf{x})^2$ due to the presence of a particle a position $\mathbf{x}$. Furthermore we introduce dimensionless field amplitudes

$$\mathbf{a}_n = \sqrt{\frac{2\epsilon_0 V}{\hbar \omega_p}} \mathbf{e}_n \tag{2.25}$$

$$\frac{\mathbf{s}_n}{\kappa} = \sqrt{\frac{2\epsilon_0 V}{\hbar \omega_p}} \mathbf{e}_n^{ext} \tag{2.26}$$

$$-\frac{\eta}{U_0} \mathbf{h} = \sqrt{\frac{2\epsilon_0 V}{\hbar \omega_p}} \mathbf{H}. \tag{2.27}$$

where $|a_n|^2$ is the photon number in the nth mode. η/U_0 is the dimensionless transverse field amplitude. The field amplitude scattered into the cavity mode is given by $\eta/U_0 \cdot U_0 = \eta$. η is now the transverse cavity pump rate. The total dimensionless electric field $\mathbf{e}_T$ is given by

$$\mathbf{e}_T(\mathbf{x}) = \sum_n \mathbf{a}_n f_n(\mathbf{x}) - \frac{\eta}{U_0} \mathbf{h}(\mathbf{x}). \tag{2.28}$$

Now equation 2.23 can be written as

$$\dot{\mathbf{a}}_n = (i\Delta_C - \kappa)\mathbf{a}_n - iU_0 \sum_{j=1}^{N} \mathbf{e}_T(\mathbf{x}_j) f_n(\mathbf{x}_j) + \mathbf{s}_n(t), \tag{2.29}$$

where $\mathbf{x}_j$ is the position of the j-th particle. Here, the term $(i\Delta_C - \kappa)\mathbf{a}_n$ is the evolution of the $n^t h$ mode in absence of cavity pumping and particles. The sum $U_0 \sum_{j=1}^{N} \mathbf{e}_T(\mathbf{x}_j) f_n(\mathbf{x}_j)$ contains the field amplitudes of the other modes and the transverse pumping field. Therefore the different modes are coupled to the transverse pump field and to each other with the coupling strength U_0 due to the presence of particles.

The potential energy V of a particle with induced dipole moment $\mathbf{p}_j = \alpha \cdot \mathbf{E}_T$ in a electric field $\mathbf{E}_T$ is given by

$$V = -\alpha \mathbf{E}_T^2 = \hbar U_0 |\mathbf{e}_T|^2. \tag{2.30}$$

By applying the gradient one gets the force $\mathbf{F}$ acting on the j-th particle with mass m and velocity $\mathbf{v}$

$$\mathbf{F} = m\ddot{\mathbf{x}}_j = m\dot{\mathbf{v}}_j = -\hbar U_0 \nabla_j |\mathbf{e}_T|^2. \tag{2.31}$$

The time evolution of the field amplitudes, equation 2.31, and the forces acting on each particle, equation 2.29, suffice to describe our cavity-particle system completely.

For now, we take only one direction of polarization into account. Therefore we can drop the vector character of the fields $\mathbf{a}_n$, $\mathbf{s}_n$, $\mathbf{h}$ and $\mathbf{e}_T$.

We want to derive the photon scattering rate for one particle into M degenerate cavity modes. Equation 2.29 can therefore be written as

$$\dot{a_n} = (i\Delta_C - \kappa)a_n - iU_0 \sum_{i=1}^{M} a_i f_i + i\eta f_n. \tag{2.32}$$

For simplicity, we assume the particle to be positioned at x_0, where all mode function take the value $f_n(x_0) = 1$. Due to this assumption all modes can be treated on an equal footing. Therefore we can expect the steady state amplitudes of a_n to be equal and to take the value

$$a_{ss} = \frac{i\eta}{\kappa - i(\Delta_C - M\ U_0)}. \tag{2.33}$$

The steady state photon number in each mode is given by

$$|a_{ss}|^2 = \frac{\eta^2}{\kappa^2 + (\Delta_C - M\ U_0)^2}. \tag{2.34}$$

The energy loss per time of the cavity is given by $\int \mathbf{J} \cdot \mathbf{E} dV$ [37]. This can be written in terms of $|a_{ss}|^2$

$$\int \mathbf{J} \cdot \mathbf{E} dV = 2\kappa M |a_{ss}|^2 \hbar\omega_p. \tag{2.35}$$

Therefore, the scattering rate Γ_S, the number of photons scattered per time, by a single particle reads

$$\Gamma_S = 2\kappa M |a_{ss}|^2. \tag{2.36}$$

This means the scattering rate is enhanced by M (number of modes). This expression holds for M degenerate and equal modes. In realistic setups the different modes are not exactly degenerate, they have different decay rates κ and the higher order mode functions are smaller than one. However, utilizing many degenerate modes can significantly increase the scattering rate and therefore the particle-field coupling.

2.2 Self-Organization

For certain parameters equation 2.29 and 2.31 predict self-organization of the particles into the lattice of period lambda [30]. By contrast, a regular optical lattice (standing wave) yields intensity maxima displaced by $\lambda/2$. This section will follow closely a derivation given in [38]. We consider a single mode cavity with one dimensional mode function $f(\mathbf{x}) = \cos(kx)$ and transverse pump $h(\mathbf{x}) = 1$. Further we assume that $s(t) = s\, e^{i\Delta_p t}$.Hence (2.29) simplifies to

$$\dot{a} = (i\Delta_C - \kappa)a - iNU_0 \left\langle \cos^2(kx) \right\rangle a + iN\eta \left\langle \cos(kx) \right\rangle + se^{i\Delta_p t}, \qquad (2.37)$$

where $\langle f(\mathbf{x}) \rangle = 1/N \sum_{j=1}^{N} f(\mathbf{x}_j)$ is the average of the function f(x) over all particle positions. Now we want to make a time averaged mean-field approach [38]. This means that the cavity field is always in a steady state (zero response time). We assume that the steady state amplitude consists of a constant and a term proportional to the time dependence of s(t)

$$a = a_0 + s_0\, e^{i\Delta_p t}. \qquad (2.38)$$

Solving equation 2.37 with ansatz 2.38 leads to

$$a_0 = \frac{iN\eta \left\langle \cos(kx) \right\rangle}{(\kappa - i\Delta_C) + iNU_0 \left\langle cos^2(kx) \right\rangle} \qquad (2.39)$$

$$s_0 = \frac{s}{i(\Delta_p - \Delta_C) + \kappa + iNU_0 \left\langle cos^2(kx) \right\rangle}. \qquad (2.40)$$

The next step is to calculate $|\mathbf{e}_T|^2$ to get an expression for the potential energy of the particle. Therefore we introduce the bunching and the order parameter

$$B = \left\langle \cos^2(kx) \right\rangle \qquad (2.41)$$

$$O = \left\langle \cos(kx) \right\rangle. \qquad (2.42)$$

The bunching parameter B takes the value $1/2$ for a random distribution and 1, if all particles are situated at the antinodes of the mode function. For $O = 1(-1)$ the particles are perfectly ordered at the positive (negative) sites of the mode function $\cos(kx)$ with a periodicity of λ. The steady state field results in

$$a_{ss} = \frac{iN\eta O}{(\kappa - i\Delta_C) + iNU_0 B} + \frac{s}{i(\Delta_p - \Delta_C) + \kappa + iNU_0 B}e^{i\Delta_p t}. \qquad (2.43)$$

Here, $|a_{ss}|^2$ denotes the steady state photon number inside the cavity. For $\Delta_p = 0$ the the steady state photon number is given by

$$|a_{ss}|^2 = \frac{|s|^2 + N^2 O^2 \eta^2}{(\Delta_C - BNU_0)^2 + \kappa^2}. \tag{2.44}$$

The term $|a_{ss}|^2$ consists of the pump and the scattered photons. Once the particles are sufficiently ordered with periodicity λ $(O > 0)$, the particles scatter in phase and this superradiance yields a photon scattering rate proportional to $N^2 O^2$.

The potential energy $V = \hbar U_0 |\mathbf{e}_T|^2$ then reads

$$V = \hbar U_0 |a_{ss}|^2 \cos^2(kx) + \hbar \frac{\eta^2}{U_0} - \hbar \eta (a_{ss} + a_{ss}^*) \cos(kx) \cos(kz). \tag{2.45}$$

For now we neglect the constant potential energy term $\hbar \frac{\eta^2}{U_0}$ We split the potential V into two parts, one proportional to $\cos^2(kx)$ and the other one proportional to $\cos(kx)$.

$$V = \hbar U_0 |a_{ss}|^2 \cos^2(kx) - \hbar \eta (a_{ss} + a_{ss}^*) \cos(kx) = U_2 \cos^2(kx) + U_1 \cos(kx) \tag{2.46}$$

As we will see later, varying phases between the transverse field and the cavity pump field are undesirable. Therefore we set $\Delta_p = 0$. U_1 and U_2 result in

$$U_1 = -2\hbar\eta \frac{\kappa |s| \cos(\phi) - \Delta_{eff}(NO\eta + |s| \sin(\phi))}{\Delta_{eff}^2 + \kappa^2} \tag{2.47}$$

$$U_2 = \hbar U_0 \frac{|s|^2 + N^2 O^2 \eta^2}{\kappa^2 + \Delta_{eff}^2}, \tag{2.48}$$

where we introduced the effective detuning $\Delta_{eff} = \Delta_C - BNU_0$ and the phase ϕ of the cavity pumping field s. In figure 2.1 you can see the potential energy along the cavity axis for different values of $|U_1| / |U_2|$.

For Small $|U_1| / |U_2|$ the potential wells exist every $\lambda/2$. Once

$$|U_1| > 2 |U_2| \tag{2.49}$$

is reached every second well disappears and an optical lattice of period λ forms. This can be understood in terms of interference. The polarization of a particle oscillates with the frequency and phase of the transverse pumping field but also
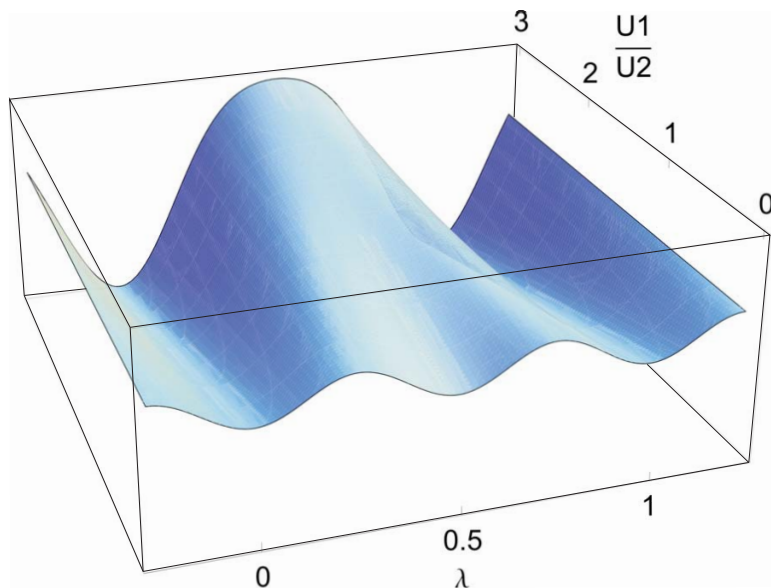
Figure 2.1: Potential energy for different values of $|U_1| / |U_2|$ along one period λ. By increasing U_1/U_2 the local minimum at $\lambda/2$ disappears and turns into a maximum of the potential energy.

with the phase of the cavity field. At certain positions the two fields are in phase (out of phase), and induce strong (weak) polarization oscillations. A strong (weak) polarization amplitude results in a deep (shallow) potential well.

To support the self-organization process it seems advisable to provide a lattice with period λ. Therefore one needs to maximize $|U_1|$ concurrent with keeping $|U_1| > 2|U_2|$. $|U_1| / 2|U_2|$ is given by

$$\frac{|U_1|}{2|U_2|} = \frac{\eta}{U_0} \frac{|s| \ \kappa \ \cos(\phi) - \Delta_{eff}(NO\eta + s \ \sin(\phi))}{|s|^2 + N^2 O^2 \eta^2}. \tag{2.50}$$

We want to calculate equation 2.50 in two limits. First we consider the case of $NO\eta \gg s$. This means that due to the high order O the scattered field is a lot stronger than the cavity pump field s. By setting $s = 0$ one gets

$$\frac{|U_1|}{2|U_2|} = \frac{\Delta_{eff}}{NOU_0}. \tag{2.51}$$

As long as the effective detuning Δ_{eff} is larger than the frequency shift NOU_0 the potential will yield a λ periodicity. The second limit is characterized by $NO\eta \ll s$. Therefore the order O is negligible. We set $O = 0$ and $\Delta_{eff} = -\kappa$,

which is the optimal choice to maximize U_1. One gets

$$\frac{|U_1|}{2|U_2|} = \frac{\eta}{U_0} \frac{\kappa}{s'} \tag{2.52}$$

$$s' = |s| \left(\cos(\phi) + \sin(\phi) \right) = |s| \sqrt{2} \sin(\frac{\pi}{4} + \phi). \tag{2.53}$$

For $\eta/U_0 > s'/\kappa$ the potential yields again a λ periodicity. By satisfying the inequalities for both limits one can provide a potential energy surface, which enables the onset and the continuation of a particle lattice with period λ.

Now we want to analyze, under which conditions self-organization can arise. We consider the spatial density of the particles in the potential V(x), which is given in the canonic ensemble by

$$\rho(x) = \frac{e^{-V(x)/k_B T}}{\int e^{-V(x)/k_B T} dx}. \tag{2.54}$$

We start out with $O = 0$. Therefore

$$U_2 = \hbar U_0 \frac{|s|^2}{\kappa^2 + \Delta_{eff}^2} \tag{2.55}$$

$$U_1 = -2\hbar\eta \frac{\kappa |s| \cos(\phi) - \Delta_{eff} |s| \sin(\phi)}{\Delta_{eff}^2 + \kappa^2}. \tag{2.56}$$

For $\Delta_{eff} = -\kappa$ the equations simplify to

$$U_2^{(0)} = \hbar U_0 \frac{|s|^2}{2\kappa^2} \tag{2.57}$$

$$U_1^{(0)} = -\hbar\eta \frac{s'}{\kappa}, \tag{2.58}$$

where $s' = |s| \sqrt{2} \sin(\frac{\pi}{4} + \phi)$. For $s \neq 0$ a potential with period lambda already exists despite vanishing order. Therefore, O=0 cannot be a state of equilibrium. Steps towards the steady state can be made by iterating equation 2.54 and hoping for a convergence. We assume the potentials $U_{1,2}$ to be very shallow compared to $k_B T$. Therefore, the first iteration can easily be made

$$\rho(x)^{(0)} = \frac{e^{(-U_2^{(0)} \cos^2(kx) - U_1^{(0)} \cos(kx))/k_B T}}{\int e^{(-U_2^{(0)} \cos^2(kx) - U_1^{(0)} \cos(kx))/k_B T} dx}. \tag{2.59}$$

This leads to

$$O^{(1)} = \frac{\int e^{(-U_2 \cos^2(kx) - U_1 \cos(kx))/k_B T} \cos(kx) dx}{\int e^{(-U_2 \cos^2(kx) - U_1 \cos(kx))/k_B T} dx}. \tag{2.60}$$

We set $e^x \approx 1 + x$

$$O^{(1)} = \frac{\int (1 - U_2 \cos^2(kx) - U_1 \cos(kx))/k_B T \cos(kx) dx}{\int (1 - U_2 \cos^2(kx) - U_1 \cos(kx))/k_B T dx} \approx -\frac{U_1}{2k_B T}. \quad (2.61)$$

Due to the opposing sign of $O^{(1)}$ and U_1 potential minima and density maxima coincide, which is reasonable. For $O \neq 0$ the potentials $U_{1,2}$ read

$$U_2 = \frac{\hbar U_0}{2\kappa^2} \left(|s|^2 + N^2\eta^2 O^2 \right) \quad (2.62)$$

$$U_1 = -\frac{\hbar \eta}{\kappa} \left(s' + NO\eta \right). \quad (2.63)$$

Now we insert equation 2.61 into equation 2.63

$$U_1^{(1)} = -\frac{\hbar \eta}{\kappa} \left(s' - N\frac{U_1^{(0)}}{2k_B T}\eta \right) \quad (2.64)$$

$$\overset{2.58}{\rightarrow} U_1^{(1)} = -\frac{\hbar \eta}{\kappa} \left(1 + \frac{N\hbar\eta^2}{2k_B T\kappa} \right) s'. \quad (2.65)$$

One crucial factor can be seen in equation 2.58 and 2.65. The arising potential U_1 is proportional to s'. Therefore, the phase ϕ between cavity pumping field s and η has to be constant over time, i.e. $\Delta_p = 0$, otherwise the sign of U_1 will change periodically. This means the potential wells transform into hills and so forth, which is naturally suppressing the self-organization process. As long as the potentials $U_{1,2} \ll k_B T$ one can proceed with further iteration steps. However, near the self-organization threshold $U_{1,2}$ are on the order of $k_B T$, i.e. analytical treatment gets much more sophisticated. The importance of s' has already been observed in numerical simulations [33]. For $\phi = 3/4\pi$,s'=0, the self-organization process can not start, see figure 2.2. The best performance is achieved at $\phi = \pi/4$, which coincides with the maximum value of s'. This strongly indicates the usefulness of cavity pumping (seeding) for an efficient self-organization and improved particle cooling.

Although it will be required to calculate O for a wider parameter range[1], we can already gain some qualitative insight. Firstly, the phase of s has to be chosen correctly to allow self-organization. Secondly, for all other parameters fixed, the order O is suppressed by a high temperature (equation 2.61).

---

[1]especially for parameters close to the self-organization threshold
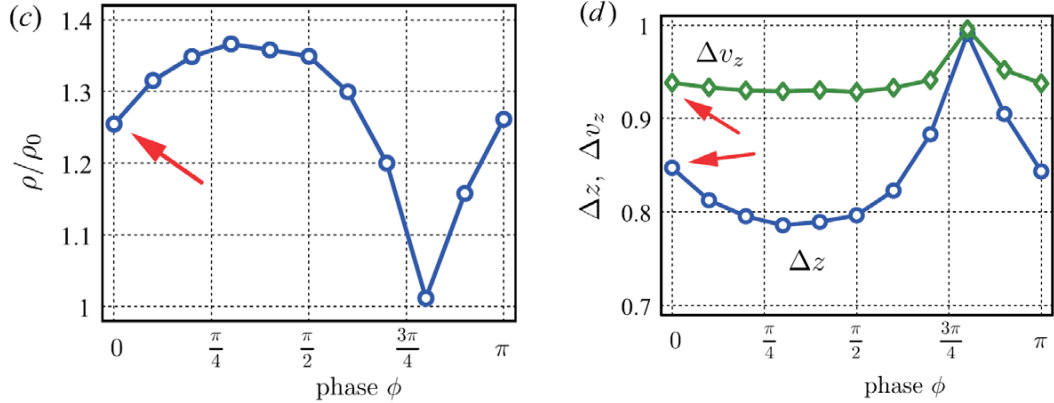
Figure 2.2: Simulations of a molecular cloud passing through a cavity waist. These graphs
were taken from [33] by *Salzburger et al.* Graph (c) shows the ratio of the phase
space densities ρ/ρ_0 as a function of the cavity pump phase ϕ. ρ is the phase
space density after passing through the cavity, while transverse and cavity pump
fields are switched on. ρ_0 denotes particle's phase space density after the passage
through the cavity without any pump fields. For $\phi = 3/4\pi$,s'=0, the phase space
density is unchanged by the pumping fields. This means that no organization
occurred. For $\phi = \pi/4$ s' is maximal, the best phase space compression is
observed. Graph (d) shows the reduction of the velocity variance Δv along the
cavity axis as a function of ϕ. Again the best reduction of the velocity variance
is achieved for $\phi = \pi/4$.

Also the case without cavity seeding ($s = 0$) can be analyzed in detail, as done
in [30, 38, 39]. In this case, U_1 vanishes for $O = 0$ and only small perturbations
with period λ remain to initiate self-organization. Such small perturbations only
grow, if the transverse pump strength η exceeds a certain threshold η^* [33].

$$\eta > \eta^* = \sqrt{\frac{(\kappa^2 + \Delta_C^2)k_B T}{2N\hbar(-\Delta_C)}} \tag{2.66}$$

In terms of the laser pump power P equation 2.66 can be written as

$$\frac{P}{\omega_0^2 \pi} > \frac{(\kappa^2 + \Delta_C^2)k_B T c}{(-\Delta_C)\omega_p} \frac{V}{N} \left(\frac{\alpha}{\epsilon_0}\right)^{-2} \tag{2.67}$$

and for $\delta = -\kappa$ this equation reads

$$\frac{P}{\omega_0^2 \pi} > \frac{\kappa k_B T c}{\omega_p} \frac{V}{N} \left(\frac{\alpha}{\epsilon_0}\right)^{-2}. \tag{2.68}$$

Therefore, this phase transition can either be observed by increasing the trans-
verse pumping power or the particle number N inside the cooling cavity above this

threshold. Above this threshold the particles are self organized and scatter the pump light in the same phase. However, achieving this transition for molecules seems to be very difficult.

2.3 Friction Force

In this section friction forces are derived to make clear, how the interaction with cavity fields can actually cool particles. Furthermore, the friction force arising in the cavity pump setup, as shown in figure 2.3, and in the transverse pump setup, figure 2.4, are compared.

In contrast to the previous section we are now including the delayed reaction of the cavity field to the particle motion, to obtain an expression for the friction force, that is exerted by the optical field in the cavity on the passing particle. The position $x(t)$ of our test particle is given by $x(t) = x_0 + v \cdot t$ and we are searching for a force whose strength grows in proportion to the particle's velocity. It will only be valid for a kinetic energy $E_{kin} \gg V$, where V is the potential generated by the light fields. First we want to derive a relation for one particle in a single mode with cavity pump field s, see figure 2.3.
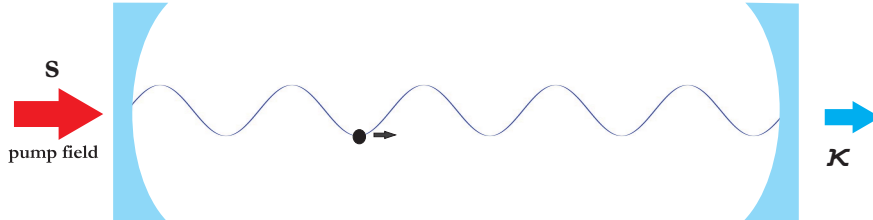
Figure 2.3: Cavity pump setup: Single particle in a cavity mode, which is pumped by the field s.

Equation (2.29) can therefore be written as

$$\dot{a} = (i\Delta_C - \kappa)a - iU_0 \cos^2(kx)a + s. \tag{2.69}$$

To obtain a velocity dependent mode amplitude $a(t)$, we expand $a(t)$ in orders of U_0. We make the following ansatz

$$a(t) = a_{ss}(1 + U_0 f(t) + O(U_0^2)). \tag{2.70}$$

Inserting 2.70 into equation 2.69 yields equations in different orders of U_0. In our experiment U_0 (mHz) typically is at least six orders of magnitude smaller than κ(1.2 MHz), η (10 kHz) , s (> 1 MHz), $k \cdot v$(MHz) and Δ_C(MHz). Therefore, we can restrict ourselves to the first order of U_0.

$$0 = (i\Delta_C - \kappa)a_{ss} + s \tag{2.71}$$

$$\dot{f}(t) = (i\Delta_C - \kappa)f(t) - i \ \cos^2(kx) \tag{2.72}$$

Again a_{ss} is the steady state amplitude similar to section 2.2.

$$a_{ss} = \frac{s}{\kappa - i\Delta_C} \tag{2.73}$$

Equation 2.72 provides a solution for f(t) and we neglect terms decaying with $e^{-\kappa t}$

$$f(t) = -\frac{1}{2(i\Delta_C - \kappa)} - \frac{(i\Delta_C - \kappa)\cos(2k(tv + x_0))}{2(4k^2v^2 + (i\Delta_C - \kappa)^2)} + \frac{2kv \ \sin(2k(tv + x_0))}{4k^2v^2 + (i\Delta_C - \kappa)^2}. \tag{2.74}$$

Now that we found an expression for the field amplitude a up to the first order of U_0, one can use equation 2.31 to calculate the forces acting on the particle. The velocity dependent part f_{fric} of the total force is

$$f_{fric} = 2\hbar k \frac{s^2 U_0^2}{\Delta_C^2 + \kappa^2} \frac{kv\kappa\Delta_C}{(\kappa^2 + (\Delta_C - 2kv)^2)(\kappa^2 + (\Delta_C + 2kv)^2)}. \tag{2.75}$$

This expression can be interpreted as a Doppler friction force, see also [40]. Due to the dependence on $\Delta_C \pm 2kv$ in the denominator one can interpret this friction force as a two photon process. Ideally, the particle scatters a photon, which is counter propagating to its velocity v, into the direction of v. This effect then reduces the particle's momentum by $2 \cdot \hbar \, k$.

In comparison to the cavity pump setup, where only the cavity mode is being pumped, we now want to derive an expression for the transverse pump case, see figure 1.6. We consider a single particle inside the cavity mode with transverse pump η and a vanishing cavity pumping s. Equation 2.29 therefore reads

$$\dot{a} = (i(\Delta_C - U_0 \ \cos^2(kx)) - \kappa)a + i\eta\cos(kx). \tag{2.76}$$
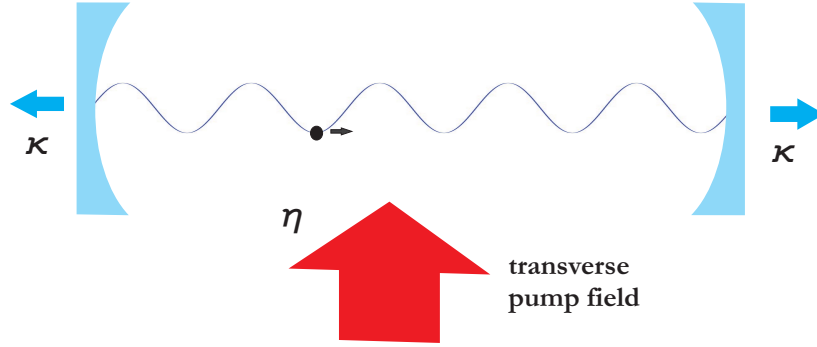
Figure 2.4: Transverse pump setup: transverse pumping field applied to a single particle in a cavity mode, which is only pumped by the particle.

Since $U_0 \ll \Delta_C$, we can neglect the term $U_0 \cos^2(kx)$. Equation 2.76 can now be solved by

$$a(t) = i\eta \frac{(\kappa - i\Delta_C)\cos(kx_0 + kvt)) + kv\sin(kx_0 + kvt)}{k^2v^2 + (\kappa - i\Delta_C)^2} + O(e^{-\kappa t}). \quad (2.77)$$

After a few cavity life times κ^{-1} the fast decaying terms $O(e^{-\kappa t})$ vanish and the photon number inside the cavity takes the value $|a|^2$

$$|a|^2 = \eta^2 \frac{\Delta_C^2 + \kappa^2 + k^2v^2}{2(\kappa^2 + (\Delta_C - kv)^2)(\kappa^2 + (\Delta_C + kv)^2)}. \quad (2.78)$$

As we will see in section 5.1, the photon number in equation 2.78 can be used to calculate the velocity of the particle by analyzing it as a function of the detuning Δ_C. From equation 2.77 we can derive a Doppler-friction force f_{fric} again

$$f_{fric} = 2\hbar k\eta^2 \frac{kv\kappa\Delta_C}{(\kappa^2 + (\Delta_C - kv)^2)(\kappa^2 + (\Delta_C + kv)^2)}. \quad (2.79)$$

In this case the particle scatters photons from the transverse pumping beam into the cavity mode dependent on its velocity v, which leads for appropriate detuning Δ_C to a cooling force. By comparing the friction forces in equation 2.75 and 2.79 one finds their different scaling behavior with the detuning Δ_C. By imposing the relation $\eta = \frac{s|U_0|}{\kappa}$, wi.e. by choosing the cavity field and the transverse pump field to be equally strong, we can directly compare the forces, see figure 2.5.

Despite increasing the detuning, the maximum friction force originating from the transverse pump, equation 2.79, stays constant and moves towards higher velocities. Therefore one can cool a particle with $k \cdot v \gg \kappa$. In the case of cavity
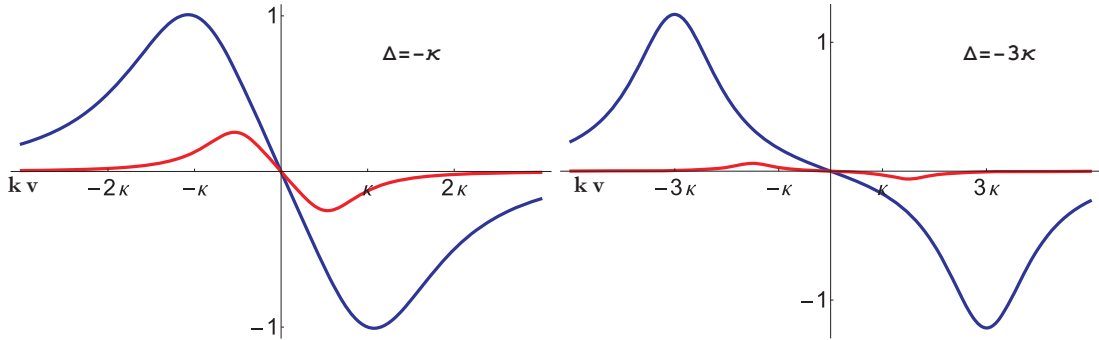
Figure 2.5: Friction force plotted against the the Doppler shift k v in units of the cavity line width κ. The red curves shows the friction force arising in the cavity pump setup, figure 2.3. The blue curve indicates the friction force in the transverse pump setup, figure 2.4. The forces are shown in arbitrary units (a.u.). The transverse pump setup offers a stronger friction force, larger capture range and superior scaling with the detuning Δ_C.

pumping, equation 2.75, the friction force decreases fast for higher detunings. At large detunings the cavity field changes only very little due to the frequency shift U_0. Additionally, the capture range, i.e. the velocity class that can be efficiently cooled, is larger for the transverse than for the cavity pump setup. Summing up the transverse pump scheme is more powerful.

As stated in the beginning these friction forces only apply to high velocities or short interaction times [2]. To analyze the dynamics of the complete system, with many modes and large particle numbers, numerical methods have to be applied. Nevertheless, with equation 2.79 we are able to estimate the friction force and the corresponding cooling effect. For a particle with velocity of $1 m/s$, a cavity line width $\kappa = 1.2$ MHz, a cavity detuning $\Delta_C = -3.36\kappa$ and a transverse pump power of $5 \cdot 10^4$ W ($\eta = 5 \cdot 10^4$) one gets a deceleration of $260 m/s^2$ per amu. However, due to the short transit times the the total velocity change amounts to only $8 \cdot 10^{-6} m/s$ for a C_{60} molecule (720 amu) arriving at the cavity with a longitudinal velocity of 20 m/s longitudinal velocity. To amplify this small friction force we need a collective enhancement s provided by superradiance (see section 2.2). This collective effect can lead to an enhancement by the factor of the particle number N, which can take values up to 10^8. Additionally we aim for an enhancement of U_0 that increases η linearly, see section 3.1.

---

[2] In the case of strong coupling ($U_0 \approx \kappa$) the derived forces also do not apply

3 Cavity Design

In this chapter we want to discuss different cavity geometries that can provide and enhance cavity cooling. A brief introduction to optical resonators[1] can be found in [41] and a detailed overview is given in [42]. An important parameter of a cavity is its line width κ, which is half width half maximum (HWHM) of the transmission spectrum $T(\omega)$ of the fundamental cavity mode. It can be written in terms of the finesse F or the cavity enhancement factor $E = F/\pi$ as

$$\kappa = \frac{\pi c}{2dF} = \frac{c}{2dE}. \tag{3.1}$$

Here, d is the cavity length and c the speed of light. All cavity cooling schemes strongly depend on κ. In the cavity pump setup [28] both the cooling times and the forces depend on κ^{-4}. The friction force in section 2.3 depends on κ^{-2}. A friction force, however can only arise if $k\, v^2$ is on the order of the line width κ, see figure or [35]. Therefore a small cavity line width κ limits the number of particles that can be cooled.

The intensity inside a cavity can be enhanced by the factor E over the input intensity. The pumping cavity should have a large enhancement factor E to provide a strong transverse pumping field. For fixed cavity length this means small κ. On the other hand κ has to be bigger than the laser line width, otherwise parts of the incident pump beam will be reflected and pump power lost. Therefore, the value of κ has to be a tradeoff between these criteria.

The cooling cavity has to be designed so that the particle-field coupling U_0 can be maximized. The parameter U_0 is proportional to the inverse mode volume V^{-1}. Therefore V should be minimized. Additionally the interaction between

---

[1]Cavity and resonator will be used interchangeably

[2]$k = 2\pi/\lambda$, v is the velocity of the particle.

the particle and the cavity fields can be enhanced by using highly degenerate modes [43]. Especially promising is the confocal cavity, which combines a high degeneracy with a large waist size [44, 45].

3.1 Cooling Cavity

As shown in section 2.1, the scattering rate into a resonator can be enhanced by utilizing a highly degenerate mode structure. In the case of proper detuning an enhanced scattering rate results in a stronger cooling force.

Near-concentric, near-confocal as well as near-planar cavities all offer highly degenerate mode frequencies. Near-concentric cavities offer the highest degeneracy. However, the near-concentric cavities have very small waist sizes (approximately diffraction limited). For a significant cooling effect a large particle number inside the mode volume is required. Therefore small waist sizes are unfavorable.

Near-planar cavities offer large waists and small degeneracy compared to the two other types. Additionally the adjustment precision is very demanding.

Confocal cavities offer good degeneracy and a satisfying waist size. Therefore this design is optimal for our cooling cavity [44, 45].

Confocal Cavity

A confocal setup is reached when the curvature of the mirrors R equals their distance d. The eigenfunctions of a resonator with finite sized mirrors can be found by applying Huygens-principle [46] [47]. Round mirrors impose cylindrical boundary conditions to the unknown eigenfunctions . Assuming the electric field to be linearly polarized and to be described by $E_0 f_{p,l}(r', \phi')$ at the surface S' of the first mirror, p and l will denote the transverse mode numbers.

By propagating every point $P'(r', \phi')$ of S' to a point $P(r, \phi)$ on the second mirror surface, one can calculate the electric field on the second mirror, see figure 3.1.

$$E(P(r, \phi)) = \int \frac{ik(1 + \cos(\theta))}{4\pi\rho} e^{-ik\rho} E_0 f_{p,l}(r', \phi') dS' \tag{3.2}$$

Here, ρ is the distance between P and P', k equals $2\pi/\lambda$. One expects the eigenfunctions to have the same field distribution on the mirrors except for a
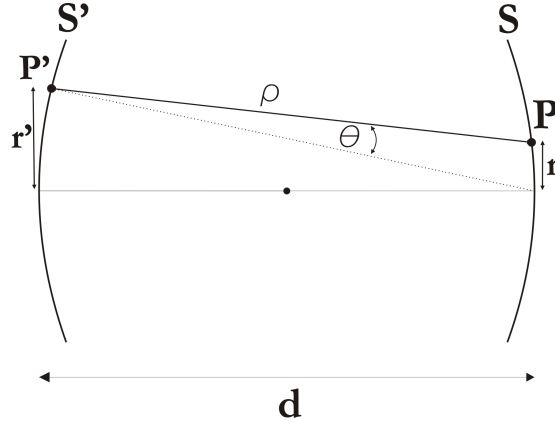
Figure 3.1: Two mirror surfaces sperated by the distance d. The field distribution at the point P on the second mirror can be obtained by propagating all points P' from the first mirror surface S' to this point P.

change in phase and amplitude which is described in 3.3.

$$\sigma_{p,l} f_{p,l}(r, \phi) = \int \frac{ik(1 + \cos(\theta))}{4\pi\rho} e^{-ik\rho} f_{p,l}(r', \phi') dS' \tag{3.3}$$

The factor $\sigma_{p,l}$ denotes the change in phase and amplitude of the field distribution function $f_{p,l}(r, \phi)$. For $\cos(\theta) \approx 1$ and $r \ll d$ equation 3.3 can be solved analytically by spheroidal wave functions for the confocal case [46,47]. With the analytic expressions for the eigenfunctions $f_{q,p,l}$ an expression for diffraction losses, due to the finite sized mirrors, can be obtained. Diffraction loss α and phase shift β of $f_{q,p,l}$ are given by [36]

$$\alpha = \frac{2\pi(8\pi N)^{2p+l+1}e^{-4\pi N}}{p!(p+l+1)!} \left[1 + O(\frac{1}{2\pi N}) \right] \tag{3.4}$$

$$\beta = (2p + l + 1)\frac{\pi}{2}. \tag{3.5}$$

Equation 3.4 shows that the diffraction loss rather depends on the mode number p than on the mode number l. A cavity mode is resonant, if the phase change after one round trip is equal to $q \cdot 2\pi$, where q is an integer. This implies that the wave vector $k_{q,p,l}$ of a confocal cavity mode has to fulfill

$$k_{q,p,l} = \frac{\pi}{d} \left(q + \frac{2p + l + 1}{2} \right), \tag{3.6}$$

where q is the longitudinal mode number. Therefore, the mode functions are characterized by the mode numbers (q, p, l).

The spheroidal wave functions can be approximated by Laguerre-Gaussian functions for $N \gg 1$ [42]. N is the Fresnel number of the resonator and is given by

$$N = \frac{a^2}{d\lambda}, \tag{3.7}$$

where a is radius of the aperture. In this case the aperture equals the size of the mirror. This parameter N also denotes the ratio between the area of the aperture and the spot size of the fundamental mode on the mirror.

Usually, Laguerre-Gaussian modes are denoted as complex functions [48]. However, in a standing-wave resonator (two mirrors) the mode functions have to vanish at the mirror surfaces. Therefore, it is convenient to utilize real mode functions, which can be written as

$$f_{q,p,l}(r, \phi, z) = c_{p,l} \; g_{p,l}(r, \phi, z) e^{-r^2/\omega(z)^2}$$
$$\times \begin{cases} \cos(k_{q,p,l}z - (2p+l+1)\tan^{-1}(\frac{z}{z_0}) + k_{q,p,l}\frac{r^2}{2R(z)}) & \text{for } q \text{ odd} \\ \sin(k_{q,p,l}z - (2p+l+1)\tan^{-1}(\frac{z}{z_0}) + k_{q,p,l}\frac{r^2}{2R(z)}) & \text{for } q \text{ even} \end{cases} \tag{3.8}$$

$$g_{p,l}(r, \phi, z) = \frac{1}{\omega(z)} \left(\frac{\sqrt{2}r}{\omega(z)} \right)^l L_p^l \left(\frac{2r^2}{\omega(z)^2} \right) \cos(l\phi) \tag{3.9}$$

$$c_{p,l} = \left(\int g_{p,l} dV \right)^{-1} \tag{3.10}$$

$$\omega(z) = \omega_0 \sqrt{1 + \frac{z^2}{z_0^2}} \tag{3.11}$$

$$R(z) = z + \frac{z_0^2}{z}, \tag{3.12}$$

where ω_0 denotes the waist of the fundamental mode and z_0 the Rayleigh range. For confocal cavity they are given by $\omega_0 = \sqrt{\lambda d/2\pi}$ and $z_0 = d/2$. L_p^l denotes the associate Laguerre polynoms. $R(z)$ is the wavefront curvature of the mode. The normalization constant $c_{p,l}$ is defined so that every mode has the mode volume [3] $V = \pi\omega_0^2 d/3$. Near the cavity center, $z = 0$, the cosine (sinus) term in equation 3.8 can be approximated by $\cos(\pi \, q/d \cdot z)$ respectively by $\sin(\pi \, q/d \cdot z)$.

---

[3] The mode volume is defined in equation 4.13

The transverse modes of higher order have a wider spatial extent, as shown in figure 3.2. This can be taken into account by introducing the waists for higher order modes [42]

$$\omega_{p,l} = \omega_0 \sqrt{2p + l + 1}. \tag{3.13}$$

In a confocal cavity many transverse modes will be resonant at the same cavity length. Therefore the effective waist, that includes all resonant modes, will be much larger than the fundamental waist ω_0. This will be beneficial for the experiment, because the particle number that is required for the collective enhancement of the cooling can be accommodated more easily in a larger waist.

For a small deviation from confocality, $d = R$, the resonance condition, equation 3.6, changes into [47]

$$\frac{2d}{\lambda} = q + \frac{2p + l + 1}{\pi}(\pi/2 - (1 - \frac{d}{R})). \tag{3.14}$$

This condition can be rewritten in terms of the frequency ν using $2d/\lambda = \nu/\nu_{FSR}$. Here, $\nu_{FSR} = c/2d$ is the free spectral range. Under perfect confocality, $d = R$. The resonance condition reads

$$\nu_{q,p,l} = \nu_{FSR}\left(q + \frac{2p + l + 1}{2}\right). \tag{3.15}$$

For small deviations from confocality the expression becomes

$$\nu_{q,p,l} = \nu_{FSR}\left(q + \frac{2p + l + 1}{\pi}(\pi/2 - (1 - \frac{d}{R}))\right). \tag{3.16}$$

It follows from equation 3.15 that the resonance frequencies occur are equally spaced by $\nu_{FSR}/2$. Therefore all the modes with mode numbers satisfying $q + p + l/2 = const.$ are degenerate. In a lossless (infinitely extended and perfectly reflective) resonator an infinite number of degenerate modes exists. On resonance the degenerate modes of a confocal cavity form a complete set of even or odd functions. This means that an arbitrary even (odd) field distribution inside the cavity is resonant, because it can be fully expanded into the eigenmodes of the resonator. Light can be efficiently coupled into the resonator without the need of matching the laser beam to the cavity modes [49]. Additionally for a confocal cavity the diffraction losses are minimal [36].

3 Cavity Design

In realistic setups the damping increases with the transverse mode number though 3.4. The degeneracy of the transverse modes is lifted for small deviations e from the confocal distance. Assuming $R = d + e$, the frequency splitting is calculated using equation (3.16). We calculate the frequency difference of the modes $\nu_{q,p,l}$ and $\nu_{q-k,p+n,l+m}$ with $-k + n + m/2 = 0$

$$\nu_{q-k,p+n,l+m} - \nu_{q,p,l} = \nu_{FSR}\left(-(n+m/2) + (\pi/2 - (1 - \frac{R+e}{R}))\frac{2n+m}{\pi}\right). \tag{3.17}$$

If one denotes $2n + m$ as maximum mode number M and equation 3.18 follows:

$$\nu_{q-k,p+n,l+m} - \nu_{q,p,l} = \Delta_m = \nu_{FSR}\frac{Me}{\pi R}. \tag{3.18}$$

This can be rewritten in terms of the line width $\delta\nu$ [4] of the fundamental mode

$$\Delta_m = \delta\nu\frac{e}{R}ME. \tag{3.19}$$

The transmission spectrum of a cavity can either be obtained by varying the applied laser frequency or by changing the displacement between the mirrors with fixed laser frequency. When varying the distance d it has to be considered that also Δ_m (3.18) is changed.

The transmission profile of a resonator mode with mirror reflectivity R [5] and round-trip loss $\gamma = 1 - \alpha$ can be calculated by [42]

$$T(\nu) = \frac{(1-R)\gamma}{(1-R\gamma)^2 + 4R\gamma\sin^2(\frac{\pi}{\nu_{FSR}}\nu)}, \tag{3.20}$$

where ν is the frequency deviance from the resonance frequency. With equation (3.4),(3.18) and (3.20) it is possible to obtain the transmission spectrum of a confocal cavity with a small deviation from the confocal distance.

In figure 3.3 the transmission of the single modes with maximum mode number M can be seen. The depicted cavity is 15 μm longer than the confocal distance.

Assuming that the incident laser field is constant over the mirror surface. The transmission spectrum of the cavity is the sum of the transmission of all modes. The number of modes K, which are exactly degenerate (e.g. (q,p=1,l=0) and

---

[4] $\delta\nu = \kappa/\pi$

[5] In the case of asymmetric reflectivies R_1 and R_2 one can write $R = \sqrt{R_1 R_2}$.

(q,p=0,l=2)), with fixed maximum mode index M is given by $K = M/2$. Therefore, this increasing degeneracy also shows up in the total transmission spectrum, see figure 3.4.

The transmission spectrum of a cavity close to confocality can be seen in figure 3.5. The asymmetry of the transmission peak gives information whether the cavity is longer or shorter than the confocal distance.

In this experiment we will vary the cavity length d. If d fulfills equation 3.14, the mode (q,p,l) is resonant inside the cavity and a transmission peak appears. The resonance condition 3.14 can be rewritten as

$$d = R\,\lambda\frac{\pi(2q + 2p + l + 1) - 2(2p + l + 1)}{2\left(2\pi R - \lambda(2p + l + 1)\right)} = \frac{\pi(2q + M + 1) - 2(M + 1)}{2\left(2\pi R - \lambda(M + 1)\right)}, \quad (3.21)$$

where M equals $2p + l$. Varying the cavity length d by $\lambda/2$ transmission peaks of the modes (q,p,l) and (q+1,p,l) appear at d and $d + \lambda/2$. Therefore, increasing the cavity length by $\lambda/2$ correspond to a frequency shift of ν_{FSR}. For $d < R$ the higher order modes appear at a larger cavity length than the fundamental mode. For $d = R$ the higher order modes are degenerate and for $d > R$ the higher order modes appear at a shorter cavity length than the fundamental mode, see figure 3.6.

To achieve exact degeneracy the fundamental mode has to be resonant at $d = R$. This implies, see equation 3.6, that $\frac{2R}{\lambda} - \frac{1}{2}$ has to be a positive integer. This condition can be fulfilled by slightly varying the wavelength λ.
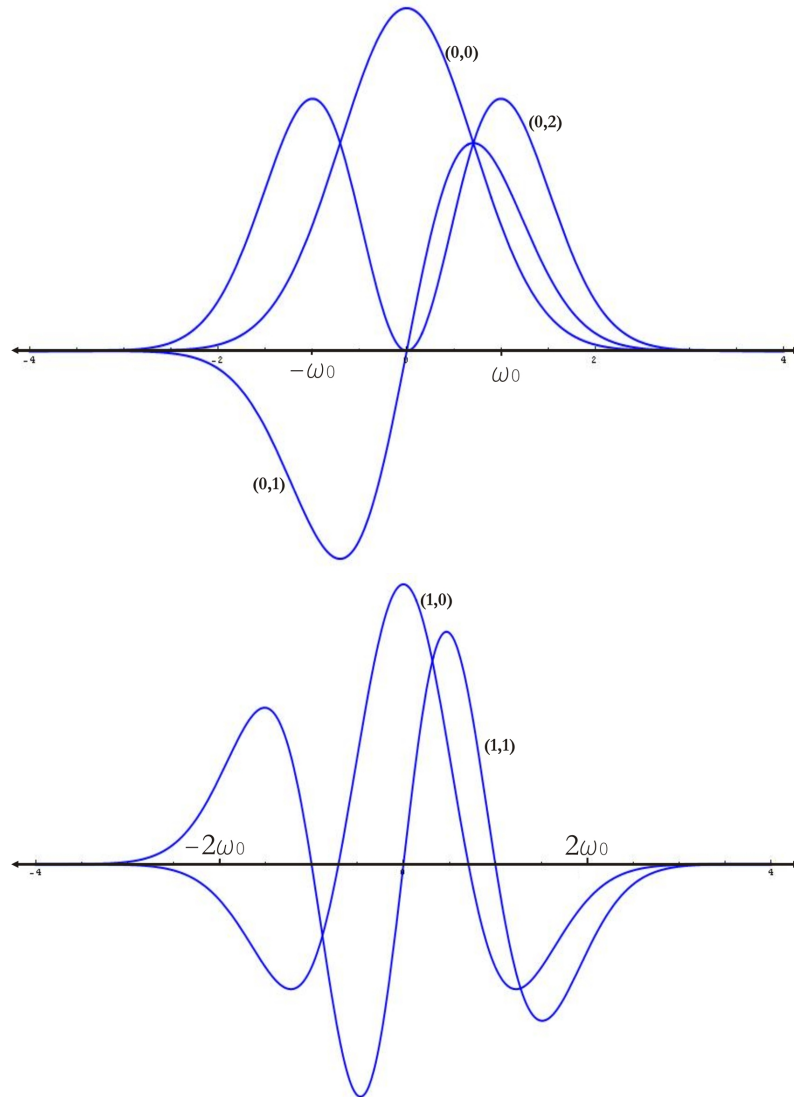
Figure 3.2: Laguerre-Gaussian modes.(p,l) denotes the transverse mode numbers. The mode functions are depicted as a function of r (distance from the cavity axis) at the cavity center for $\phi = 0$.
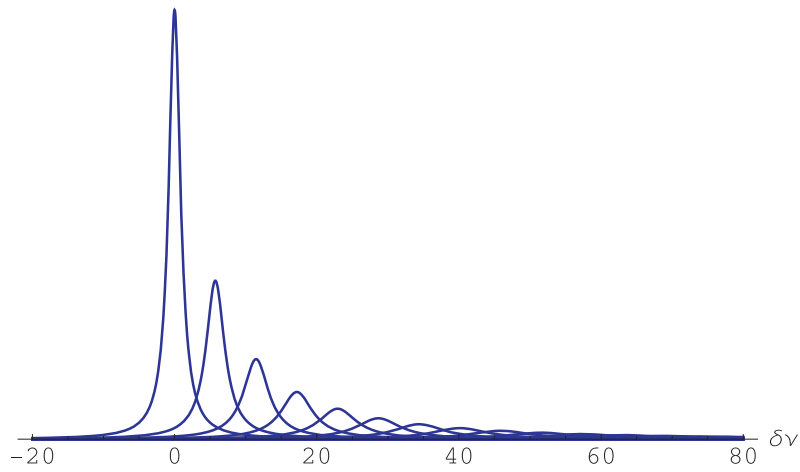
Figure 3.3: Schematic illustration of the transmission profiles of modes with increasing mode number and therefore with increased damping. The cavity deviates $+15$ μm from confocality. Unit on the x-axis is the cavity line-width $delta_\nu$.
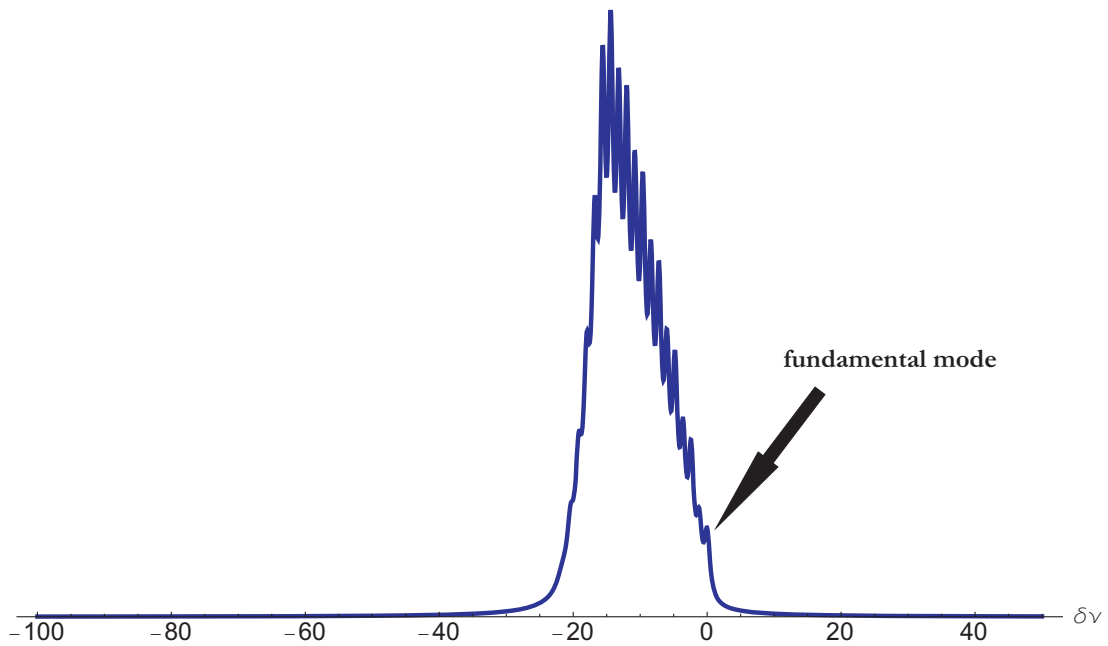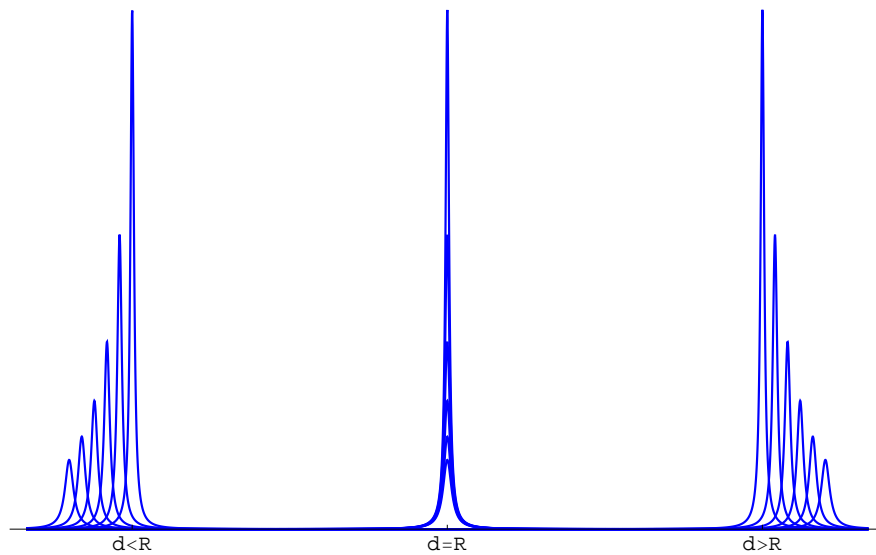

Figure 3.4: Transmission spectrum of a cavity that deviates -6 μm from confocality, $E = 5000$, $d = 25mm$ and Fresnel number $N = 5$. Due to increasing degeneracy of the transverse modes, the transmission peak of the fundamental mode is smaller than the transmission peak resulting from the higher order transverse modes.
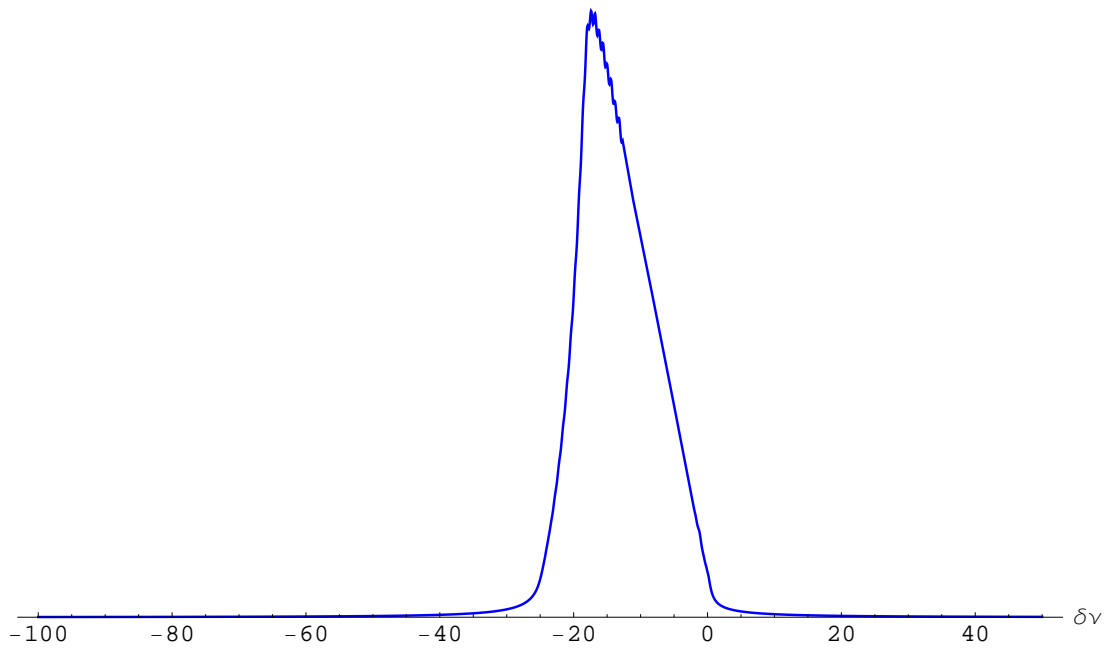
Figure 3.5: Transmission spectrum of a cavity that deviates -3 μm from confocality, $E = 5000$, $d = 25mm$. The fundamental mode is completely covered by the broader higher order modes.

Figure 3.6: Transmission spectrum as a function of the cavity length d. The large peaks denote the fundamental modes and the smaller peaks the higher order modes.

3.2 Pumping Cavity

The main purpose of the pumping cavity is to dramatically enhance the incoming laser power in order to provide a strong pumping field. To maximize the intensity in the cavity the incident laser beam has to be mode matched and the cavity has to be impedance matched. The incoming laser beam is mode matched, when the beam profile of the laser matches the beam profile of the fundamental mode, which can be achieved by several lenses. Impedance matching means to adjust the mirror reflectivities to minimize the back reflections from the input mirror. A cavity is impedance matched when the transmission through the first mirror equals the round trip scattering losses and the transmission of the second mirror [50]. In our experiments the cavities were operating in ultra high vacuum. So that scattering losses would be diminished. For two equal mirrors the intensity can be enhanced up to the cavity enhancement factor E.

$$E = \frac{1}{1-R},$$ (3.22)

where R is the mirror reflectivity.

The simplest design for the pumping cavity is a linear resonator (Fabry-Perot cavity). The alignment is rather easy. And in spite of the strong dipole forces that arise due to large field gradients along the standing wave this arrangement was chosen for the first experiments.

Ring cavity

A more advanced configuration would be a ring cavity. A ring cavity can be operated as a running wave resonator. Therefore the strong field gradients along the cavity axis would be avoided. There exists a counter propagating mode, which is degenerate in frequency. If the second mode is also populated with photons, a standing wave arises. But in contrast to the counter propagating beams in a linear cavity these counter propagating modes of a ring cavity have an arbitrary phase in respect to each other.

Contary to linear cavities the laser beam does no longer hit the mirror perpendicularly, therefore astigmatism occurs. This results in an elliptical cavity waist. The waist size in the sagittal plane is described by ω_s and in the tangential plane
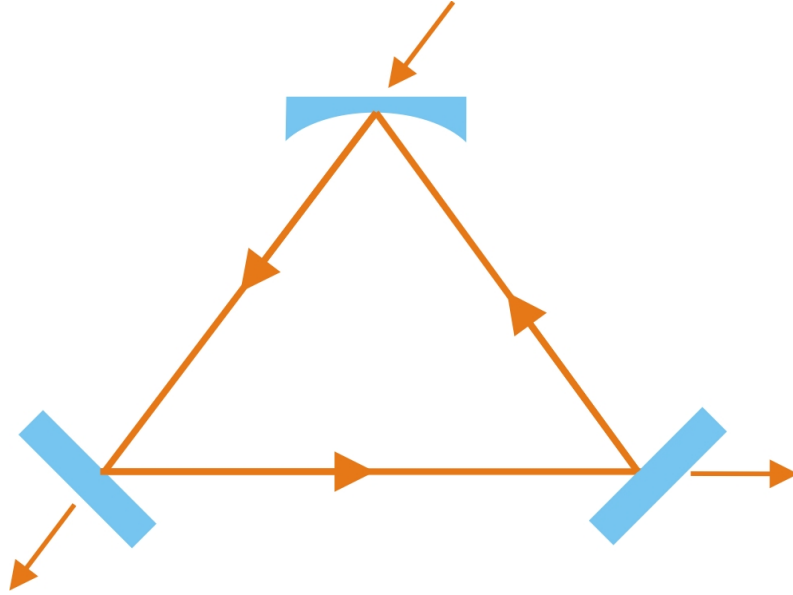
Figure 3.7: Running wave cavity

by ω_t. [6] [42]

$$\omega_t = \frac{\lambda d}{2\pi}\sqrt{\frac{2R\cos(\phi)}{d} - 1} \tag{3.23}$$

$$\omega_s = \frac{\lambda d}{2\pi}\sqrt{\frac{2R}{\cos(\phi)d} - 1}, \tag{3.24}$$

where ϕ is half the angle of the incoming and the reflected beam at the curved mirror. The different size of the waists adds complexity to mode matching, because the ordinary gauss mode of the laser has to be shaped additionally. On the other hand an elliptical waist offers the possibility to increase the overlap of the cooling and the pumping cavity mode, see figure 3.8.

cool
cavity
waist

pump cavity waist
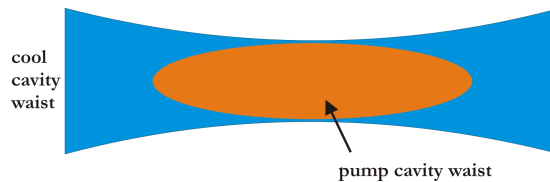
Figure 3.8: If the sagittal plane coincides with the cooling cavity axis, the overlap between pumping and cooling cavity mode can be increased.

For experiments with molecular beams, however, this seems impractical due to

---

[6]The ring cavity spans the tangential plane, which is orientated perpendicularly to the sagittal plane.
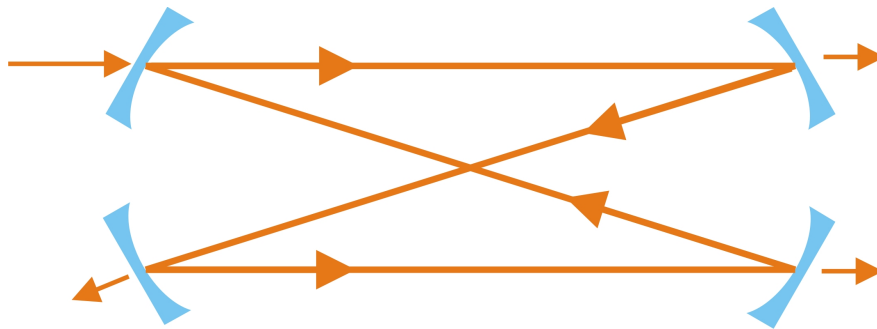
geometrical reasons. Therefore, we propose a combination of the cooling and the ring cavity, see figure 3.9.
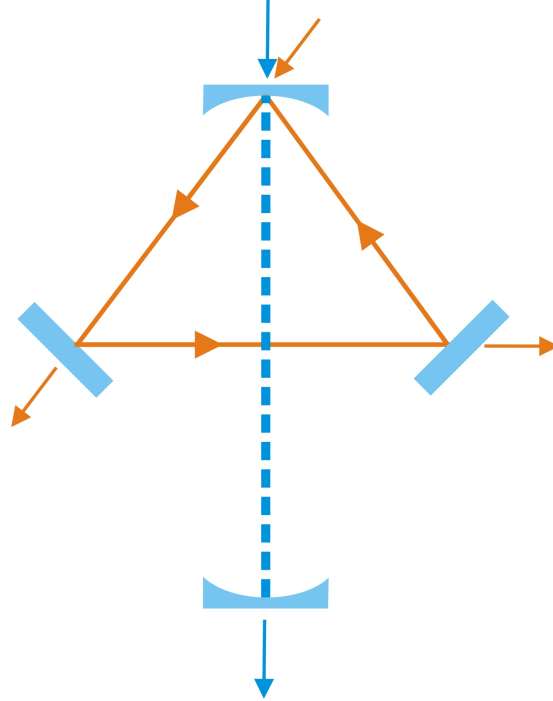
Figure 3.9: Here proposed cooling-pumping cavity. For practical reasons it is possible to combine a confocal cooling cavity and a pump ring cavity.

A more complex realization of a ring cavity is the Bow-Tie resonator, see figure 3.10.

Figure 3.10: Bow-Tie resonator

The interesting feature of this cavity design is the intersection of beams in the center. At this intersection the electric fields of the beams superpose. We assume the intersection to coincide with the cavity waist. Therefore we can approximate the electric fields of the beams to be plane waves with amplitudes E_0, which

are polarized perpendicularly to the cavity plane. The wave vector $\mathbf{k}$ of the electric field is identical for both of the beams except for an opposite sign in the y-component, see figure 3.11.

$$E_1(t, \mathbf{x}) + E_2(t, \mathbf{x}) = E_0 \left(e^{i(\omega t - k_x x - k_y y)} + e^{i(\omega t - k_x x + k_y y + \phi)} \right) \tag{3.25}$$

$$= 2E_0 e^{i(\omega t - k_x x)} e^{i\phi/2} \cos(k_y y + \phi/2) \tag{3.26}$$

Here, ϕ is a global phase difference of the beams, that can originate from unequal path lengths. Equation 3.26 shows a standing wave at the intersection in y-direction. The electric field of this standing wave has a period of $2\pi/k_y$, the intensity profile has a period of π/k_y. By choosing the angle of the beams appropriately the period results in λ or 2λ. This standing wave can be helpful when combining a Bow-Tie pumping cavity with a confocal cooling cavity, see figure 3.11.
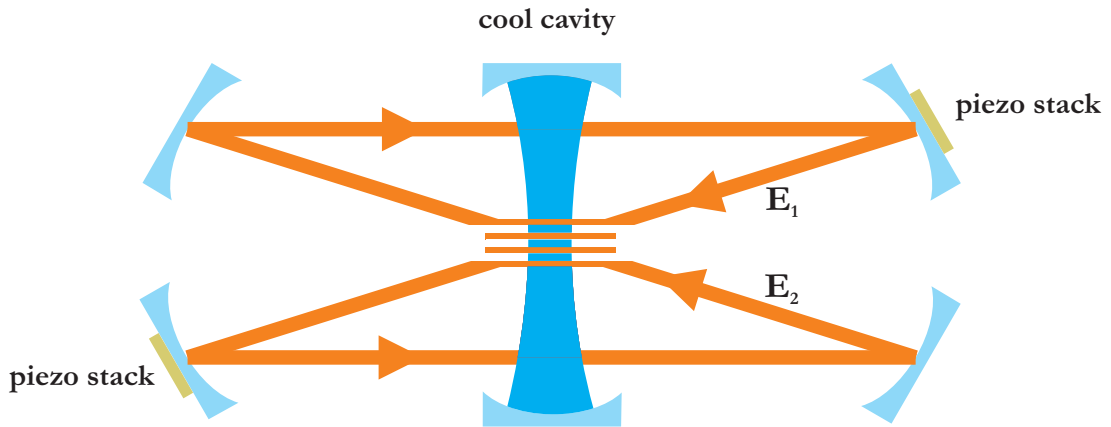
Figure 3.11: Combination of a cooling cavity and a Bow-Tie pumping cavity. In the center of the Bow-Tie cavity a standing wave arises. This standing wave can be used to assist in the cooling process due to its helpful periodicity. The piezo stacks are essential to optimize the position of the Bow-Tie standing wave in respect to the cooling cavity mode.

This setup could assist the cooling process by providing a strong potential for particles with the period lambda, see section 2.2. To optimize this desired effect

the antinodes of the standing wave from the Bow-Tie resonator have to match the antinodes of the cooling cavity mode. This can be achieved by two piezo stacks. One stack expands the cavity length and the other one compresses it. One cavity arm will become longer and the other one shorter. The cavity length remains the same but phase ϕ is changed. We will discuss this setup again later on in a separate section, where we propose longitudinal cooling of molecules.

4 Experimental setup

The experiment described in this section is designed to explore the dynamics of a molecular beam interacting with the light fields of two cavities. The molecular beam is characterized by its density and divergence,which measures the cooling of the transverse degree of freedom. The light fields of the two cavities can be analyzed by the reflected and transmitted fields.

The experiment consists of two parts, the optical and the vacuum setup. The optical setup includes feedback stabilization of the cavities, proper detuning of the cavities in respect to each other and to the laser, and optical pumping of the cavities. The vacuum setup contains a molecule source, the cavities and a molecule detector.

In our first experiments the molecule C_{60} is used. Optical properties [51], laser ionization [52] and vapor pressure [53] of C_{60} were already studied in detail. Additionally, the fullerene source is well characterized and available in our research group. At the end of the chapter we will put experimental numbers into the self-organization threshold 2.68.
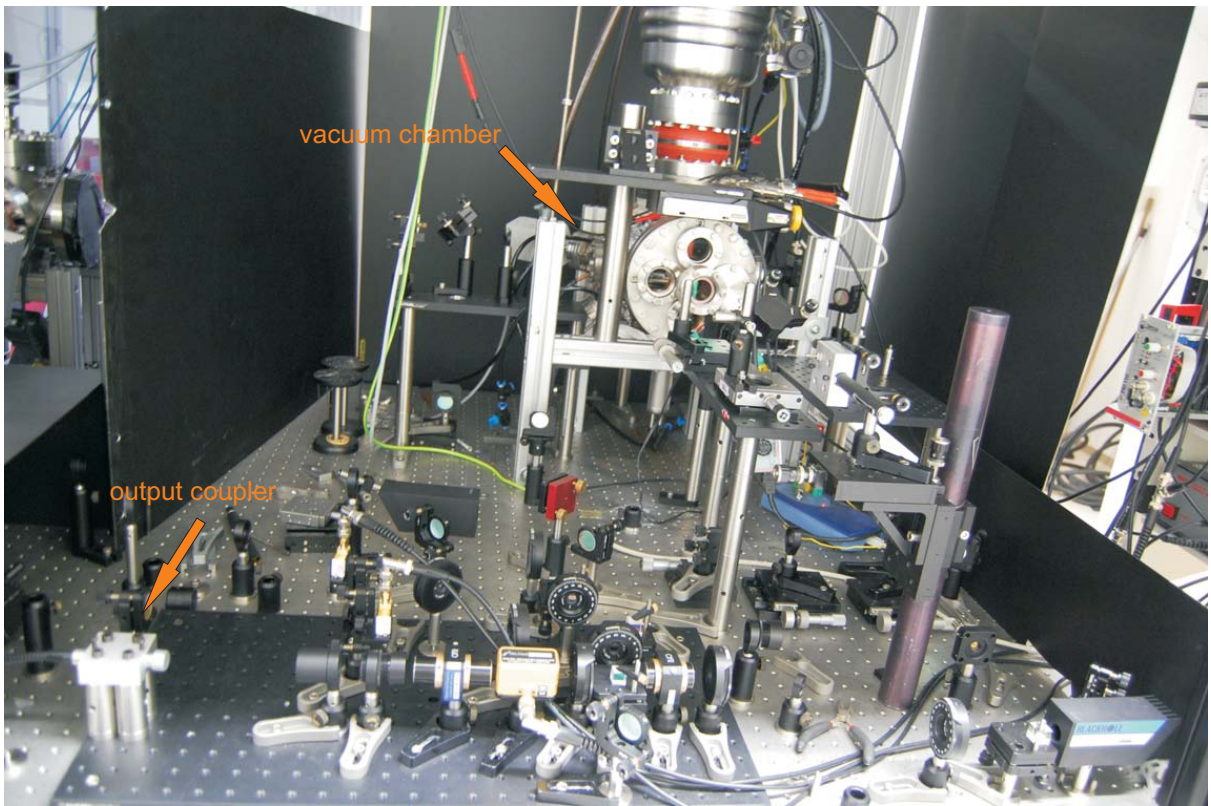
Figure 4.1: Experimental setup

4.1 Optical Setup

The optical setup is shown as a schematic drawing in figure 4.2.
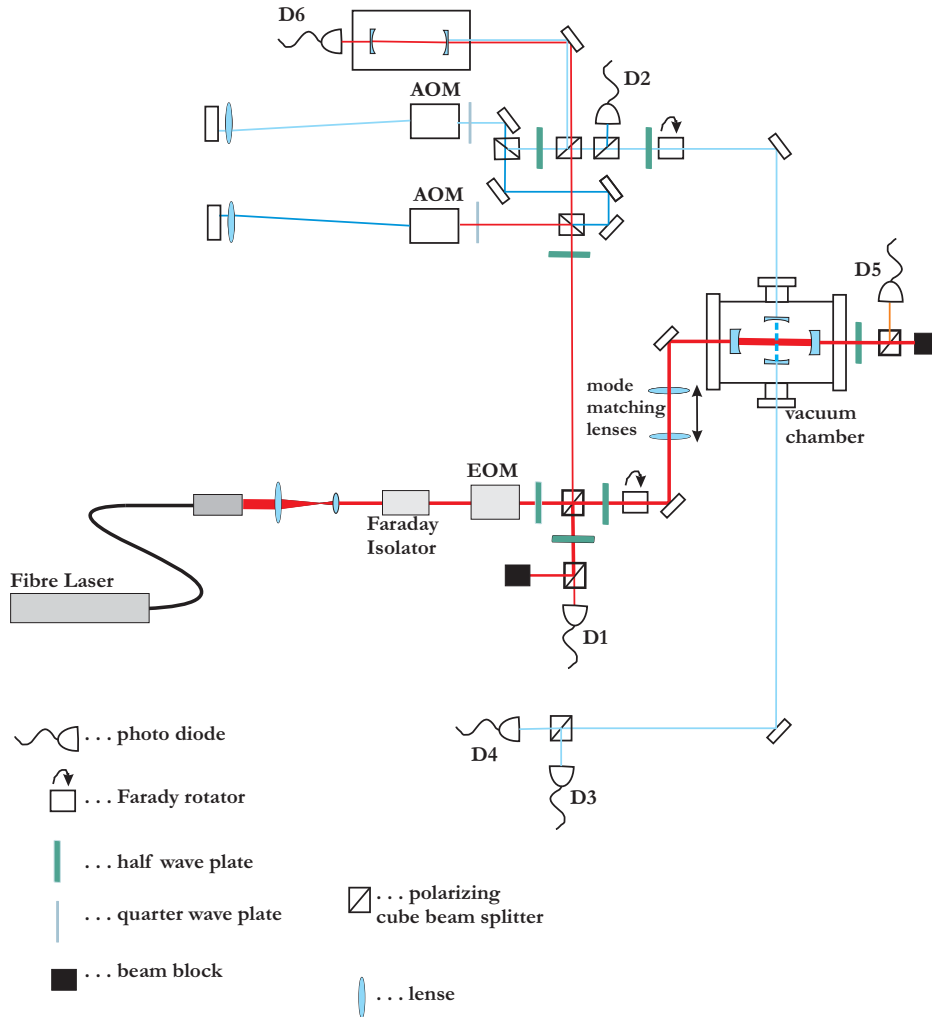
Figure 4.2: Optical setup. The cooling cavity beam, which is manipulated in the upper section, and the pumping cavity beam are applied to the cavities, which are situated in the vacuum chamber (right). In the following the details concerning this setup will be discussed.

The fiber laser employed was $ELR - 10 - 1560 - LP - SF$ from *IPG Photonics Corporation.* The laser has a wavelength of 1560 nm, 10 W cw optical power and a full width half maximum line width of 20 kHz. The output beam is a linearly polarized TEM_{00} mode with a $1/e^2$ diameter of 3.6 mm . This diameter is too large for most of the optical components in the further setup, therefore it is reduced to 800 μm in a Kepler-Type telescope.
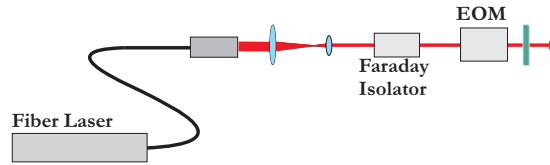

Figure 4.3

To avoid harmful back reflections into the fiber laser the telescope has to be displaced from the output coupler by several centimeters and it has to be anti-reflection coated. After collimation the beam passes through the Faraday isolator IO-5-1550-HP from *Thorlabs Gmbh.* This model endures an optical power up to 25 W. A Faraday isolator acts as an optical diode. Photons can only pass through the diode in one specified direction. This isolator protects the fiber laser from back reflections that can arise from subsequent optical components. Afterwards the beam propagates through the electro-optical phase modulator (EOM) 4063 from *New Focus Corporation.* An introduction to electro-optical effects is given in [41]. The EOM modulates the phase of the laser beam with 40 MHz. This results in frequency sidebands that are shifted by -40 MHz and +40 MHz from the initial frequency. These sidebands can be used to stabilize the cavity length to the laser frequency in a Pound-Drever-Hall (PDH) scheme [54]. The phase of the electric field leaking out of the cavity is very sensitive to the resonance condition. In the PDH scheme this strong dependence is utilized to keep the cavity on resonance.

The EOM can only modulate light with a certain direction of polarization. Therefore, the polarization of the initial light has to be adjusted accordingly.

The laser beam is split into two beams by a polarizing beam splitter (PBS) , one is applied to the cooling cavity and the other one to the pumping cavity, see figure 4.4.
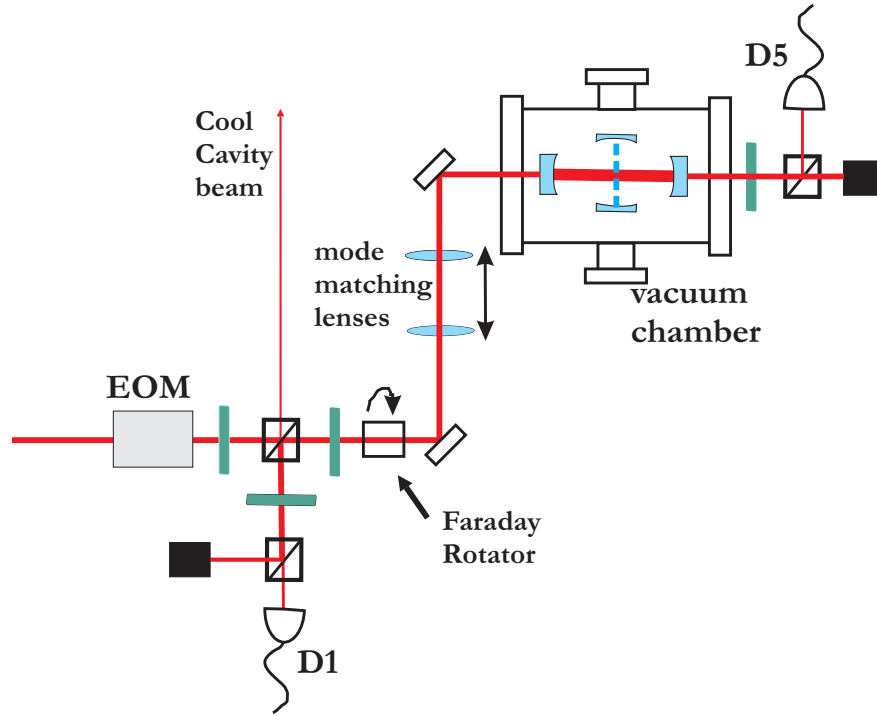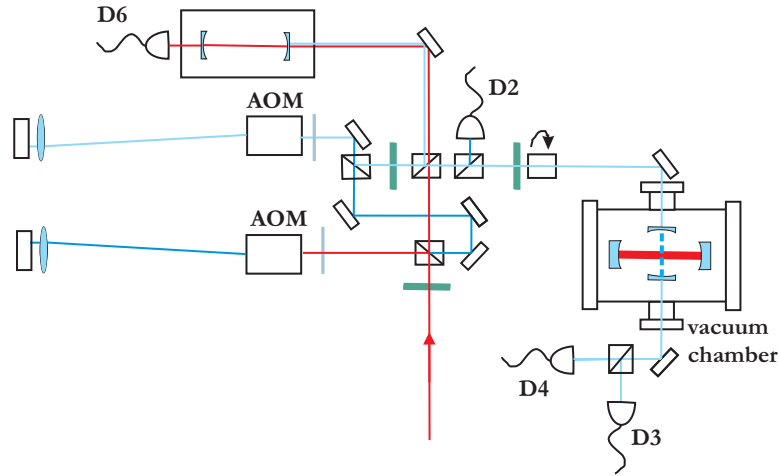
Figure 4.4: Pumping cavity beam

The polarization of the pump photons can be varied by a half wave plate. The Faraday rotator rotates the direction of polarization by 45 °. To couple into the pumping cavity efficient mode matching is required. Generally the laser beam is not resonant to any cavity mode. Therefore, the light is reflected by the cavity mirror and travels back to the PBS. The Faraday rotator rotates the direction of polarization again by 45°. The half wave plate changes the polarization by the same angle as before but now with opposite sign. As a consequence the reflected beam's polarization is now vertical after Faraday rotator. Therefore the PBS reflects the beam towards photo diode D1. The power of the reflected pump beam can be reduced by a combination of a half wave plate and another PBS to avoid damage of the photo diode.

If the pump beam is resonant with a cavity mode, light is transmitted through the cavity and detected by photo diode D5. Again the power of the transmitted beam can be reduced by combination of a half wave plate and a PBS.

One part of the cooling cavity beam is directed into an external cavity without further manipulating it, as shown in figure 4.4. The second part of the beam is sent through the acousto-optical modulator (AOM) AMF-40-5-1560 from

Figure 4.5: Cooling cavity beam. The beam is frequency shifted by two AOMs. The cooling
cavity is stabilized to this shifted beam, which results in a frequency detuning in
respect to the pumping cavity.

Brimrose Corporation. Ultrasound in the crystal generates a diffraction grating
that splits the incident beam into an unshifted and a diffracted frequency-shifted
beam [41]. The frequency of the beam is shifted by the modulation frequency
ν_m that is applied to the AOM. Additionally the beam is deflected by a certain
exit angle (25 mrad) that depends on the modulation frequency. To avoid re-
adjusting the optical setup when changing the modulation frequency, an AOM
can be operated in a double-pass configuration. After passing through the AOM
for the first time the beam is focused by a lens. The focal point of the lens
should be right in the center of the AOM. The beam is reflected by a mirror
and propagates the same way back towards the AOM. Due to the acousto-optic
effect the beam is deflected by the same angle as before and again the frequency
is changed by the modulation frequency. Summing up, after the passage through
the double-pass configuration the beam direction is inverted and the frequency is
changed to $\nu \pm 2 \cdot \nu_m$. The sign of the frequency shift can be changed by rotating
the orientation of the AOM by 180°.

Due to a quarter wave plate [1] the beam passes through the PBS towards
the second AOM. The same procedure is repeated at the second AOM. The
two AOMs have slightly different resonance frequencies 39 MHz and 40 MHz
with a bandwidth of 10MHz at 3 dB. This means the first AOM can shift the

---

[1] 2x quarter wave plate $\Longrightarrow$ half wave plate

frequency from 70 MHz up to 90 MHz with both signs. With the second AOM one can shift the light either in the same or in the opposite frequency direction. Therefore the effective light shift can take values from 0 to 22 MHz and 138 to 178 MHz. However, we can also operate only one of the AOMs in a double-pass configuration. This means one AOM will shift the frequency by $\pm 35 - 45$MHz and the other one by $\pm 68 - 88$MHz. By using only one AOM we can achieve a frequency shift of 68-88 MHz. As a result the light shift can take the values 0-22, 23-53, 68-88 and 103-133 MHz.

The frequency detuned beam can now be sent to the cavity. The beam is necessary to stabilize the cavity to the length that corresponds to the desired detuning with respect to the pumping cavity. Polarization control and detection of the reflected beam in D2 is implemented similarly to the pumping beam.

To detect the light that is scattered by the molecules one my choose the polarization of the cooling cavity beam to be perpendicular to the pump beam. The scattered light is then detected by D3 and the photons from the cooling cavity beam are then detected in D4.
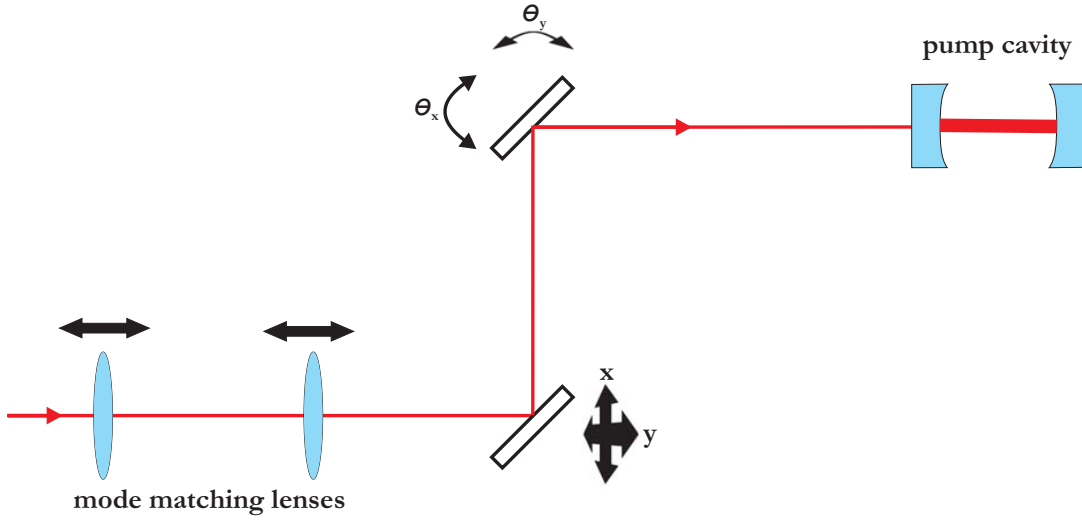
4.1.1 Mode Matching

In order To couple a laser beam efficiently into a single cavity mode, mode-matching is inevitable. This means that the shape of the laser beam has to matched to the desired cavity mode. Since we want to couple into the fundamental mode. The laser waist has to be in the centered between the mirrors and its size has to match the cavity waist, in our case 282 μm. Additionally, the laser shape has still to be Gaussian, which is not self-evident after passing through many optical elements.

We start our calculations with the waist at the end of the telescope and propagate the laser beam through several optical elements towards the cavity waist using the ABCD-law, see [41, 42],

We end up with one complex equation, which can be transformed into a set of two real equations. To solve it we need to tune two variables. Generally speaking it is more convenient to match two modes, if they are widely separated.

The simplest matching scheme consists of a single lens with fixed focal length.

Figure 4.6: Mode matching setup. To match the incoming laser beam to the cavity mode we
need two lenses, two translation stages to vary the position of the beam and a
kinematic mirror mount that changes the angle of the beam.

The two variables to be adjusted are then the distances between the lens and the
two waists. [36]. However, this scheme is highly impractical because the distance
between the initial waist and the cavity waist has to be varied and either the
laser or the vacuum chamber would have to be moved.

Therefore we use two lenses and a fixed distance between the waists. The two
variables are now the positions of the lenses between the waists. Apart from the
adequate waist in the center of the cavity mirrors the wave vector $\mathbf{k}$ of the laser
beam has to match the wave vector of the cavity mode. This means that the
incident laser beam has to be orthogonal to both curved mirror surfaces. Hence
we have to adjust the position (x and y) and the angle (θ_x and θ_y). This can be
implemented using two translation stages and one kinematic mirror mount.

It is important that the mode matching lenses can be positioned in front of the
translation stages and the mirror mount, see figure 4.6. Otherwise the alignment
of the laser beam will get very difficult.

The calculations for the positions of the two lenses are carried out in *Mathematica*.
The results are checked with a graphical beam simulation program.

We found satisfying results for two lenses with a focal length of 100 cm. The
first lens is positioned 117.6 cm and the second lens 134.5 cm displaced from the

initial waist, where the distance between the two waists is 210 cm. Each lens is mounted on a translation stage to adjust the position with μm precision.

4.1.2 Mode Structure of the Cooling Cavity

This section is dedicated to the discussion of the assembling and the mode structure of the cooling cavity. The distance of the cavity mirrors has to be exactly the confocal distance, otherwise the desired degeneracy will be destroyed.To attain the modes with maximum transverse mode number M to be displaced less than the cavity line width $\delta\nu$ from the fundamental mode, the deviation of e from confocality has to be smaller than

$$e \leq \frac{R}{ME}. \tag{4.1}$$

The expected single-mode finesse is 5000 π, the displacement and the radius of the mirrors curvature equals 25 mm. Hence equation 4.1 results in $e \leq \frac{5}{M}\mu m$.

To achieve this positioning precision the following strategy was used to setup the cavity, see figure 4.7.

The first mirror was mounted on a piezo stack. We used a HPSt $150/15 - 8/3$ from *Piezomechanik GmbH*. These piezo stacks are characterized by their high resonance frequencies (above 300 kHz) and their high stiffness (1800 N/μm). A high stiffness ensures a high resonance frequency despite the additional mass of the attached mirror. Afterwards the piezo stack was mounted on an INVAR block. INVAR is a low-thermal-expansion alloy with a linear thermal expansion coefficient of $1.5 \cdot 10^{-6}$ K^{-1} for temperatures between 20-100 °C. For a block length of 26 mm this results in 39 nm K^{-1}. The second mirror was lying loosely on a tube. The INVAR block with the first mirror attached was mounted on a translation stage. Therefore the distance between the mirrors could be varied by moving the entire INVAR block.

To measure the mirror separation we sent an unfocused laser beam with a large spot size on to the cavity. The cavity length was changed by varying the voltage across the piezo stack and the output of the cavity was monitored by a photo diode. It is a special feature of a confocal cavity that any field of arbitrary profile is resonant [2]. Deviations from confocality will lower the transmission and broaden

---

[2]At least half of it, see section 3.1
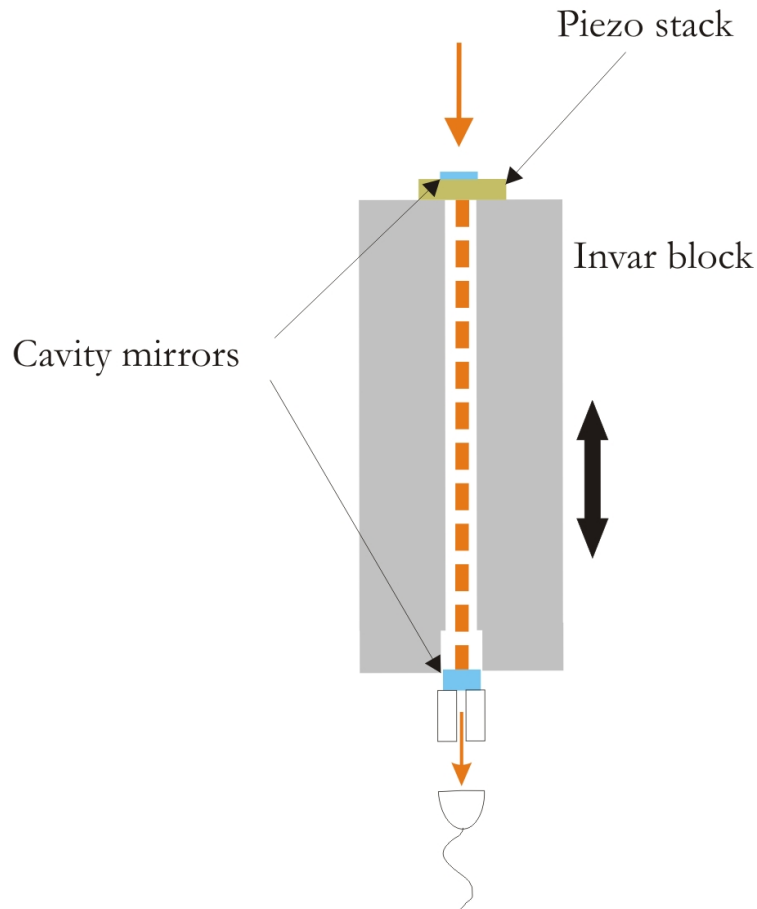
Figure 4.7: Setup for manufacturing the confocal cavity. The cavity spectrum was recorded
while adjusting the displacement of the mirrors. The red arrows indicate the
laser beams entering and leaving the cavity. The bolt black arrow indicates the
movement of the entire INVAR block.

the cavity spectrum. Therefore we changed the displacement of the mirrors until
sharp transmission peaks arise. The spectrum of the cavity, which is shorter than
the confocal distance, can be seen in figure 4.8.

The spectrum was very unstable due to the loosely lying mirror. Once the
transmission peaks were sharp and high, the second mirror was glued with a
vacuum adhesive to the INVAR block. Immediately the cavity spectrum became
very stable, see figure 4.9. By changing the voltage of the piezo stack the dis-
tance between the mirrors could be further adjusted. The effective line width of
the resonator was calculated to be 33 MHz. From the peak shape it could be
concluded that the cavity was a bit longer than the confocal distance.
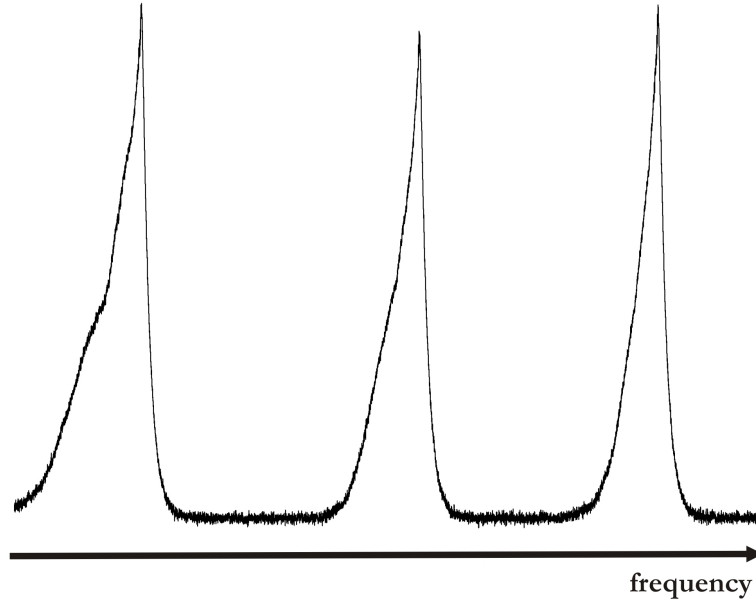
Figure 4.8: Spectrum of a near-confocal cavity. The distance between the left and the right is one free spectral range. The smaller peak in the center contains all odd modes. This transmission peak is usually smaller than the even mode peaks (left and right).

The effective cavity length is given by $d = n \cdot d_0$. At normal air pressure $n = 1 + 3 \cdot 10^{-4}$. The cavity was mounted to fulfill the condition $d = R$. In the vacuum chamber the refractive index n is equal to one. This means that in the vacuum chamber the effective cavity length equals d_0, which is 7.5 μm smaller than at air normal pressure. The transmission spectrum of the cavity can be seen in figure 4.10. The peaks are seperated by $\nu_{FSR}/2$.

We measure the frequency shift between the fundamental mode and the neighboring transverse mode. By inserting this frequency difference into equation 3.18 we can estimate the deviation from confocality. At maximum piezo voltage (maximum length) the cavity is approximately 6 μm shorter than confocality.
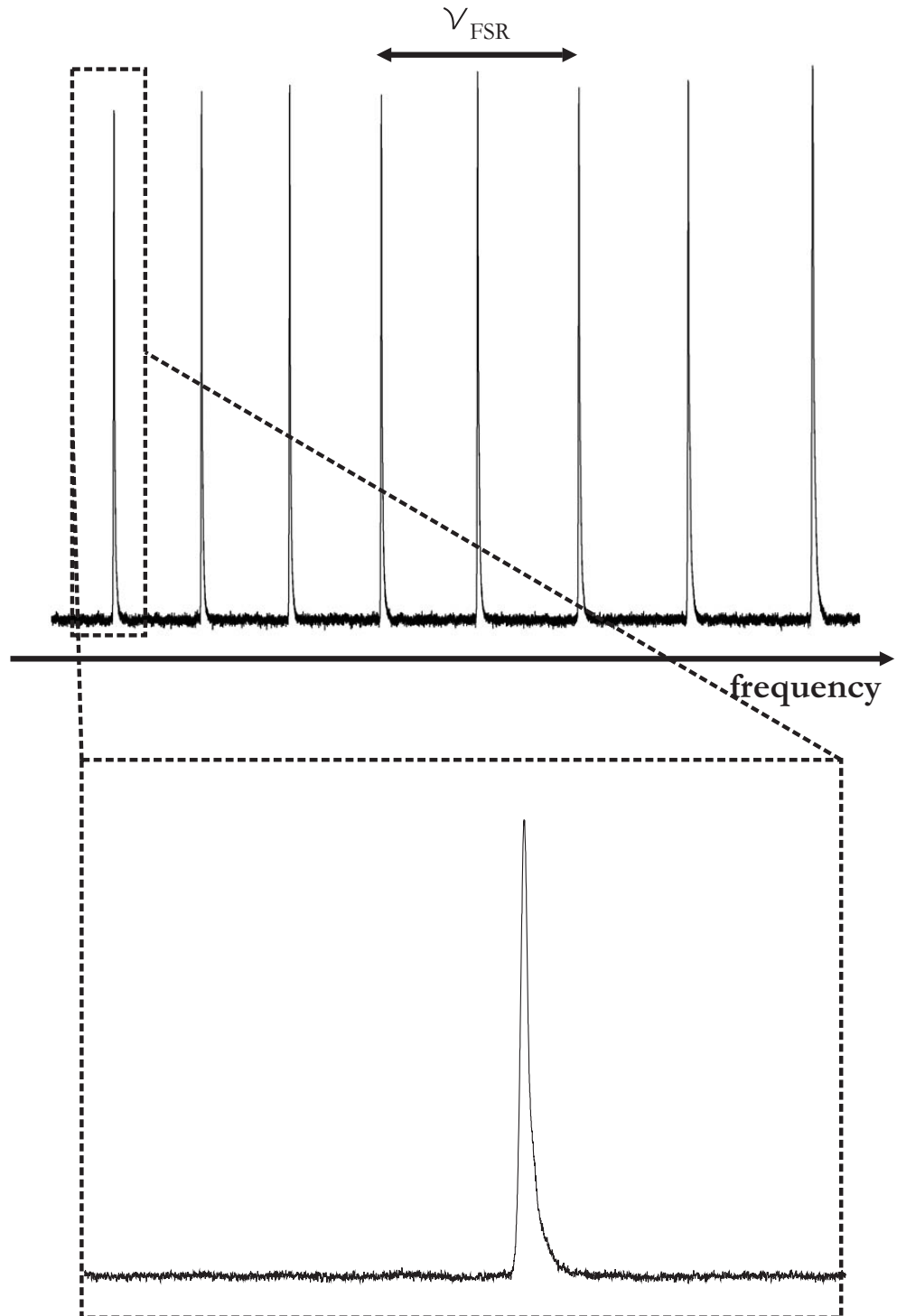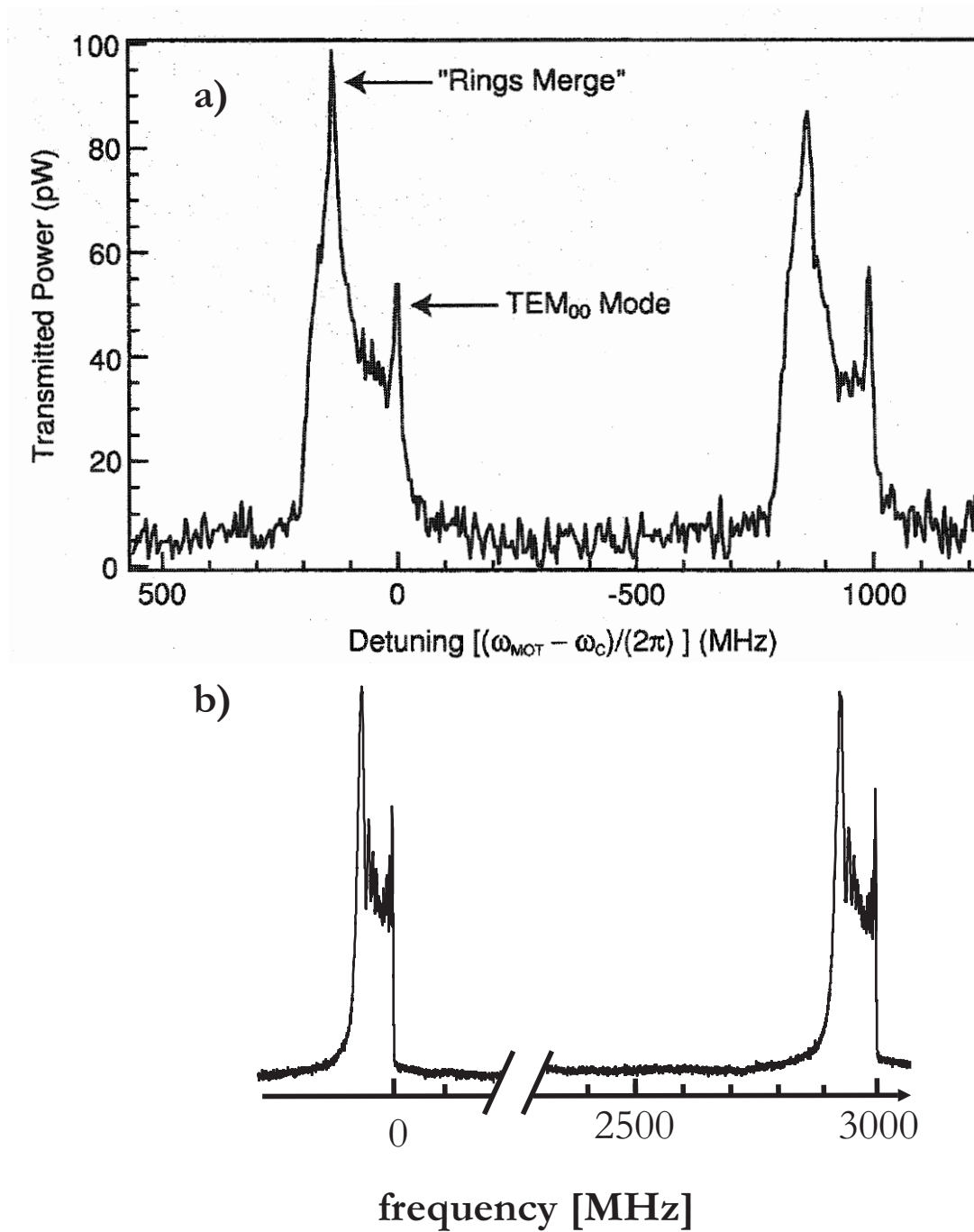
Figure 4.9: Transmission spectrum of the mounted cavity at normal pressure. $\nu_{FSR} = 6$ GHz. The peak closest to confocality is zoomed out. The line width $\delta_\nu = 33$ MHz.
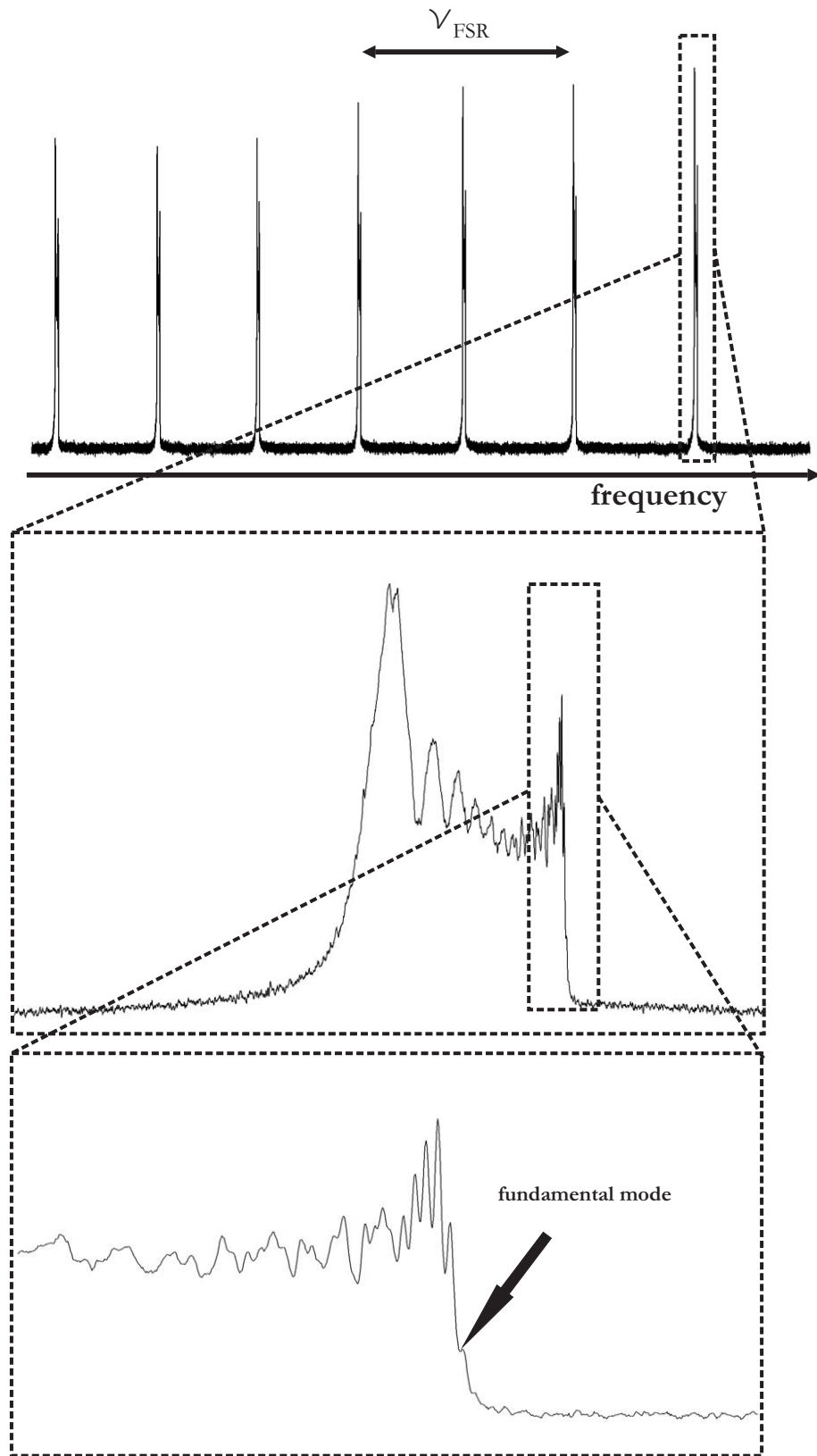
Figure 4.10: Transmission spectrum of the cavity in vacuum. The transmission peaks are three times wider than at normal pressure. $\nu_{FSR} = 6$ GHz. The peak closest to confocality (line width $\delta_\nu = 100$ MHz) is zoomed out. The lower order transverse modes including the fundamental mode are again zoomed out.

Figure 4.11: a) Transmission spectrum of a 7.5 cm long confocal cavity taken from Chan
PhD thesis 2003 [55]. This cavity has finesse of 2000 and is 28 (24) μm in
x (y) direction shorter than confocality. **b)** Transmission spectrum from our
confocal cavity, see also figure 4.10. Our cavity has a finesse of $1.9 \cdot 10^4$ and is 6
μm shorter than confocality. Both spectra look rather similar. However in our
cavity there are many more modes underneath the broad transmission peak.

4.1.3 Mode Structure of the Pumping Cavity

One pumping cavity mirror is directly mounted on the same INVAR block as the cooling cavity mirrors. The other mirror is glued to a piezo stack (the same as in 4.1.2), which is again mounted on the INVAR block, as shown in figure 4.12. The mirrors have to be mounted precisely in order to make sure the beams intersect in the center of the cavities. For a start the pumping cavity was designed with a
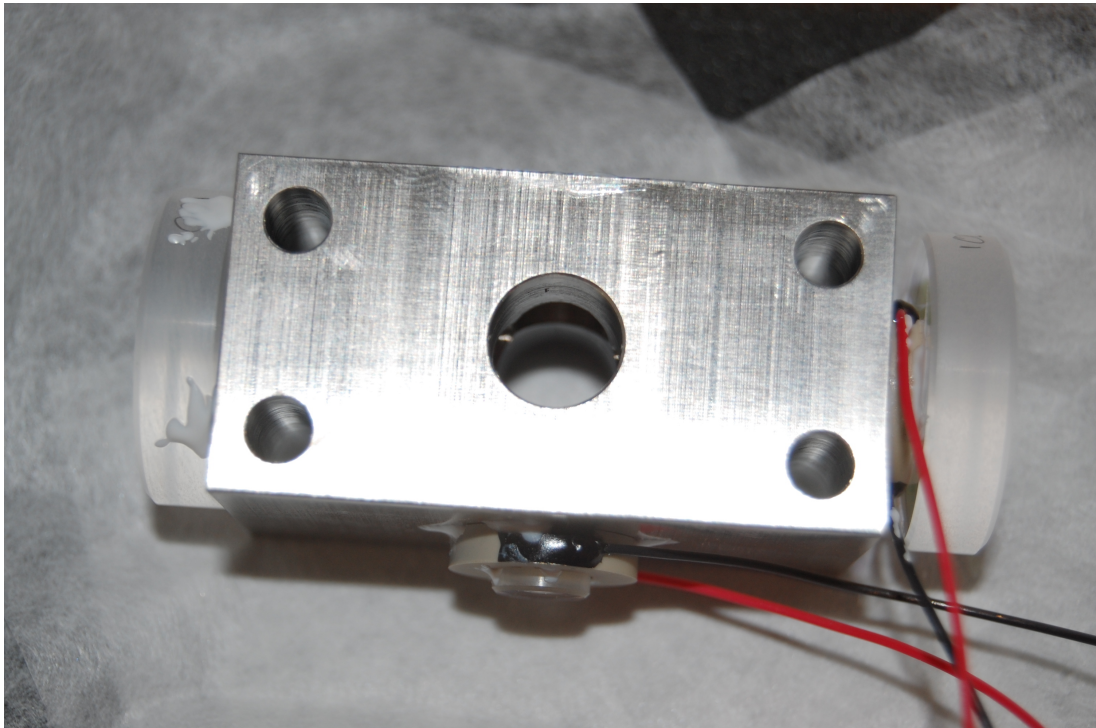

Figure 4.12: The INVAR cavity block. The pumping cavity mirrors are mounted on the long axis of the INVAR block. The cooling cavity mirrors are mounted on the short side of the block. One mirror of each cavity is glued to a piezo stack.

large waist to illuminate the bigger part of the confocal cavity's effective waist. The pumping cavity mirrors have a curvature of 1 m and are separated by 53mm. This results in a waist size of 282 μm. To observe a clean [3] spectrum one has to mode match the laser to the cavity, see section 4.1.1.

To calculate the finesse $F = \nu_{FSR}/\delta_\nu$ of our cavity one could determine the line width δ_ν with respect to the free spectral range ν_{FSR}. Another more accurate method is to measure the line width with respect to radio frequency (rf) side-

---

[3]Clean means the absence of transverse modes.
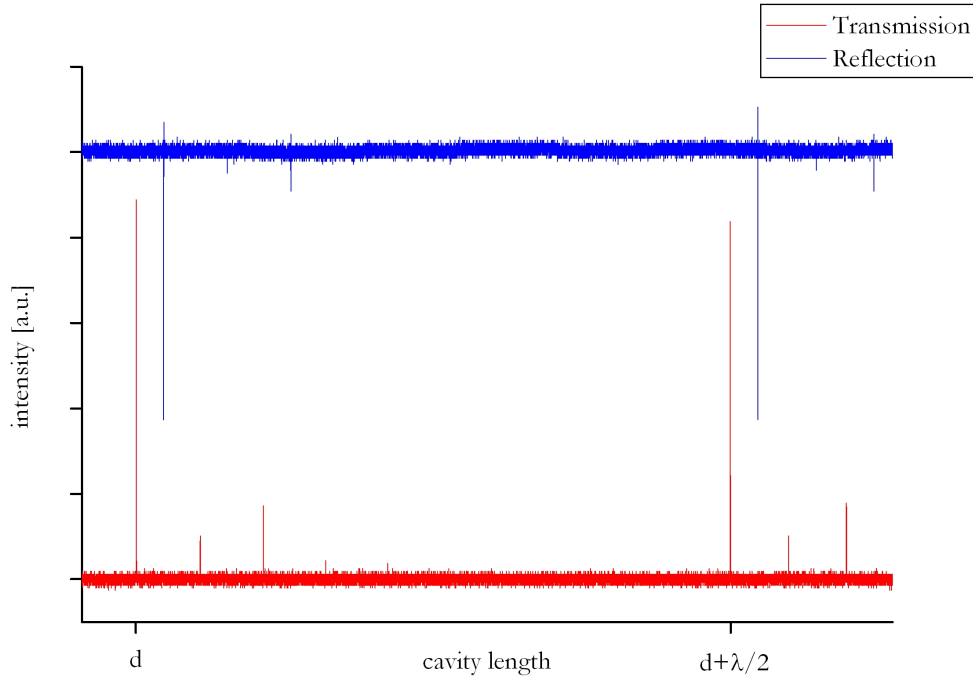
Figure 4.13: Transmission spectrum and reflection spectrum of the cavity. The cavity length
was scanned over one free spectral range ($\lambda/2$). The reflection spectrum was
shifted graphically to avoid an overlap between the fundamental mode in the
transmission and the reflection spectrum. The small peaks are low order trans-
verse modes.

bands, see section 4.1. The shift between the laser frequency and the rf sidebands
equals ± 40 MHz. This displacement acts as a frequency standard for the deter-
mination of the cavity line width, see figure 4.14.

Comparing the cavity line width $\delta\nu$ with the 40 MHz frequency standard results
in $\delta\nu = \kappa/\pi = 164$kHz. The applied laser has a line width of 20 kHz. The mea-
sured spectrum is the convolution of the laser spectrum with the cavity mode
spectrum. Therefore we have to subtract the laser line width from the measured
value. This results in the line width $\delta\nu = \kappa/\pi =$**144kHz** , a finesse $F = 1.97 \cdot 10^4$
and a cavity enhancement factor $E = 6.3 \cdot 10^3$.

In order to achieve a high intra-cavity laser power the coupling of the laser into
the cavity has to be efficient. On the one hand this implies that the cavity length
has to be stabilized to a resonance of the fundamental mode. On the other hand
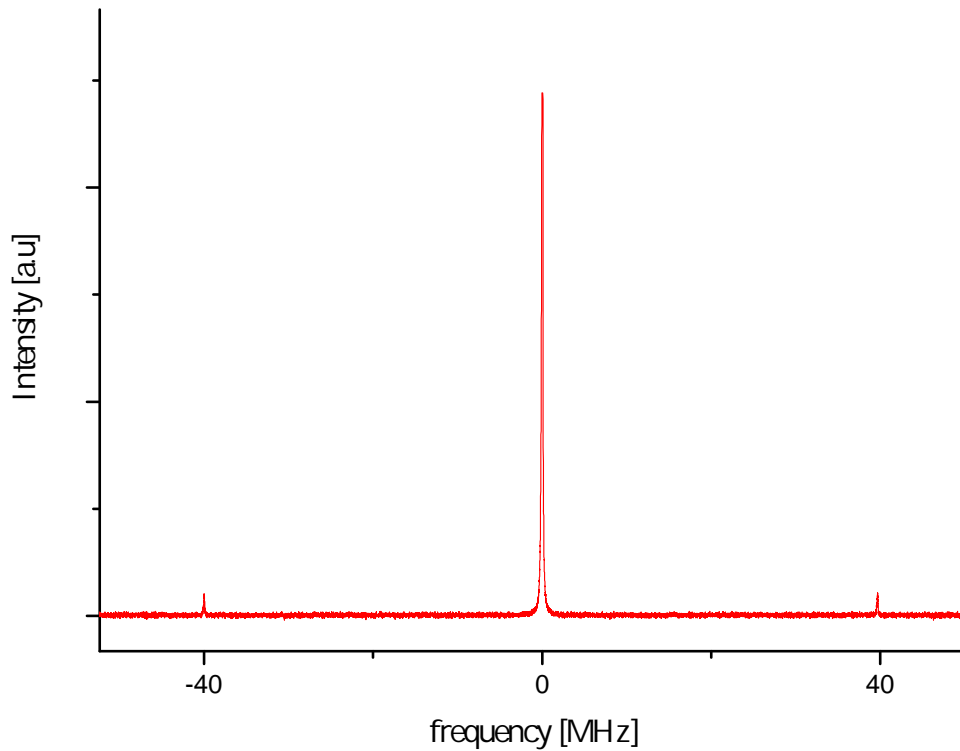
Figure 4.14: Fundamental mode of the pumping cavity with rf sidebands.

the reflection from the cavity has to be minimized. The coupling efficiency can be defined as the ratio between the reflected intensity on and off resonance. Due to the proper mode matching the coupling efficiency is already **66%**. By further opimizing the mode matching the coupling efficiency can be increased up to 90%. It has to be noted that it is not yet clear, whether the mirrors can sustain the full optical power ($5 \cdot 10^4$ W).

4.2 Vacuum Setup

The vacuum setup contains the molecule source, the cavities and the molecule detector. A schematic drawing of the setup is shown in figure 4.15
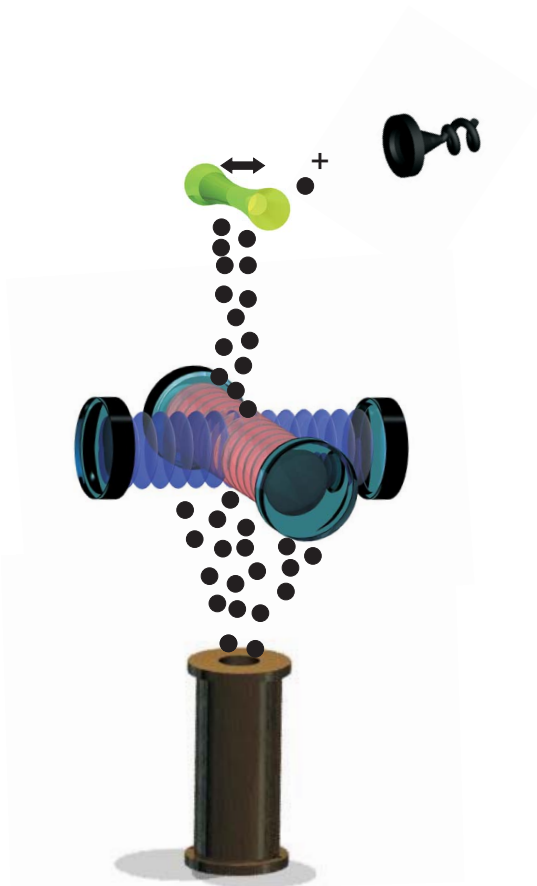
Figure 4.15: Schematic drawing of the experimental setup inside the vacuum chamber. An effusive oven emits molecules with high transverse velocities (up to 5 % of the longitudinal velocity). The particles propagate through the cavities and scatter light of the pumping cavity into the cooling cavity. In this process the transverse velocities shall be reduced, which would result in a smaller divergence angle of the molecular beam. The width of the molecular beam is measured by a scannable green ionization laser.

The particle source is an effusive oven that is heated to a certain temperature to achieve a significant vapor pressure. The molecules evaporate into the vacuum chamber [56]. The oven can be heated up to 800°C and is continuously monitored by a thermo element. To avoid oxidation, the oven should only be operated below 10^{-5} mbar.

Two problems arise when using a thermal source. Due to the high temperature of the oven the surrounding is heated with a power of typically 40 W (for temperatures near 800°C even 80 W). The heating of the chamber walls tends to degrade the vacuum. When the oven is cold the pressure inside the chamber is typically $1 \cdot 10^{-8}$mbar[4]. For temperatures beyond 600 °C the pressure rises to more than $1 \cdot 10^{-6}$mbar. The second problem is the creation of additional charges by the heating coils of the oven. Both effects spoil the detected signal to noise ratio [5]. The heating of the surroundings is predominately caused by ther-
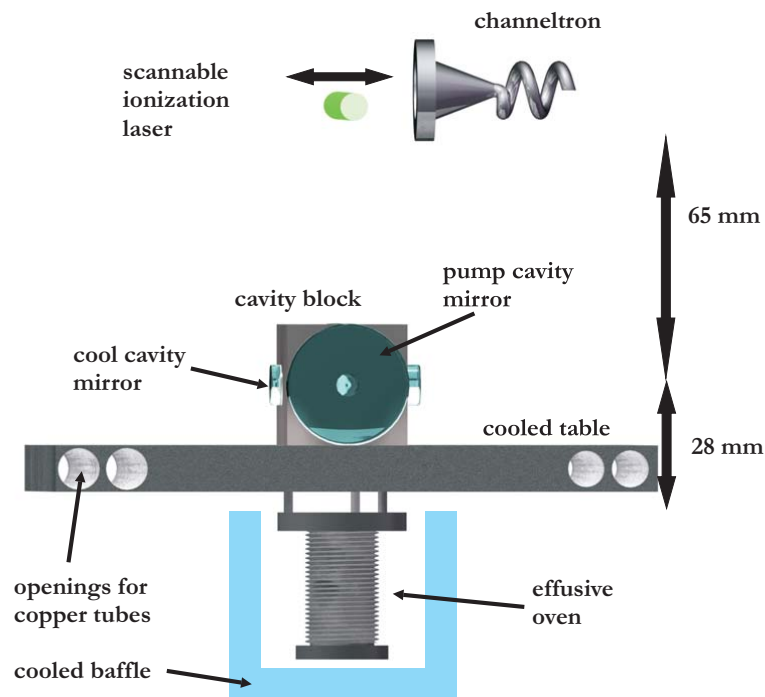
Figure 4.16: Design of the vacuum setup. The distance between oven orifice and cavity waist is 28mm, between cavity waist and channeltron 65 mm.

mal radiation. This can be shielded by a cooled baffle, which is cooled by liquid nitrogen. The cooled baffle allowed us to reduce the pressure inside the chamber again $1 \cdot 10^{-9}$mbar. Even at oven temperature of 600 °C the pressure rises only to $5 \cdot 10^{-9}$ mbar. For common operating temperatures of 630-700°C the pressure stays below $3 \cdot 10^{-8}$mbar. Thereby the heating problem can be eliminated very

---

[4] After heating the oven several times the pressure drops to $5 \cdot 10^{-9}$mbar

[5]Naturally a higher pressure also results in more collisions. However, the mean free path is under our conditions much larger than the dimensions of the experiment [57].

effectively. The oven is mounted on the same table as the cavities. To avoid temperature fluctuations of the cavity block this table is water cooled to 18°C (figure 4.16).

The cavity block is mounted on the cooled table by a clamping fork. Optical access to the cavity is given by four optical windows. The temperature of the cavity block is monitored by a thermo element. Five centimeters above the cavity block the electron multiplier (channeltron) is mounted. A green cw laser ionizes the molecules right beside the channeltron.

The laser can be scanned by about 1 cm along the axis of the cooling cavity. This suffices to measure the shape of the molecular beam after its passage through the cavity. The scanning is achieved by a computer controlled translation stage (*Micos*), which has a position accuracy of better than 1 μm. In the case of sufficient count rate the full range can be scanned very quickly, well below one second.
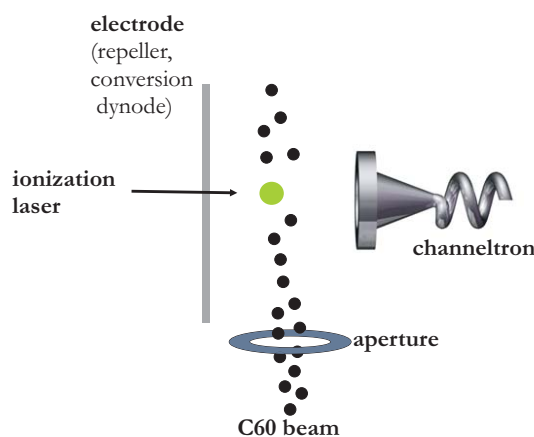
Figure 4.17: Detection scheme. The electrode is displaced by 1 cm from the channeltron. The electrode can be operated positively (repeller) or negatively charged(conversion dynode). The positively charged aperture repels free moving positive ions.

The channeltron can either be operated in the repeller or in the conversion dynode mode, see figure 4.17. In the conversion dynode mode the positive molecular ions are accelerated towards the negatively charged electrode (-5 to -10 kV). Incident molecules strike the surface and electrons are ejected. These are repelled by the dynode and accelerated towards the channeltron, where they are multiplied. When using a repeller (+5 to +10 kV) the ions are repelled towards the

channeltron, where tan electron cascade is triggered.

Using conversion dynodes yields a good ion detection probability on the one hand, but on the other hand an intolerable noise rate due to the large number of charged particles inside the vacuum chamber. The repeller mode offers only a poor ion detection probability, but the signal to noise ratio is a lot better. Therefore we utilize a repeller instead of a conversion dynode. To further improve the signal to noise ration we introduced a positively charged aperture (+3kV), which repels freely moving positive ions. However, due to the hot oven the signal to noise ratio did not exceed 1:400.

4.3 Fullerene C_{60}

The ideal molecule for the experiment should fulfill three conditions: It should have a small absorption cross-section but a high polarizability and it should form an intense molecular beam. The first test molecule is the fullerene C_{60}. The absorption spectrum of C_{60} is shown in figure 4.18. The laser wavelength is far
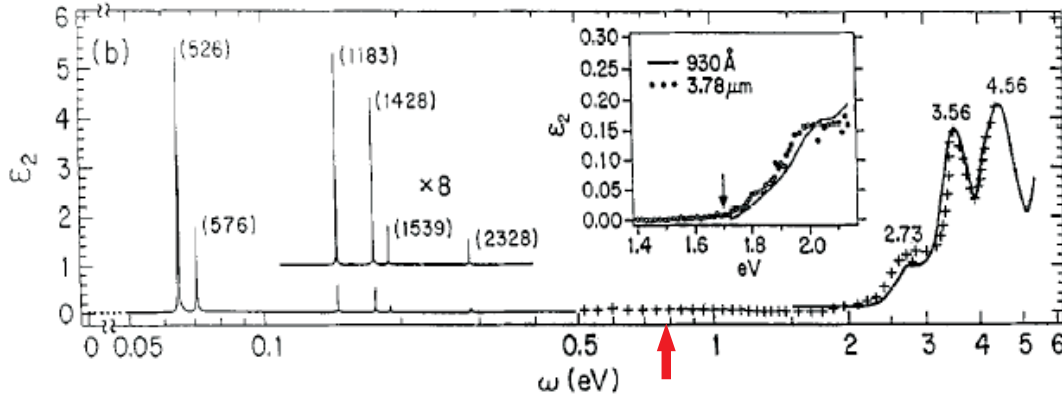
Figure 4.18: Imaginary part of the dielectric function ϵ plotted against the photon energy in eV. The graphic is taken from an article by Eklund *et al* [51]. The red arrow marks the photon energy (0.795 eV) of our fiber laser.

from any resonance. The absorption cross section of C_{60} σ_{abs} in a solvent was measured to be $6.4 \cdot 10^{-24}$ [58] for a wavelength of 1064 nm. The number of absorbed photons N_{abs} is given by

$$N_{abs} = \frac{2P}{\omega^2 \pi} \frac{\sigma_{abs}}{h\nu} \tau, \tag{4.2}$$

where τ is the mean transit time of a particle through the cavity. ν is the frequency of the utilized laser. For an optical power of 40 kW inside the pumping cavity, a waist size ω of 282 μm and an approximate absorption cross section of $\sigma_{abs} = 1 \cdot 10^{-24}$ at 1560 nm each particle would absorb about 7 photons during the transit. Both fragmentation and ionization are then very unlikely due to high mechanical stability and the thermal nature of electron emission [59]. By accelerating the ions formed in the cavity waist towards the channeltron (e.g. by applying negative voltage to the aperture) the ionization rate due to the infrared laser can be estimated.

The polarizability α at 1560 nm is slightly lower than the static polarizability due to missing vibrational contribution [51]. Measurements of thin films of C_{60}

found a static polarization of 85 $\mathring{A}^3$ and an estimated a vibrational contribution of 2 $\mathring{A}^3$, which results in a polarizability of 83 $\mathring{A}^3$ for the near infra-red region. A precise value for the static polarizability was measured to be $88.9 \pm 0.9 \pm 5.1$ $\mathring{A}^3$ [60]. Therefore a value for α of 83 $\mathring{A}^3$ at 1560 nm seems to be a conservative estimate. The polarizability α_{SI} in SI-units reads

$$\alpha_{SI} = 4\pi\epsilon_0\alpha = 4\pi\epsilon_0 \cdot 83\mathring{A}^3. \tag{4.3}$$

To calculate the molecular beam density we assume the pressure inside the oven to equal the vapor pressure of the molecules. The fraction of molecules leaving through the oven orifice is assumed to be small. The total number of particles I leaving the orifice with area σ in forward direction per second and solid angle reads [56]

$$I = \frac{n_0\bar{v}\sigma}{4\pi}, \tag{4.4}$$

where $\bar{v}$ is the mean velocity of a thermal gas at oven temperature T and n_0 is the particle density inside the oven. For an ideal gas this can be written in terms of the vapor pressure p_0 as

$$n_0 = \frac{N}{V} = \frac{p_0}{k_B T}. \tag{4.5}$$

Therefore 4.4 can be written as

$$I = \frac{\sigma p_0}{\pi\sqrt{2\pi m k_B T}} = 8.39 \cdot 10^{24} \frac{\sigma p_0}{\sqrt{M\ T}} \left[s^{-1}\ sr^{-1}\right], \tag{4.6}$$

where M is the molecular weight in atomic units (amu). The vapor pressure can be calculated from the empirical expression [53]

$$p_0 = 10^{8.28 - 9154/T}\ [kPa]\ (730 < T < 990K). \tag{4.7}$$

The big advantage of C_{60} is the possibility to detected them by laser ionization [52]. Therefore we are able to scan the molecular beam by shifting the laser beam.

Because of the small waist of the ionization laser ($15\mu m$) a high spatial resolution can be achieved along the axis of the cooling cavity. The ionization laser is a *Verdi V10* by *Coherent*. It has 10 W optical power at a wavelength of 532 nm. The absorption cross section σ_{abs} of C_{60} at this wavelength is rather low
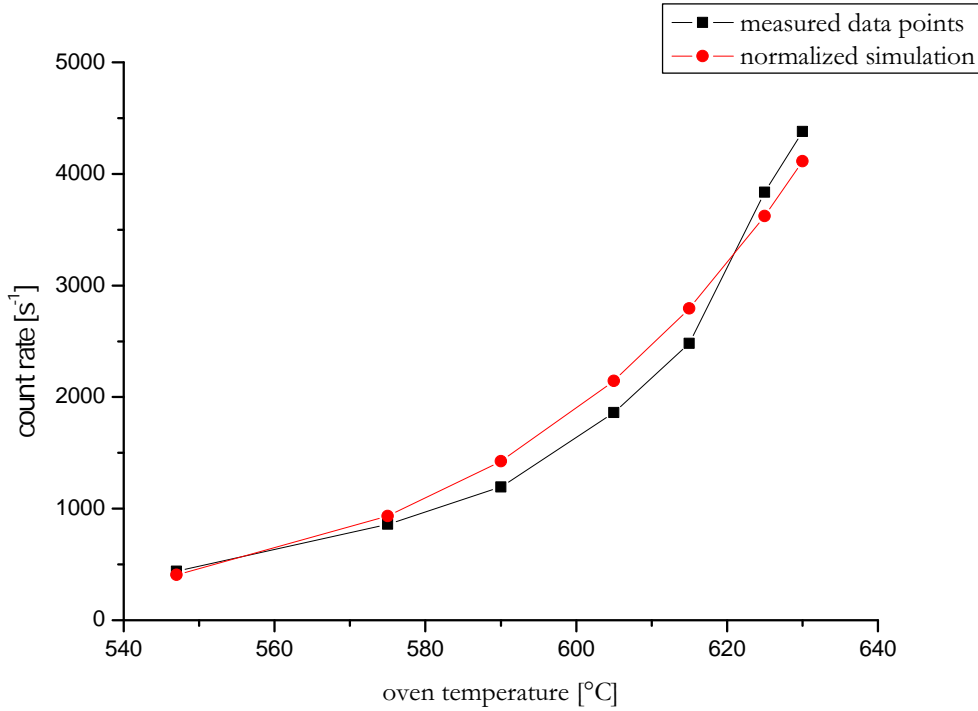
Figure 4.19: Count rate plotted against the oven temperature. The red curve was simulated by equation 4.6 and multiplied by a normalization constant.

($\sigma_{abs} = 2.89 \cdot 10^{-22}$ m^2) [58]. However, once a molecule has absorbed one photon it is very likley to undergo a transition from singlet to triplet state [61]. The absorption cross section of a molecule in a triplet state can exceed the cross section in a singlet state by one order of magnitude. This results in an uncertainty in the absorption cross section due to laser power dependency.

The ionization energy E_i of C_{60} equals $7.6eV$ [59,62]. If a C_{60} molecule absorbs a laser photon the energy is distributed rapidly over many degrees of freedom, i.e. all rotational and vibrations states. However, one can heat the molecules stepwise with several photons to high internal temperatures, where each molecule may emit an electron[6]. The mean photon number $\bar{n}$ absorbed by one molecule with velocity v can be derived from equation 4.2.

$$N_{abs} = \frac{2P}{\omega\pi} \frac{\sigma_{abs}}{\hbar\nu} \frac{1}{v}, \tag{4.8}$$

---

[6]The molecule may also emit thermal photons [63]

where the transit time τ was estimated to be ω/v. The probability to absorb n photons is given by the Poissonian photon statistics $P(\bar{n}, n) = (\bar{n}^n e^{-\bar{n}})/n!$. The probability p_i for the ionization of a molecule can be written as [52]

$$p_i(\bar{n}) = \sum_{n=0}^{\infty} P(\bar{n}, n)(1 - e^{-k_i(T_v)\tau_i}). \tag{4.9}$$

The rate constant for thermionic emission of an electron k_i is given by

$$k_i(T_v) = A_i T_v e^{-\frac{E_i}{k_B T_v}}, \tag{4.10}$$

where T_v is the intra molecular temperature. Inside the oven T_v of the molecules is equal to the oven temperature. The absorption of n photons increases the internal temperature by [59]

$$T_v[K] = 1000 + \frac{(n \cdot \hbar[eV]\omega - (7.46 - T_0[eV])}{0.01377}. \tag{4.11}$$

The absorption of n photons does not increase the temperature by $n \cdot \hbar\omega/k_B$ but
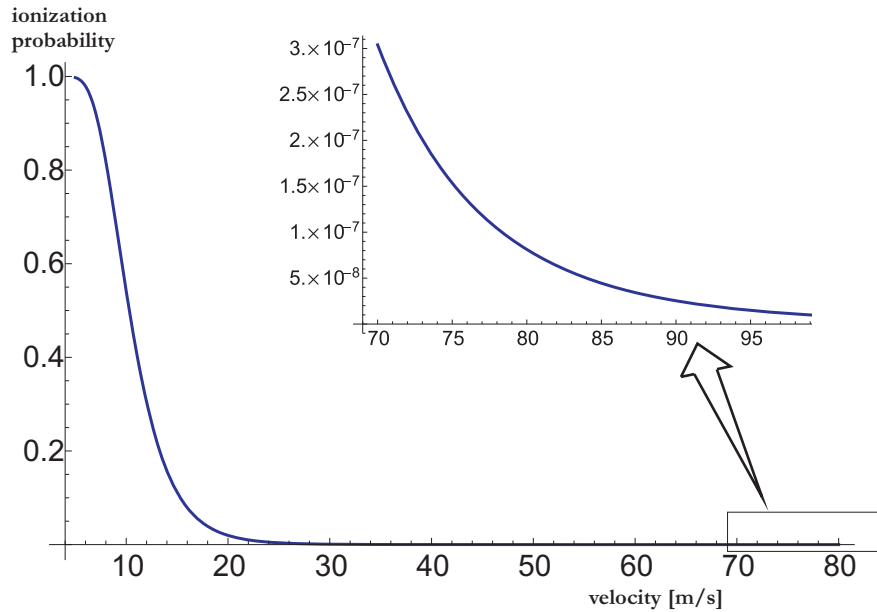
Figure 4.20: Ionization probability as a function of the particle velocity. The ionization probability drops rapidly for higher velocity due to the shorter interaction times with the ionization laser.

only by $n \cdot \frac{\hbar\omega}{k_B \, \mathbf{160}}$. This is an account of the fast energy distribution among the many degrees of freedom [64]. However, the internal temperature is still changed

by 170 K per absorbed photon. Therefore the molecule is heated until an electron is boiled off. With equations 4.10, 4.11and 4.9 we are now able to calculate the ionization probability for a C_{60} molecule with velocity v, see figure 4.20.
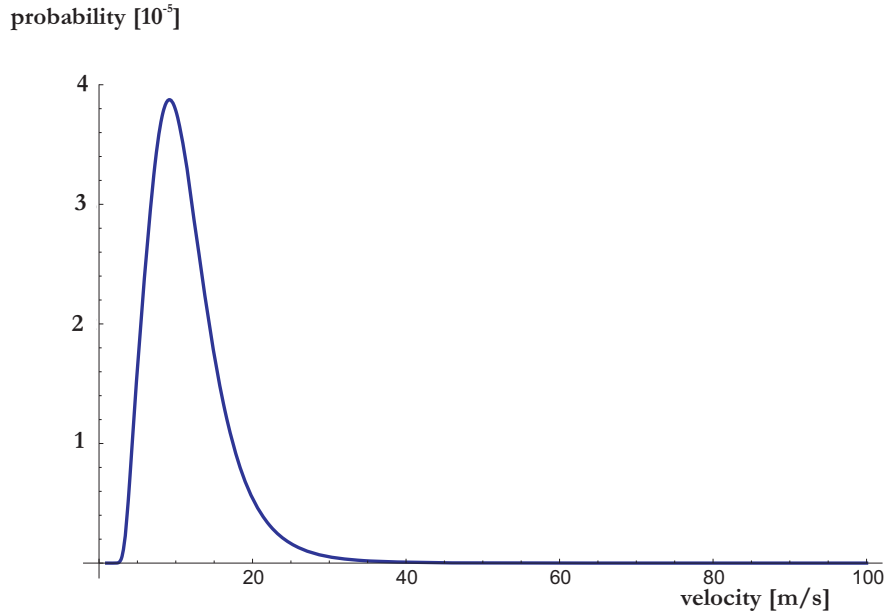
Figure 4.21: Velocity distribution of the ionized particles. By multiplying the ionization probability (figure 4.20) with the Maxwell Boltzmann distribution one gets the velocity distribution of the actually ionized particles.

The transverse cooling effect mediated by the cavities will be stronger for slow particles due to the longer interaction times with the cavity fields. Therefore it will be advisable for us to select particles with lower velocity to observe small cooling effects more easily. Fortunately our detection scheme is strongly selective towards lower velocities, see figure 4.20. Hence the velocity distribution of the ionized particles is the product of ionization probability and the Maxwell Boltzmann distribution.

Figure 4.22 shows the measured count rate in dependence of the laser power. The slowly dropping count rate at low laser power levels indicates the presence of rather slow particles of the Maxwell Boltzmann distribution. This fact is not self-evident, because slow particles are more likely to be hit from other molecules while leaving the oven. This leads to a discrimination of low velocities in a thermal beam. Additionally in the case of a long horizontal setup the very slow
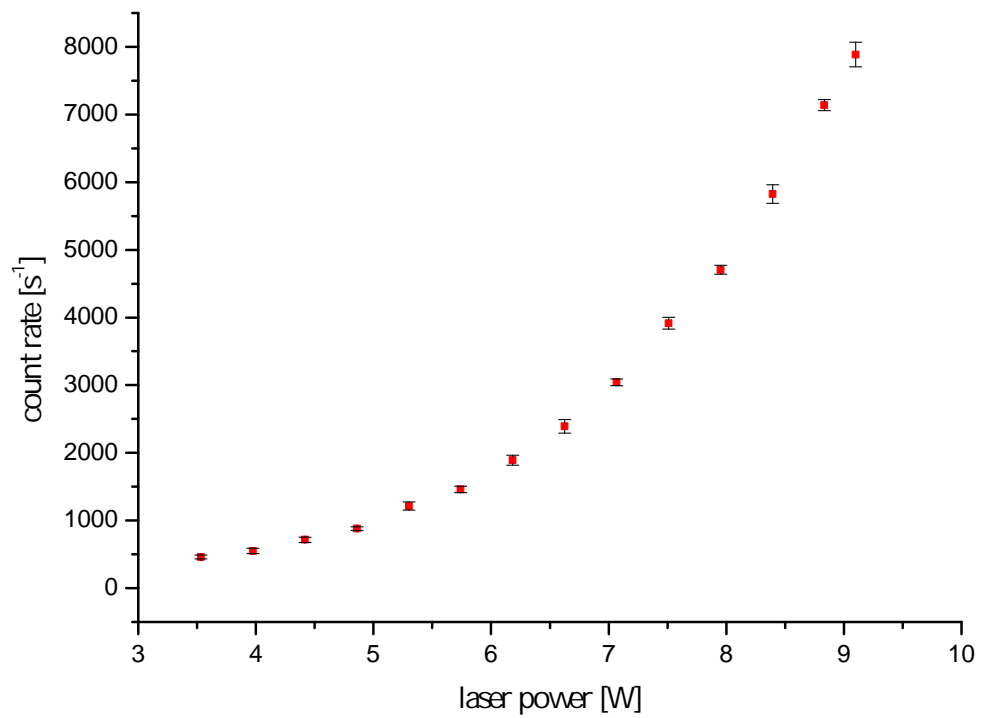
Figure 4.22: Measured count rate plotted against the ionization laser power. The black bars indicate the standard error of the data point. The curve shows the typical non-linear dependence on the laser power due to the thermal nature of ionization.

particles cannot be detected, because they drop to the ground before reaching the detector.

4.4 Self-Organization Threshold in Numbers

First we recall the self-organization threshold from section 2.2

$$\frac{P}{\omega^2 \pi} > \frac{\kappa k_B T_t c}{\omega_p} \frac{V}{N} \left(\frac{\alpha}{\epsilon_0}\right)^{-2}. \tag{4.12}$$

Now we need to adapt this equation to our experiment and to reduce the number of parameters. The mode volume V of a confocal cavity is given by

$$V = \frac{L \pi \omega_0^2}{3}, \tag{4.13}$$

where ω_0 is the waist of the confocal cavity and L the cavity length.

Furthermore we need an expression for the mean kinetic energy $k_B \cdot T_t$ in the direction of the cooling cavity axis. The maximum transverse velocity v_t can be
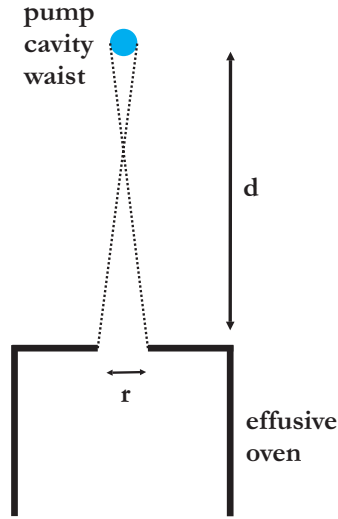
Figure 4.23

calculated by the geometry of the setup, see figure 4.23, which results in

$$v_t = v_l \frac{r + \omega \sqrt{\pi}}{2d}, \tag{4.14}$$

where v_l is the longitudinal velocity and $\omega \sqrt{\pi}$ is the effective diameter of the fundamental mode. We assume that all transverse velocities that hit the pump beam are equally probable, which is equivalent to $\cos(\theta) \approx 1$. Here, θ is the polar angle of the cavity waist for a coordinate system situated in the center of the oven. Therefore the mean square velocity (rms) $\bar{v}_t^2$ is given by

$$\bar{v}_t^2 = \frac{1}{2v_t} \int_{-v_t}^{v_t} v^2 dv = \frac{v_t^2}{3}. \tag{4.15}$$

The molecules have the same longitudinal temperature, because of the small angles. It equals the oven temperature and does not depend on the transverse temperature. Hence, the rms longitudinal velocity v_l can be expressed by the oven Temperature T

$$\bar{v}_l^2 = \frac{8k_BT}{\pi m}. \tag{4.16}$$

With the equations 4.14, 4.16 and 4.15 we are now able to write the transverse Temperature T_t in terms of the oven temperature T

$$k_BT_t = k_BT\frac{(r + \omega\sqrt{\pi})^2}{12d^2}. \tag{4.17}$$

The particle number N inside the cooling cavity mode volume V can be obtained easily by the total beam intensity, equation 4.6, times the solid angle of the cavity mode intersection. The effective intersection area of the pumping cavity mode, with waist ω, and the fundamental cooling cavity mode, with waist ω_0, equals to $\pi\omega\omega_0$. For a start the confocality of the cooling cavity is neglected. The mean transit time τ through the intersection reads

$$\tau = \sqrt{\frac{2m}{k_BT}}\tilde{\omega}, \tag{4.18}$$

where $\tilde{\omega}$ is the smaller of the two waists. Therefore $\tilde{\omega}$ equals ω_0. Hence the particle number N in the cavity intersection is given by

$$N = \frac{\sigma p_0}{\pi\sqrt{2\pi mk_BT}}\frac{\pi\omega\omega_0}{d^2}\tau. \tag{4.19}$$

Finally we insert the obtained expressions 4.13, 4.17 and 4.19 into equation 4.12

$$P_c = \frac{\sqrt{\pi}c\lambda}{144\ E}\ \omega\ \frac{(r + \omega\sqrt{\pi})^2}{r^2}\ \frac{(k_BT)^2}{p_0(T)}\ \frac{\epsilon_0^2}{\alpha^2}. \tag{4.20}$$

Now we want to minimize the critical pump power P_c. When neglecting that the cooling cavity is confocal the optimal value of ω is ω_0. The orifice radius r should be sufficiently big to minimize $\frac{(r+\omega\sqrt{\pi})^2}{r^2}$. The temperature dependence of the critical pump power is shown in figure 4.24. For our experimental setup the maximum achievable pumping power equals $5 \cdot 10^4$ W. For a temperature around 800 °C the self-organization threshold would therefore be reached.
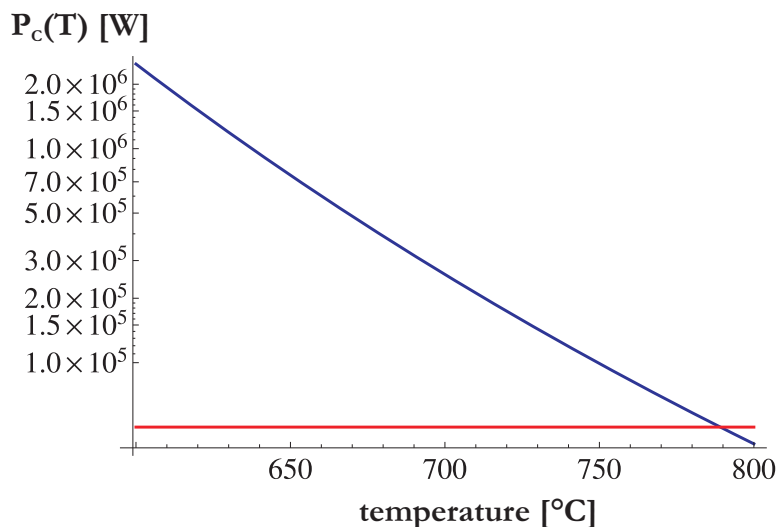
Figure 4.24: The blue curve shows the critical pump power P_c. The red curve is the available pump power inside the pumping cavity.

So far we have neglected the mode degeneracy of the confocal cooling cavity. Transverse modes of the confocal cavity have a wider spatial extent, which results in an effective waist that is about 10 times larger than the waist of the fundamental mode ω_0. Therefore the pump waist ω can be chosen larger to illuminate the bigger part of the effective cooling cavity waist. The mode degeneracy does not only results in a larger waist, but also in an enhanced coupling strength U_{eff}. Simulations in [28, 65] (cavity pump setup) observe that $U_{eff} = MU_0$, where M is the number of equal modes. Calculations in section 2.1 (transverse pump setup) suggest that $U_{eff} = \sqrt{M}U_0$. These scalings apply for the ideal case. In realistic setups the line width κ of the higher order modes increases, which leads to a reduced coupling strength. Nevertheless, every enhancement in the coupling strength U_{eff} will lower the critical pump strength P_c quadratically.

Equation 4.20 is only valid for thermal effusive beams. It seems favorable to evaporate substance at lower temperatures. A promising replacement for C_{60} would be Tryptophan, which offers a very high vapor pressure at temperatures around 300°C [66] [7]. Carbon tetrachloride CCl_4 or benzene derivates substituted with several iodine atoms appear to be even more promising [8]

Substances other than C_{60} cannot be ionized by green laser. Hence a quadrupole

---

[7]The boiling point of Trypthophan under normal pressure is 290°C

[8]Unfortunately these substances are rather unhealthy.

mass spectrometer (QMS) equipped with electron impact ionization has to be used to detect these substances. This has, however, some disadvantages. Achieving the spatial resolution of the laser beam seems to be difficult and one would have to abandon the beneficial velocity selection of laser ionization. In exchange an improved signal to noise ratio due to the mass selectivity of the detection could be achieved.

5 Outlook

Apart from transverse cavity cooling the interaction of molecules with cavities may also be utilized to detect molecules. In the next section I will present a few estimations for the detection and even for a velocity measurement of the interacting particles. This detection scheme can be realized in the current experimental setup.

Another future experiment shall implement longitudinal deceleration and cooling of molecules, which is a prerequisite if one wants to trap them. Once the particles are trapped and translationally cold, the internal degrees of freedom may be cooled by a cavity cooling scheme as well. Cooling of internal degrees of freedom will be especially important when considering quantum computation utilizing polar molecules, because the molecules have to be prepared in their rotational and vibrational (ro-vibronic) ground state.

5.1 Molecule Detection

A particle moving inside a cavity mode can have two effects on the cavity field. On the one hand it shifts the resonance frequency of the combined system by U_0. On the other hand the particle can scatter light from a transverse pumping field into the cavity mode. In principle, both effects can be used to detect a molecule. However, it seems even more favorable to combine them in a coincidence scheme. This means, if these both effects are measured both measured within a certain time interval, the particle is detected. This can be advantageous with respect to the signal to noise ratio.

The detection of single atoms with a high-finesse cavity was first observed in 1996 by *Mabuchi et al.* [67]. They observed single cesium atoms falling from MOT through the cavity. The atoms were strongly coupled ($U_0 \geq \kappa$) to the

cavity mode. Therefore the presence of the particle could shift the resonance by more than a line width. This results in a transmission drop of over 50%, which can be measured easily.

For our cooling cavity and a C_{60} molecule the frequency shift U_0 equals only $4 \cdot 10^{-3}\ Hz$, which is eight orders of magnitude smaller than the cavity line width κ. Therefore one would have to make incredible efforts to reduce all other sources of noise to be sensitive enough to detect this frequency shift.

However, one particle illuminated by our pumping cavity scatters about 30 photons per second into the fundamental mode of the cooling cavity. Again it is expected that the scattering rate into all cooling cavity modes is at least an order of magnitude higher. A particle with a longitudinal velocity of 20 m/s has a transit time through the cavities of 25 μs. Therefore one particle scatters $7.5 \cdot 10^{-3}$ photons into all cooling cavity modes. For a convenient detection efficiency we assume one scattered photon per transit will be adequate [1]. To reach one scattered photon per transit we would need a C_{60} molecule with a velocity of 1 m/s and a pumping cavity waist of 40 μm. However, we hope for even better enhancement due to the degenerate mode structure of the cooling cavity.

Molecule cavity thermometer

In section 2.3 we derived an expression for the cavity photon number in the fundamental mode for one scattering particle, see equation 2.78.

$$|a|^2 = \eta^2 \frac{\Delta_C^2 + \kappa^2 + k^2 v^2}{2(\kappa^2 + (\Delta_C - kv)^2)(\kappa^2 + (\Delta_C + kv)^2)} \tag{5.1}$$

Now one can measure the light power leaking out from one cavity mirror $|a|^2 \kappa$ while varying the detuning Δ_C, see figure 5.1.

The width or the displacement of the peaks provides us with information about the particle's velocity. The peaks are displaced from the center by $\pm k \cdot v$. For $kv < \kappa$ the two peaks merge to one broad peak. The width of this peak again can be used to determine the particle's velocity. Due to the low scattering rate single photon sensitivity would be needed to measure the scattered light as a function of detuning.

---

[1]This only holds for a light detection scheme with single photon sensitivity
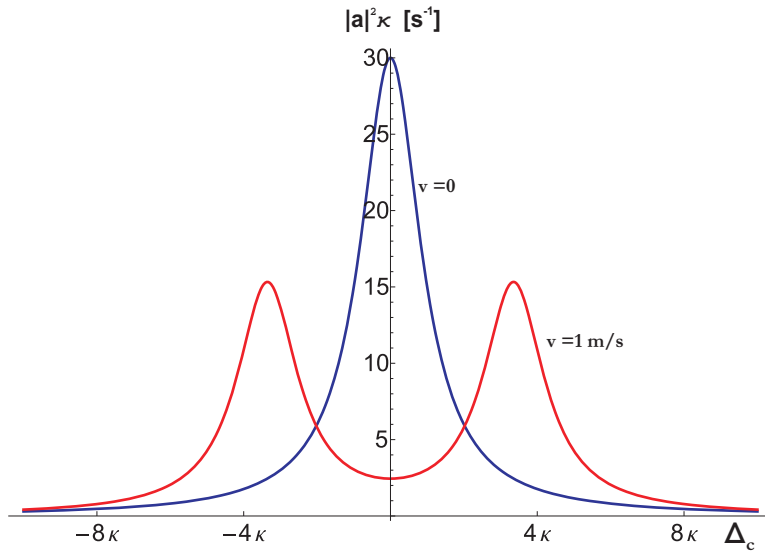
Figure 5.1: Photons emitted from the cavity as a function of the cavity deuning Δ_C for a particle velocity of zero (red curve) and 1 m/s (blue curve).

In our beam-type experiment one could measure the transverse velocity and therefore the transverse temperature of the beam. By taking into account the geometry of the setup the temperature of the oven could be determined as well. Below the self-organization threshold the cavity field can only arise due to fluctuations in the particle density. For Poissonian fluctuations this leads to to an order parameter $|O| \approx \sqrt{N}$, where N is the particle number inside the cavity mode. Summing up the N particles scatter N times the photons of a single particle [44, 45]. Figure 5.2 shows the emitted photons scattered from a molecular beam, as described in 4.4, into the fundamental cooling cavity mode.

This cavity thermometer can also be used to measure the temperature of a (thermal) cloud in a trap. Figure 5.3 shows the emission spectrum of the cavity for a thermal cloud with temperature of 10 K and 1 K.

It seems especially promising to apply the proposed methods to large metallic clusters due to their large polarizability (5 Å^3 per atom).
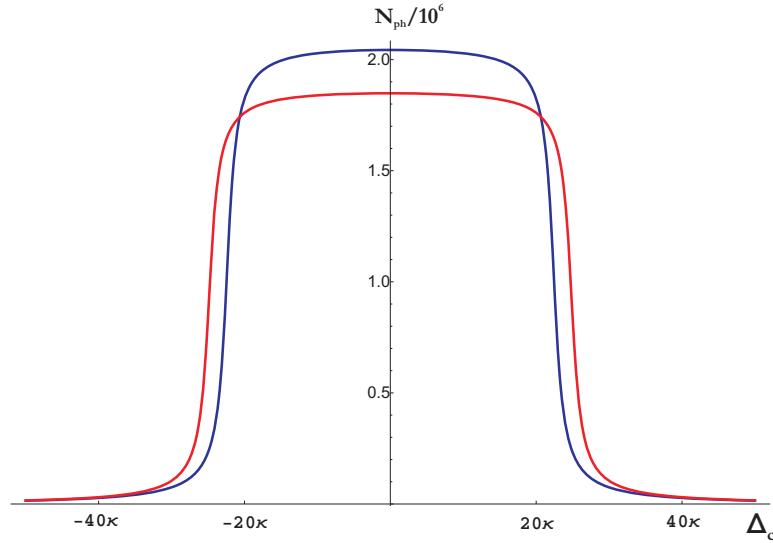
Figure 5.2: Scattered photons from a molecular beam at an oven temperature of T=600 °C (blue curve) and T=800 °C (red curve). N_{ph} denotes the number of photons emitted from the cavity. The particle number inside the cavity was set to 10^6.
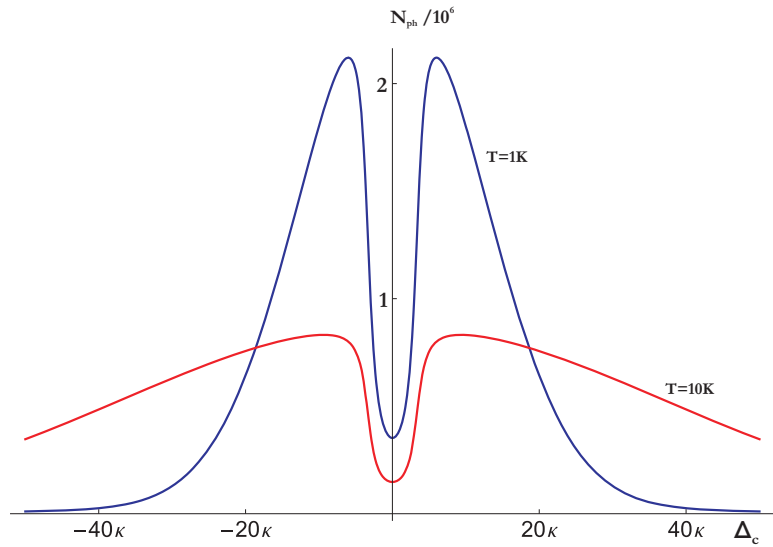
Figure 5.3: Scattered photons of a thermal cloud with temperature T=1K (blue curve) and T=10 K (red curve). N_{ph} denotes the number of photons emitted by the cavity. The particle number inside the cavity was set to 10^6.

5.2 Longitudinal Cooling of Molecules

cool cavity
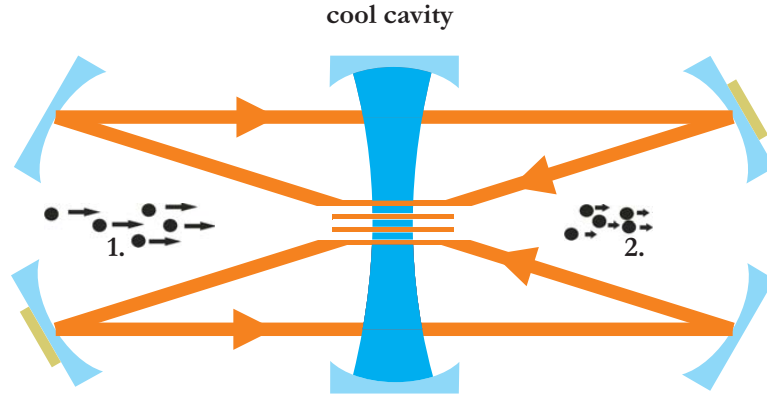
Figure 5.4: Longitudinal cooling of molecules with a Bow-Tie pumping cavity. Fast molecules enter the cavity waist (1.). They scatter photons, which originate from the pumping cavity, into the cooling cavity. Each scattered photon reduces the momentum of the particles by $\hbar k_x$. After passing through the cavity waists the molecules are decelerated and also cooled, if the laser frequency is appropriately tuned (2.).

As already mentioned in section 3.2 one could use a Bow-Tie pumping cavity to decelerate and cool the longitudinal temperature of molecules, see figure 5.4. Photons, with momentum $\hbar\mathbf{k}$ from the pumping cavity are scattered into the cooling cavity. On average the particle momentum $\mathbf{p}$ is reduced by $\hbar k_x$ for each scattered photon, see figure 5.5. Here, k_x is the vector component of $\mathbf{k}$ in the direction of $\mathbf{p}$.
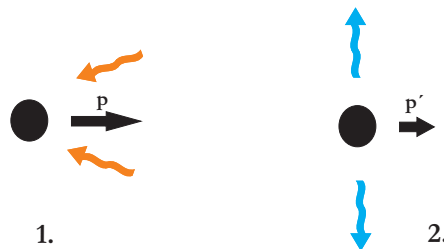
Figure 5.5: A molecule with momentum p is illuminated by photons of the pumping cavity(1.). Preferentially the molecule scatters the photons into the cooling cavity (2.). After scattering a photon the momentum p is reduced on average by $\hbar k_x$.

Every particle moving through the cavity waists will be decelerated in the longitudinal direction of the beam (cloud). By detuning the cavity to be resonant with the scattered light from the faster particles, however, the molecular beam (cloud) will also be cooled. In addition to longitudinal cooling the Bow-Tie pumping cavity offers another advantage: Due to the standing wave of the pumping field along the cooling cavity axis the self organization process can be supported with a λ-periodicity. Combining this setup with a buffer gas cell [68] seems especially promising, see figure 5.6.
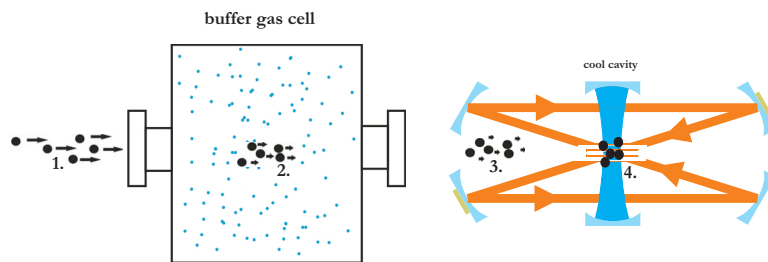
Figure 5.6: Longitudinal cavity cooling combined with a buffer gas cell. By transiting a buffer gas cell the molecules can be cooled down to below 5 K. Due to the deceleration (cooling) force mediated by the cavities a small fraction of the particles will even be trapped inside the cavity waist.

After transiting the buffer gas cell the particles will enter the cavities already at temperatures below 5 K. Due to the longitudinal cooling forces some particles will be trapped inside the cavity waist. Alternatively one can also combine the cavities with different trapping techniques, see 5.3. However, by applying longitudinal cavity cooling would be able to **continuously** load a trap. This cooling an trapping scheme would similar to the very successful techniques available for atoms. But much experimental effort still has to be invested to verify the validity of these concepts.

5.3 Trapping of Molecules

A few light molecular species with strong magnetic dipole moments can be trapped in magnetic fields. These magnetic traps are usually situated in a cryogenic buffer gas cell, which suffices for cooling the particles below the trap depth [69–71]. The advantage of this scheme is its enormous trap depth (up to 3 K). However, the lifetime of the particles inside the trap is strongly limited by inelastic collisions with the buffer gas and other molecules, which can result in untrappable states of the molecules.

Further cooling by means of evaporative cooling [11] relies on collisions. Until now the relatively large inelastic cross sections for molecules have prohibited evaporative cooling.

Polar molecules in low field seeking states (positive Stark effect) have also been trapped in a minimum of a static electric field with trap depths up to 1 K [72,73]. However, molecules in low field seeking states are at risk of inelastic collisions, which leads to untrappable states, again. Unfortunately all molecular ground states and nearly all states of large molecules are high field seekers (hfs), i.e. they seek a time-averaged maximum of the electric field. Only time dependent electric fields can yield a maximum of the field in free space, which means that only traps with varying electric fields can be utilized to trap hfs molecules and especially large molecules.

Traps for hfs can be realized by slowly varying ($\approx 1kHz$) superpositions of inhomogenous and homogenous eletric fields [74], by microwave fields [75] or by off-resonant optical light fields. The potential energy V_{tr} of a particle with polarizability α in a beam with intensity I is given by [76]

$$V_{tr} = -\frac{Re(\alpha)\ I}{2\epsilon_0 c}. \tag{5.2}$$

For a Gaussian laser beam with waist ω the intensity I is given by $I = \frac{2P}{\pi\omega^2}$. For a C_{60} molecule the trap depth V_{tr} in an antinode of our pumping cavity ($5 \cdot 10^4 W$) would be $V_{tr}/k_B = 50mK$. However, in the case of large molecules the continuous absorption of photons will reduce the trapping time severely. Naturally, by using molecules (clusters) with higher polarizabilities the trap depth can be even larger.

5.4 Cooling Internal Degrees of Freedom

The internal degrees of freedom can be cooled by collisions (buffer gas or supersonic expansion) to about 1 K [56,77]. One promising scheme to cool molecules internally and externally to ultra-cold temperatures is evaporative cooling [78,79]. As already mentioned collisions are obligatory for this scheme. Therefore this cooling methods works best for particles with large collisional cross sections that are unlikely to undergo transitions to untrappable states due to inelastic collisions.

Apart from evaporative cooling the internal degrees can also be cooled by raman transitions [2] assisted by a cavity. Cavity cooling of internal degrees of freedom was proposed in 2007 by *Morigi et al.* [81,82]. By tuning a cavity to resonance with a certain anti-stokes transition and off resonance with all stokes transitions, one ro-vibronic state can be depopulated. The molecules are pumped by photons that are far off resonant from the electronic transitions. The particle can scatter light with the same frequency (Rayleigh peak), with higher frequency (anti-Stokes lines) or with lower frequency (Stokes lines). When scattering with higher frequency than the pumping light, internal energy is removed from the particle. The energy difference between the pumping and scattered photon is given by the difference between the initial and the final ro-vibrionic state.

First, one has to tune the high finesse cavity such that one mode is resonant to the highest occupied ro-vibronic state. Then the pumping laser field is applied and the state is depopulated. Afterwards the pumping field is switched off and the cavity has to be detuned to the next transition. It is important that the laser is switched off during detuning the cavity, otherwise the Stokes lines will be enhanced unintentionally.

Raman transitions are two-photon processes, which obey the selection rule $\Delta J = 0, \pm 2$. Therefore particles with even (odd) rotational quantum number J will end up in the electronic and vibrational ground state with $J = 0$ ($J = 1$). This means, even ideally, only 50% of the molecules will end up in the absolute ground state.

---

[2]An introduction to raman transitions is given in [80]
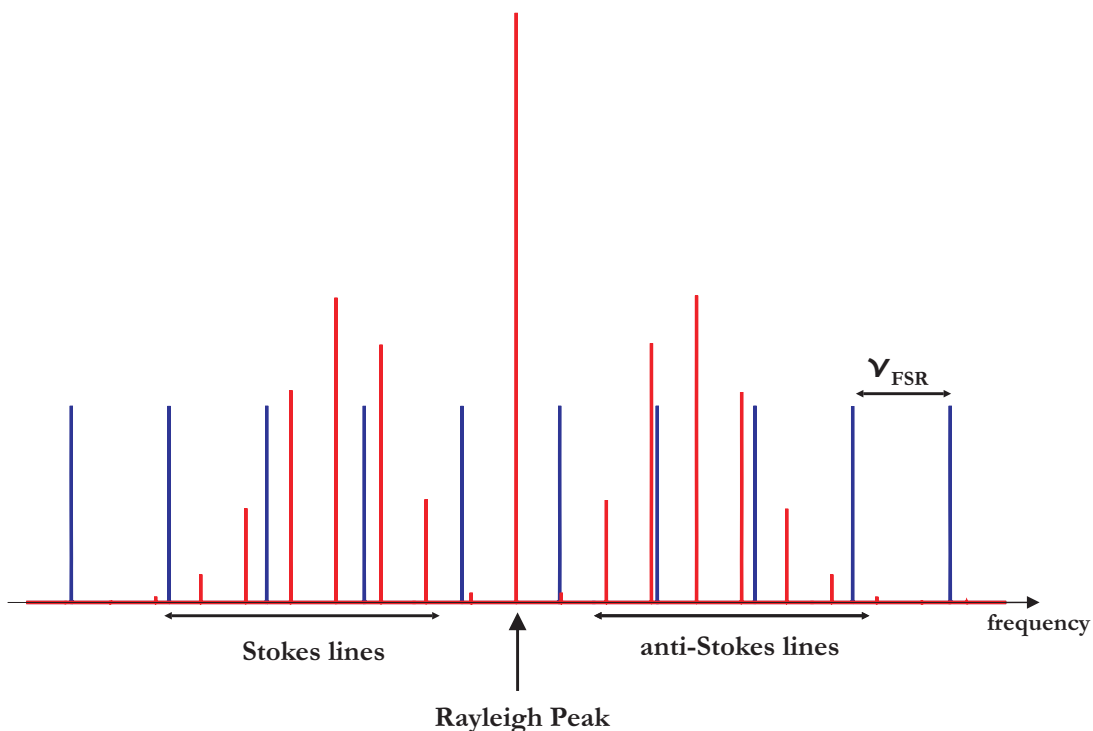
Figure 5.7: Cavity cooling of internal degrees of freedom. The blue bars indicate the longitudinal modes of the cavity spaced by ν_{FSR}. The red bars indicate frequencies of raman transitions. Stokes lines have a lower frequency and anti-Stokes lines a higher frequency than the Rayleigh peak frequency. For resting molecules the frequency of the Rayleigh peak and the pumping frequency are equal. The frequency comb formed by the cavity modes is shifted to be resonant to one anti-Stokes line.

5.5 Quantum Computation with Molecules

One of the most exciting applications of ultracold molecules would be quantum computation. Quantum computing with polar molecules was proposed by David DeMille in 2002 [83, 84]. One can use the ground state $|J = 0\rangle$ and the first excited rotational level $|J = 1, M_j = 0\rangle$ [3] to encode a qubit. In the case of a polar molecule the energy difference between the two levels depends on the external electric field E (Stark effect). For $E = 0$ the energy splitting $\hbar\omega$ equals $\hbar\omega_0$, for $E \neq 0$ $\hbar\omega = \hbar\omega_0 + D_{eff}E$. D_{eff} is the difference between the dipole moments in the two levels.

The molecules have to be trapped in an optical lattice with one molecule at

---

[3] M_j is the projection quantum number along the dipole axis
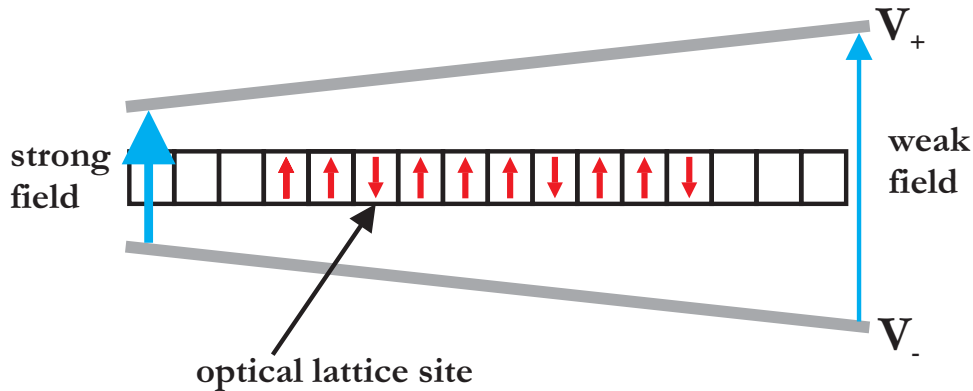
Figure 5.8: Quantum computation with polar molecules. The red arrows indicate one molecule either in the up state (ground state) or in the down state (excited state). The blue arrows indicate the electric field between charged metal plates.

each site. Additionally, one has to apply an inhomogeneous electric field with a constant gradient along the lattice axis, see figure 5.8. Therefore, each lattice site has a different energy splitting between the two states due to the linear change of the electric field. Hence one can apply single qubit rotations on one desired qubit by applying microwave photons with a frequency that fit the specific energy splitting.

The electric field at a certain lattice site consists of the strong external gradient field and also of the dipole field induced by the neighbor. Due to the different dipole moments of the two states, the energy splitting depends on the state of the neighboring molecules. Summing up one can choose to change the state of a desired molecule in dependency of the state of the neighboring particle. This suffices for quantum computation. The advantages of this quantum computation scheme are the strong dipole-dipole interaction, the long lifetimes of excited rotational states and that the transition frequencies are situated in the microwave regime.

It has to be noted that the outlined experiment is quite complex and still far away from its realization. By now various modifications of this scheme have been proposed [85–90]. However, apart from using molecules as qubits one can also think of using them for higher dimensional quidits states, which would be an obvious step to utilize the rich internal structure of molecules [91–93].

6 Conclusions

In this diploma thesis I have presented the progress in the setup of a new cavity cooling experiment, which is unique in its design features. A thorough year ago, I started designing and constructing the experiment from an empty table. By now the vacuum, the cavity setup and laser manipulation are fully functional and the first measurements of the molecule-cavity interaction are about to begin.

At the heart of the experiment lies the high finesse ($F \approx 1.9 \cdot 10^4$) confocal cavity. It was set up with a deviation of 6 μm from confocality (compared to 24 (28) μm in the x (y) direction in [16]) and contains a few thousands modes over a frequency range of 100 MHz.

The aim of this experiment is to achieve the first cooling of complex molecules, i.e. we search for a measurable reduction of the molecule's transverse velocity. A key feature to cooling is the collective enhancement provided in a self-organized pattern (superradiance). By utilizing a suitably prepared molecular beam, low transverse temperature concurrent with high particle density, the demanding requirements for self-organization can be fulfilled. Apart from cooling the combination of a pumping cavity with a confocal cavity promises various applications for the coherent manipulation of molecules.

Compared to existing cooling techniques for molecules, cavity cooling does not rely on collisions and it is therefore conceptually not limited to the temperature of a buffer gas. It may eventually lead to final temperatures below well 1 mK. Additionally, by combining a longitudinal cavity cooling scheme with a trap, continuous loading of the trap may be possible in an advanced version of the setup.

In spite of the great interest in cold and ultracold molecules [84] cooling and trapping schemes are sill rare. Therefore the experiment opens a window to a new domain of future implementations of molecular cavity cooling.

Bibliography

[1] T. W. Hänsch and A.W. Schawlow. Cooling of gases by laser radiation. *Opt. Commun.*, 13(1):68–69, 1975.

[2] D. Wineland and H. Dehmelt. Proposed $10^{14}\delta\nu < \nu$ laser fluorescence spectroscopy on Tl$^+$ mono-ion oscillator III (side band cooling). *Bull. Am. Phys. Soc.*, Ser. II, 20:637, 1975.

[3] E. Arimondo, W. D. Phillips, and F. Strumia, editors. *Laser Manipulation of Atoms and Ions*, volume Course CXVIII of *Proc. Int. School of Physics*, Amsterdam, 1993. Italian Physical Society, North-Holland.

[4] P. Maunz, T. Puppe, I. Schuster, N. Syassen, P. W. H. Pinkse, and G. Rempe. Cavity cooling of a single atom. *Nature*, 428:50 – 52, 2004.

[5] J. McKeever, J. R. Buck, A. D. Boozer, A. Kuzmich, H.-C. Nägerl, D. M. Stamper-Kurn, and H. J. Kimble. State-insensitive cooling and trapping of single atoms in an optical cavity. *Phys. Rev. Lett.*, 90(13):133602, Apr 2003.

[6] H. J. Metclaf and P. van der Straten. Laser cooling and trapping of atoms. *J. Opt. Soc. Am. B*, 20(5):887–908, 2003.

[7] S. Chu. Nobel lecture: The manipulation of neutral particles. *Rev. Mod. Phys.*, 70(3):685–706, Jul 1998.

[8] C. N. Cohen-Tannoudji. Nobel lecture: Manipulating atoms with photons. *Rev. Mod. Phys.*, 70(3):707–719, Jul 1998.

[9] W. D. Phillips. Nobel lecture: Laser cooling and trapping of neutral atoms. *Rev. Mod. Phys.*, 70(3):721–741, Jul 1998.

[10] C. Cohen-Tannoudji, J. Dupont-Roc, and G. Grynberg. *Atom-Photon Interactions.* John Wiley & Sons, Inc., 1992.

[11] H. J. Metclaf and P. van der Straten. *Laser cooling and trapping.* Springer, 1999.

[12] J. Dalibard and C. Cohen-Tannoudji. Laser cooling below the doppler limit by polarization gradients: simple theoretical models. *J. Opt. Soc. Am. B*, 6(11):2023–2045, 1989.

[13] A. Aspect, E. Arimondo, R. Kaiser, N. Vansteenkiste, and C. Cohen-Tannoudji. Laser cooling below the one-photon recoil energy by velocity-selective coherent population trapping. *Phys. Rev. Lett.*, 61(7):826–829, Aug 1988.

[14] M. Kasevich and S. Chu. Laser cooling below a photon recoil with three-level atoms. *Phys. Rev. Lett.*, 69(12):1741–1744, Sep 1992.

[15] W. Neuhauser, M. Hohenstatt, P. Toschek, and H. Dehmelt. Optical-sideband cooling of visible atom cloud confined in parabolic well. *Phys. Rev. Lett.*, 41(4):233–236, Jul 1978.

[16] H. W. Chan, A. T. Black, and V. Vuletić. Observation of collective-emission-induced cooling of atoms in an optical cavity. *Phys. Rev. Lett.*, 90(6):063003, Feb 2003.

[17] J. T. Bahns, W. C. Stwalley, and P. L. Gould. Laser cooling of molecules: A sequential scheme for rotation, translation, and vibration. *The Journal of Chemical Physics*, 104(24):9689–9697, 1996.

[18] M. D. Di Rosa. Laser-cooling molecules. *The European Physical Journal D - Atomic, Molecular, Optical and Plasma Physics*, 31(2):395–402, November 2004.

[19] B. K. Stuhl, B. C. Sawyer, D. Wang, and J. Ye. Magneto-optical trap for polar molecules. *Physical Review Letters*, 101(24):243002, 2008.

[20] P. Horak, G. Hechenblaikner, K. M. Gheri, H. Stecher, and H. Ritsch. Cavity-induced atom cooling in the strong coupling regime. *Phys. Rev. Lett.*, 79(25):4974–4977, Dec 1997.

[21] P. Münstermann, T. Fischer, P. Maunz, P. W. H. Pinkse, and G. Rempe. Dynamics of single-atom motion observed in a high-finesse cavity. *Phys. Rev. Lett.*, 82(19):3791–3794, May 1999.

[22] P. W. H. Pinkse, T. Fischer, P. Maunz, and G. Rempe. Trapping an atom with single photons. *Nature*, 404(6776):365–368, March 2000.

[23] C. J. Hood, T. W. Lynn, A. C. Doherty, A. S. Parkins, and H. J. Kimble. The Atom-Cavity Microscope: Single Atoms Bound in Orbit by Single Photons. *Science*, 287(5457):1447–1453, 2000.

[24] S. Nussmann, K. Murr, M. Hijlkema, B. Weber, A. Kuhn, and G. Rempe. Vacuum-stimulated cooling of single atoms in three dimensions. *Nature Physics*, 1:122–125, 2005.

[25] A. D. Boozer, A. Boca, R. Miller, T. E. Northup, and H. J. Kimble. Cooling to the ground state of axial motion for one atom strongly coupled to an optical cavity. *Physical Review Letters*, 97(8):083602, 2006.

[26] J. K. Asbóth, P. Domokos, and H. Ritsch. Correlated motion of two atoms trapped in a single-mode cavity field. *Phys. Rev. A*, 70(1):013414, Jul 2004.

[27] T. Fischer, P. Maunz, T. Puppe, P. W. H. Pinkse, and G. Rempe. Collective light forces on atoms in a high-finesse cavity. *New Journal of Physics*, 3(1):11, 2001.

[28] P. Horak and H. Ritsch. Scaling properties of cavity-enhanced atom cooling. *Phys. Rev. A*, 64(3):033422, Aug 2001.

[29] M. Gangl and H. Ritsch. Collective dynamical cooling of neutral particles in a high-q optical cavity. *Phys. Rev. A*, 61(1):011402, Dec 1999.

[30] P. Domokos and H. Ritsch. Collective cooling and self-organization of atoms in a cavity. *Phys. Rev. Lett.*, 89(25):253003, Dec 2002.

[31] A. T. Black, H. W. Chan, and V. Vuletić. Observation of collective friction forces due to spatial self-organization of atoms: From rayleigh to bragg scattering. *Phys. Rev. Lett.*, 91(20):203001, Nov 2003.

[32] S. Deachapunya, P. J. Fagan, A. G. Major, E. Reiger, H. Ritsch, A. Stefanov, H. Ulbricht, and M. Arndt. Slow beams of massive molecules. *The European Physical Journal D - Atomic, Molecular, Optical and Plasma Physics*, 46:307–313, 2008.

[33] T. Salzburger and H. Ritsch. Collective transverse cavity cooling of a dense molecular beam. *New J. Phys.*, 11(5):055025, May 2009.

[34] P. Domokos and H. Ritsch. Mechanical effects of light in optical resonators. *J. Opt. Soc. Am. B*, 20(5):1098–1130, 2003.

[35] G. Hechenblaikner, M. Gangl, P. Horak, and H. Ritsch. Cooling an atom in a weakly driven high-q cavity. *Phys. Rev. A*, 58(4):3030–3042, Oct 1998.

[36] H. Kogelnik and T. Li. Laser beams and resonators. *Applied Optics*, 7(5):1550–1567, October 1966.

[37] J. D. Jackson. *Classical Electrodynamics*. Walter de Gruyter, 3rd edition, 2002.

[38] J. K. Asbóth, P. Domokos, H. Ritsch, and A. Vukics. Self-organization of atoms in a cavity field: Threshold, bistability, and scaling laws. *Physical Review A*, 72:053417, 2005.

[39] D. Nagy, J. K. Asboth, P. Domokos, and H. Ritsch. Self-organization of a laser-driven cold gas in a ring cavity. *EPL (Europhysics Letters)*, 74(2):254, 2006.

[40] V. Vuletić and S. Chu. Laser cooling of atoms, ions, or molecules by coherent scattering. *Phys. Rev. Lett.*, 84(17):3787–3790, Apr 2000.

[41] B. E. A. Saleh and M. C. Teich. *Fundamentals of Photonics*. John Wiley & Sons, Inc., 1991.

95

[42] N. Hodgson and H. Weber. *Laser resonators and beam propagation.* Springer, second edition, 2005.

[43] P. Domokos and H. Ritsch. Collective cooling and self-organization of atoms in a cavity. *Phys. Rev. Lett.*, 89(25):253003, Dec 2002.

[44] B. Lev, A. Vukics, E. R. Hudson, B. C. Sawyer, P. Domokos, H. Ritsch, and J. Ye. Prospects for the cavity-assisted laser cooling of molecules. *Phys. Rev. A*, 77(2):023402, 2008.

[45] V. Vuletic, H. W. Chan, and A. T. Black. Three-dimensional cavity doppler cooling and cavity sideband cooling by coherent scattering. *Phys. Rev. A*, 64:033405–1 – 033405–7, 2001.

[46] G. D. Boyd and J. P. Gordon. Confocal multimode resonator for milimeter through optical wavelength masers. *The Bell system technical journal*, 40:489–508, March 1961.

[47] G. D. Boyd and H. Kogelnik. Generalized confocal resonator theory. *The Bell system technical journal*, 41:1347–1369, July 1962.

[48] A. E. Siegman. *Lasers.* University Science Books, 1986.

[49] M. Hercher. The spherical mirror fabry-perot interferometer. *Appl. Opt.*, 7(5):951–966, 1968.

[50] R. D. van Zee and J. P. Looney, editors. *Cavity-enhanced Spectroscopies*, volume 40 of *Experimental methods in the physical sciences.* Academic Press, 2002.

[51] P. C. Eklund, A. M. Rao, Y. Wang, P. Zhou, K. A. Wang, J. M. Holden, M. S. Dresselhaus, and G. Dresselhaus. Optical properties of c_{60}- and c_{70}-based solid films. *Thin Solid films*, 257:211–232, 1995.

[52] D. Ding, J. Huang, R. N. Compton, C. E. Klots, and R. E. Haufler. cw laser ionization of C_{60} and C_{70}. *Phys. Rev. Lett.*, 73(8):1084 – 1087, 1994.

[53] V. Piacente, G. Gigli, P. Scardala, A. Giustini, and D. Ferro. Vapor pressure of C_{60} Buckminsterfullerene. *J. Phys. Chem.*, 99:14052 – 14057, 1995.

[54] E. D. Black. An introduction to pound–drever–hall laser frequency stabilization. *American Journal of Physics*, 69(1):79–87, 2001.

[55] H. W. P. Chan. *Cavity cooling of cesium atoms*. PhD thesis, Stanford University, 2003.

[56] G. Scoles, D. Bassi, and D. Buck, U. Laine, editors. *Atomic and Molecular Beam Methods*, volume 1. Oxford University Press, 1988.

[57] M. Arndt, O. Nairz, J. Voss-Andreae, C. Keller, G. Van der Zouw, and A. Zeilinger. Wave-particle duality of c60 molecules. *Nature*, 401:680–682, 1999.

[58] N. Gotsche, H. Ulbricht, and M. Arndt. Uv-vis absorption spectroscopy of large molecules for applications in matter wave interferometry. *Laser Physics*, 17(4):583 – 589, 2009.

[59] A. Bekkerman, B. Tsipinyuk, A. Budrevich, and E. Kolodney. Direct experimental evidence for the thermal nature of delayed electron emission from a superhot c 60 molecule. *J. Chem. Phys.*, 108:5165 – 5168, 1998.

[60] M. Berninger, A. Stéfanov, S. Deachapunya, and M. Arndt. Polarizability measurements in a molecule near-field interferometer. *Phys. Rev. A*, 76:013607, 2007.

[61] M. S. Dresselhaus, G. Dresselhaus, and P. C. Eklund. *Science of Fullerenes and Carbon Nanotubes*. Acad. Press, San Diego, 2 edition, 1998.

[62] I. V. Hertel, H. Steger, J. de Vries, B. Weisser, C. Menzel, B. Kamke, and W. Kamke. Giant plasmon excitation in free c60 and c70 molecules studied by photoionization. *Phys. Rev. Lett.*, 68(6):784–787, Feb 1992.

[63] L. Hackermüller, K. Hornberger, B. Brezger, A. Zeilinger, and M. Arndt. Decoherence of matter waves by thermal emission of radiation. *Nature*, 427:711, 2004.

[64] B. Tsipinyuk, A. Budrevich, M. Grinberg, and E. Kolodney. Impact induced vibrational exciation in surface scattering of hyperthermal neutral C_{60} molecule. *J. Chem. Phys.*, 106:2449 – 2457, 1997.

BIBLIOGRAPHY

[65] P. Domokos, T. Salzburger, and H. Ritsch. Dissipative motion of an atom with transverse coherent driving in a cavity with many degenerate modes. *Phys. Rev. A*, 66(4):043406, Oct 2002.

[66] J. S. Gaffney and R. C. Pierce. Mass spectrometer study of evaporation of α-amino acids. *Journal of the American Chemical Society*, 99:4293–4298, 1977.

[67] H. Mabuchi, Q. A. Turchette, M. S. Chapman, and H. J. Kimble. Real-time detection of individual atoms falling through a high-finesse optical cavity. *Opt. Lett.*, 21(17):1393–1395, 1996.

[68] D. Egorov, T. Lahaye, W. Schöllkopf, B. Friedrich, and J. M. Doyle. Buffer-gas cooling of atomic and molecular beams. *Phys. Rev. A*, 66(4):043401, Oct 2002.

[69] J. D. Weinstein, R. deCarvalho, T. Guillet, B. Friedrich, and J. M. Doyle. Magnetic trapping of calcium monohydride molecules at millikelvin temperatures. *Nature*, 395:148–150, 1998.

[70] W. C. Campbell, E. Tsikata, H.-I. Lu, L. D. van Buuren, and J. M. Doyle. Magnetic trapping and zeeman relaxation of nh (x [sup 3] sigma[sup -]). *Physical Review Letters*, 98(21):213001, 2007.

[71] M. Stoll, J. M. Bakker, T. C. Steimle, G. Meijer, and A. Peters. Cryogenic buffer-gas loading and magnetic trapping of crh and mnh molecules. *Physical Review A (Atomic, Molecular, and Optical Physics)*, 78(3):032707, 2008.

[72] H. L. Bethlem, G. Berden, F. M. H. Crompvoets, A. J. A. Van Roij R. T. Jongma, and G. Meijer. Electrostatic trapping of ammonia molecules. *Nature*, 406:491–494, 2000.

[73] T. Rieger, T. Junglen, S. A. Rangwala, P. W. H. Pinkse, and G. Rempe. Continuous loading of an electrostatic trap for polar molecules. *Phys. Rev. Lett.*, 95(17):173002, Oct 2005.

[74] H. L. Bethlem, J. van Veldhoven, M. Schnell, and G. Meijer. Trapping polar molecules in an ac trap. *Physical Review A (Atomic, Molecular, and Optical Physics)*, 74(6):063403, 2006.

[75] D. DeMille, D. R. Glenn, and J. Petricka. Microwave traps for cold polar molecules. *The European Physical Journal D - Atomic, Molecular, Optical and Plasma Physics*, 31:375–384, 2004.

[76] R. Grimm, M. Weidemüller, and Y. B. Ovchinnikov. Optical dipole traps for neutral atoms. *Adv. At. Mol. Opt. Phys. 42, 95 (2000*, 42:95, 2000.

[77] H. L. Bethlem, G. Berden, and G. Meijer. Decelerating neutral dipolar molecules. *Phys. Rev. Lett.*, 83(8):1558–1561, Aug 1999.

[78] S. Ospelkaus, K. K. Ni, M. H. G. de Miranda, B. Neyenhuis, D. Wang, S. Kotochigova, P. S. Julienne, D. S. Jin, and J. Ye. Ultracold polar molecules near quantum degeneracy, 2008.

[79] P. Barletta, J. Tennyson, and P. F. Barker. Towards sympathetic cooling of large molecules: cold collisions between benzene and rare gas atoms. *New Journal of Physics*, 11(5):055029, 2009.

[80] W. Demtroeder. *Molekülphysik*. Oldenburg, 2003.

[81] G. Morigi, P. W. H. Pinkse, M. Kowalewski, and R. de Vivie-Riedle. Cavity cooling of internal molecular motion. *Physical Review Letters*, 99(7):073001, 2007.

[82] M. Kowalewski, G. Morigi, P. W. H. Pinkse, and R. de Vivie-Riedle. Cavity cooling of translational and ro-vibrational motion of molecules: ab initio-based simulations for oh and no. *Applied Physics B: Lasers and Optics*, 89(4):459–467, 2007.

[83] D. DeMille. Quantum computation with trapped polar molecules. *Phys. Rev. Lett.*, 88(6):067901, Jan 2002.

[84] L. D. Carr, D. Demille, R. V. Krems, and J. Ye. Cold and ultracold molecules: science, technology and applications. *New Journal of Physics*, 11(5):055049, 2009.

[85] A. André, D. DeMille, J. M. Doyle, M. D. Lukin, S. E. Maxwell, P. Rabl, R. J. Schoelkopf, and P. Zoller. A coherent all-electrical interface between polar molecules and mesoscopic superconducting resonators. *Nature Physics*, 2:636–642, 2006.

[86] P. Rabl, D. DeMille, J. M. Doyle, M. D. Lukin, R. J. Schoelkopf, and P. Zoller. Hybrid quantum processors: Molecular ensembles as quantum memory for solid state circuits. *Physical Review Letters*, 97(3):033003, 2006.

[87] E. Kuznetsova, R. Côté, K. Kirby, and S. F. Yelin. Analysis of experimental feasibility of polar-molecule-based phase gates. *Physical Review A (Atomic, Molecular, and Optical Physics)*, 78(1):012313, 2008.

[88] C. Lee and E. A. Ostrovskaya. Quantum computation with diatomic bits in optical lattices. *Phys. Rev. A*, 72(6):062321, Dec 2005.

[89] S. F. Yelin, K. Kirby, and R. Côté. Schemes for robust quantum computation with polar molecules. *Physical Review A (Atomic, Molecular, and Optical Physics)*, 74(5):050301, 2006.

[90] E. Charron, P. Milman, A. Keller, and O. Atabek. Quantum phase gate and controlled entanglement with polar molecules. *Physical Review A (Atomic, Molecular, and Optical Physics)*, 75(3):033414, 2007.

[91] R. Zadoyan, D. Kohen, D. A. Lidar, and V. A. Apkarian. The manipulation of massive ro-vibronic superpositions using time-frequency-resolved coherent anti-stokes raman scattering (tfrcars): from quantum control to quantum computing. *Chemical Physics*, 266(2-3):323 – 351, 2001.

[92] Z. Bihary, D. R. Glenn, D. A. Lidar, and V. A. Apkarian. An implementation of the deutsch-jozsa algorithm on molecular vibronic coherences through four-wave mixing: a theoretical study. *Chemical Physics Letters*, 360(5-6):459 – 465, 2002.

[93] D. R. Glenn, D. A. Lidar, and V. A. Apkarian. Quantum logic gates in iodine vapor using time-frequency resolved coherent anti-stokes raman scattering: a theoretical study. *Molecular Physics*, 104(8):1249–1266, 2006.

Curriculum Vitae

Personal Data

Name	Peter ASENBAUM
Birth	2 October 1986
Place of Birth	Vienna, Austria
Parents	Augustinus und Susanne Asenbaum
Nationality	Austria

Education

2008	Research activities in the Quantum Optics group of Markus Arndt
2005-2009	Studies of Physics and Chemistry at the University of Vienna
2004-2005	Mandatory military service
1996-2004	Grammar school: 'Albertus Magnus Schule', Vienna